

1. Report No. FHWA/TX-83/26+256-4		2. Government Accession No.		3. Recipient's Catalog No.	
4. Title and Subtitle EVALUATION OF MODULI AND THICKNESSES OF PAVEMENT SYSTEMS BY SPECTRAL-ANALYSIS-OF-SURFACE-WAVES METHOD				5. Report Date December 1983	
				6. Performing Organization Code	
7. Author(s) Soheil Nazarian and Kenneth H. Stokoe II				8. Performing Organization Report No. Research Report 256-4	
9. Performing Organization Name and Address Center for Transportation Research The University of Texas at Austin Austin, Texas 78712-1075				10. Work Unit No.	
				11. Contract or Grant No. Research Study 3-8-80-256	
12. Sponsoring Agency Name and Address Texas State Department of Highways and Public Transportation; Transportation Planning Division P. O. Box 5051 Austin, Texas 78763				13. Type of Report and Period Covered Interim	
				14. Sponsoring Agency Code	
15. Supplementary Notes Study conducted in cooperation with the U. S. Department of Transportation, Federal Highway Administration Research Study Title: "The Study of New Technologies for Pavement Evaluation"					
16. Abstract <p>The Spectral-Analysis-of-Surface-Waves (SASW) method is a nondestructive method for evaluating the moduli and thicknesses of pavement systems. By means of a transient impact applied to the surface of a pavement system or soil deposit, a group of waves with different frequency components is transmitted to the medium. By analysis of the phase information for each frequency determined between two receivers located on the surface, Rayleigh wave velocity, shear wave velocity, and eventually elastic moduli and thicknesses of the various layers in the pavement system are determined. The method has the advantages of being: (1) fast and economical, (2) nondestructive, and (3) capable of full automation.</p> <p>Preliminary studies of the feasibility and testing procedure of the SASW method were presented in Research Report 256-2. This initial work has been improved and expanded in the following areas: (1) the testing procedure has been refined with a resulting reduction in scatter in the data, and (2) a simple inversion method for elimination of the effect of high- or low-velocity shallow layers has been developed.</p> <p>Three series of tests were performed on State Highway 71 near Columbus, Texas. These tests were performed on a continuously reinforced concrete pavement, an asphaltic-concrete shoulder, and a soil median. The moduli determined with the SASW method are at most within 11 to 20 percent of those determined by the crosshole seismic method.</p>					
17. Key Words seismic testing, spectral analysis, elastic moduli, propagation velocity, pavement systems, Rayleigh waves, compression waves, shear waves			18. Distribution Statement No restrictions. This document is available to the public through the National Technical Information Service, Springfield, Virginia 22161.		
19. Security Classif. (of this report) Unclassified		20. Security Classif. (of this page) Unclassified		21. No. of Pages 138	22. Price

EVALUATION OF MODULI AND THICKNESSES OF PAVEMENT SYSTEMS
BY SPECTRAL-ANALYSIS-OF-SURFACE-WAVES METHOD

by

Soheil Nazarian
Kenneth H. Stokoe II

Research Report Number 256-4

The Study of New Technologies for Pavement Evaluation
Research Project 3-8-80-256

conducted for

Texas
State Department of Highways and Public Transportation

in cooperation with the
U. S. Department of Transportation
Federal Highway Administration

by the

CENTER FOR TRANSPORTATION RESEARCH
BUREAU OF ENGINEERING RESEARCH
THE UNIVERSITY OF TEXAS AT AUSTIN

December 1983

The contents of this report reflect the views of the authors, who are responsible for the facts and the accuracy of the data presented herein. The contents do not necessarily reflect the official views or policies of the Federal Highway Administration. This report does not constitute a standard, specification, or regulation.

PREFACE

This work was supported by the Texas State Department of Highways and Public Transportation under Research Project 3-8-80-256. The technical assistance and funding support provided by that organization are gratefully acknowledged. The writers specifically wish to thank Messers Gerald Peck, Richard Rogers, and Kenneth Hankins for their interest, advice and support.

Appreciation is extended to Drs. Alvin H. Meyer and W. R. Hudson for their constructive advice. The writers would also like to thank Scott R. Heisey and Waheed Uddin for their field assistance, Fred Redd for drafting the figures, and Sarah Clark and Teresa Tice-Boggs for assistance in typing the report.

LIST OF REPORTS

Report No. 256-1, "Comparison of the Falling Weight Deflectometer and the Dynaflect for Pavement Evaluation," by Barry Eagleson, Scott Heisey, W. Ronald Hudson, Alvin H. Meyer, and Kenneth H. Stokoe, II, presents the results of an analytical study undertaken to determine the best model for pavement evaluation using the criteria of cost, operational characteristics, and suitability.

Report No. 256-2, "Determination of In Situ Shear Wave Velocities From Spectral Analysis of Surface Waves," by J. Scott Heisey, Kenneth H. Stokoe II, W. Ronald Hudson, and A. H. Meyer, presents a method for determining elastic moduli at soil and pavement sites. Criteria considered in developing this method included the restraint of nondestructive testing, accuracy of moduli for all layers regardless of thickness, and quickness and efficiency for rapid, extensive testing.

Report No. 256-3, "Detection of Cracks on Highway Pavements," by C. H. Chien, W. N. Martin, A. H. Meyer, and J. K. Aggarwal, presents algorithms for the detection of cracks of highway pavements in aerial photographs.

Report No. 256-4, "Evaluation of Moduli and Thicknesses of Pavement Systems by Spectral-Analysis-of-Surface-Waves Method," by Soheil Nazarian and Kenneth H. Stokoe, presents the Spectral-Analysis-of-Surface-Waves (SASW) method for determination of moduli and thicknesses of pavement systems. The field testing procedure is simple, the method is nondestructive, and a unique solution to the problem is obtained.

ABSTRACT

The Spectral-Analysis-of-Surface-Waves (SASW) method is a nondestructive method for evaluating the moduli and thicknesses of pavement systems. By means of a transient impact applied to the surface of a pavement system or soil deposit, a group of waves with different frequencies components is transmitted to the medium. By analysis of the phase information for each frequency determined between two receivers located on the surface, Rayleigh wave velocity, shear wave velocity, and eventually elastic moduli and thicknesses of the various layers in the pavement system are determined. The method has the advantages of being: (1) fast and economical, (2) nondestructive, and (3) capable of full automation.

Preliminary studies of the feasibility and testing procedure of the SASW method were presented in Research Report 256-2. This initial work has been improved and expanded in the following areas: (1) the testing procedure has been refined with a resulting reduction in scatter in the data, and (2) a simple inversion method for elimination of the effect of high- or low-velocity shallow layers has been developed.

Three series of tests were performed on State Highway 71 near Columbus, Texas. These tests were performed on a continuously reinforced concrete pavement, an asphaltic-concrete shoulder, and a soil median. The moduli determined with the SASW method are at the most within 11 to 20 percent of those determined by the crosshole seismic method.

KEY WORDS: seismic testing, spectral analysis, elastic moduli, propagation velocity, pavement systems, Rayleigh waves, compression waves, shear waves.

SUMMARY

Many highways in the Interstate highway system are approaching the end of their serviceable lives. Due to the lack of a fast, economical, and precise method for evaluating the properties of these pavement systems, it is difficult to perform meaningful maintenance inspections regularly. Consequently, much money is spent each year in replacing pavements when it might be possible to perform preventive maintenance to extend the life of some of these pavements. Fast in situ methods for evaluating the properties of the pavement systems, such as the Dynaflect and Falling Weight Deflectometer, have drawbacks: providing a non-unique solution, requiring excessive in-house data reduction time, and employing static solutions to a dynamic testing procedure.

A new method of testing pavement systems in situ has been developed which can be used to evaluate the moduli and thicknesses of different layers. The method, which is called the Spectral-Analysis-of-Surface-Waves (SASW) method is a seismic wave propagation method which involves measurement of transiently excited Rayleigh waves propagating along the pavement surface. The method is fast, precise, and nondestructive. In addition, it requires no boreholes and has the potential of full automation.

This method has been successfully applied to an asphaltic-concrete pavement, a continuously reinforced concrete pavement, and a soil site near Columbus, Texas, and the results are presented herein.

STATEMENT OF IMPLEMENTATION

The Spectral-Analysis-of-Surface-Waves (SASW) method has many applications in the construction and maintenance of highways. With this method, elastic moduli and layer thicknesses of pavement systems can be evaluated in situ. The method can be utilized as a tool for quality control during construction and during regular maintenance inspections. Testing is nondestructive, rapid and easy to perform. In addition, it is possible to automate fully the data acquisition and reduction schemes.

The SASW method has been applied to several pavement systems, both asphalt and concrete, in the last three years, and the results have been compared with those from the other available methods. Elastic moduli determined from the SASW method are in good agreement with moduli obtained from well established seismic methods, and layer thicknesses compare well with those determined from boring logs. Case histories on several sites are presented in Research Report 256-2 and this report. However, more tests are required to study the universality and precision of the method and to define more confidently the testing criteria. Improvement is required in the analytical portion of the data reduction scheme to decrease the number of simplifying assumptions. Also, the hardware and software should be modified to minimize the testing and data reduction time.

TABLE OF CONTENTS

PREFACE	iii
LIST OF REPORTS	v
ABSTRACT	vii
SUMMARY	ix
STATEMENT OF IMPLEMENTATION	xi
 CHAPTER 1. INTRODUCTION	 1
 CHAPTER 2. BACKGROUND	
Review of Available Methods	3
Wave Propagation in Elastic Half-Space	4
Evaluation of Elastic Properties from Propagation Velocity	8
In Situ Wave Propagation Methods	12
Borehole Seismic Methods	13
Surface Seismic Methods	15
 CHAPTER 3. SPECTRAL-ANALYSIS-OF-SURFACE-WAVES METHOD	
Field Testing	20
Source	20
Location of Receivers (Geophone Array)	24
Recording Device	27
Determination of R-Wave Dispersion Curve	29
Inversion of R-Wave Dispersion Curve	31
 CHAPTER 4. EXPERIMENT NEAR COLUMBUS, TEXAS	
Description of Site	35
Set-Up and Procedure	38
 CHAPTER 5. PRESENTATION OF RESULTS	
Crosshole Seismic Test	43
Soil Section (Median)	43
Asphalt (ACP) Section	46

Spectral-Analysis-of-Surface-Waves Method	46
Soil Section (Median)	49
Asphalt (ACP) Section	53
Concrete (CRCP) Section	53
Evaluation of Elastic Properties	62
CHAPTER 6. COMPARISON OF CROSSHOLE SEISMIC AND SASW RESULTS	67
CHAPTER 7. SUMMARY, CONCLUSIONS, AND RECOMMENDATIONS	
Summary	75
Conclusions	75
Recommendations for Future Studies	76
REFERENCES	79
APPENDICES	
Appendix A. Effect of Set-Up Configuration on Dispersion Curves in SASW Method	83
Appendix B. Fourier Transform and Spectral Analysis	89
Appendix C. Inversion of Dispersion Curves	103
Appendix D. Crosshole Seismic Tests	111
THE AUTHORS	123

CHAPTER 1. INTRODUCTION

Many different methods have been proposed for evaluating the elastic properties of pavement systems. These methods apply either a static or a dynamic load to the system. Methods involving static loading have the drawback of providing a non-unique solution to the problem. In addition, only a summation of the overall stiffness of the pavement system is measured, and decomposition of this summation into the properties of the different layers is difficult if not impossible. Dynamic methods, such as the Dynaflect and Falling Weight Deflectometer, are more promising, but the equipment is expensive, the testing time is substantial, and a non-unique solution to the problem is obtained. In this report the Spectral-Analysis-of-Surface-Waves (SASW) method for determination of moduli and thicknesses of pavement systems is presented. Despite the complicated theory behind this method, the testing procedure is simple, and a unique solution to the problem is obtained. The nondestructive nature of the SASW method and the minimal time necessary to conduct this test are positive attributes. The fact that it is possible to automate fully the method by means of microprocessors makes it even more promising.

Use of the SASW method in pavement systems was originated by Heisey et al (Ref 1) and now is under continuous development. This report is an update of progress made in developing this method. Testing performed on State Highway 71 near Columbus, Texas, on a concrete pavement, an asphaltic concrete shoulder, and a soil median is presented herein. Moduli and layer thicknesses determined with the SASW method are shown to compare closely with moduli determined by crosshole seismic tests and with layering

determined with borings. This is the first time that the SASW method has been used on a concrete pavement.

CHAPTER 2. BACKGROUND

REVIEW OF AVAILABLE METHODS

Four general methods are available for evaluating the elastic properties of pavement systems, namely:

- (1) static deflections,
- (2) steady-state dynamic deflections,
- (3) impact load response, and
- (4) wave propagation methods.

An in-depth review of these methods as well as their advantages and disadvantages has been discussed by Lytton et al (Ref 2), Heisey et al (Ref 1), and Hoar (Ref 4).

Static deflection methods include the plate bearing test, curvature meter, Benkelman beam, traveling Deflectometer, and La Croix deflectograph. By means of elastic theory and the measured deflection, elastic properties of each layer are determined.

In the methods involving steady-state dynamic deflection, the deflection of the pavement system is measured at different points near a loaded area. Then, by means of elastic theory, the moduli of the pavement system are back-calculated. Current equipment includes the Road Rater, Dynaflect, and Waterways Experimental Station (WES) vibrator.

Impact load response methods involve monitoring the displacement-time response at the pavement surface due to a transient load. The pavement is

modelled as a single-degree-of-freedom system, and the average stiffness is calculated.

The main disadvantage of the three general methods described above is that the overall stiffness of the pavement is evaluated, and decomposition of the overall stiffness into the stiffness of each layer is difficult, because generally a unique solution does not exist. The number and thicknesses of the layers should really be known in advance. In addition, in methods 2 and 3 the tests are performed dynamically but the data obtained from these tests are analyzed assuming static loading, which results in significant differences between actual and assumed stress distributions.

Wave propagation methods measure the velocities of elastic waves traveling through the pavement layers. If properly used, these methods are the most direct form of evaluation of elastic moduli and thicknesses of the individual layers. Two types of wave propagation methods, the SASW and crosshole seismic methods, are used in this study. A detailed discussion of the SASW method is presented in Chapter 3. First, background material on wave propagation and different insitu wave propagation methods is presented.

WAVE PROPAGATION IN ELASTIC HALF-SPACE

Wave motion created by a disturbance within an infinite, homogeneous, isotropic, elastic medium can be described by two kinds of waves: compression and shear. These waves are called body waves because they travel in the bulk of the medium. In a half-space, a third type of motion occurs. This wave, called a Rayleigh wave, propagates near the surface of the half space. Each of these waves demonstrates a different type of particle motion and travels with different velocities.

Compression waves (also called dilatational waves, primary waves, or P-waves) exhibit a push-pull motion. As a result, wave propagation and particle motion are in the same direction. Compression waves travel faster than the other types of waves and, hence, appear first in a travel time record.

Shear waves (also called distortional waves, secondary waves, or S-waves) generate a shearing motion, which causes particle motion perpendicular to the direction of wave propagation. Shear waves travel slower than P-waves and appear as the second major wave type on a travel time record.

Rayleigh waves (R-waves) propagate near the surface at a speed approximately 90 percent of that of S-waves. Particle motion associated with R-waves is composed of both vertical and horizontal components, which, when combined, form a retrograde ellipse at the surface. The amplitude of the wave attenuates rapidly with depth, and, at a depth equal to about 1.5 times the wavelength, the amplitude is equal to approximately 10 percent of the original amplitude at the surface.

In Fig 2.1, particle motions relative to the directions of wave propagation for the different types of waves are illustrated.

The propagation of these three types of waves away from a vertically vibrating circular source at the surface of an elastic half-space is shown in Fig 2.2. Miller and Persey (Ref 6) found that, for the situation shown in Fig 2.2, approximately 67 percent of the input energy propagates in the form of R-waves while the shear and compression waves carry 26 and 7 percent of the energy, respectively. P- and S-waves propagate radially outward from the source, but R-waves propagate in a cylindrical wavefront near the surface. Although body waves travel faster than surface waves, body waves attenuate much faster at the surface than R-waves, due to geometric damping. At the

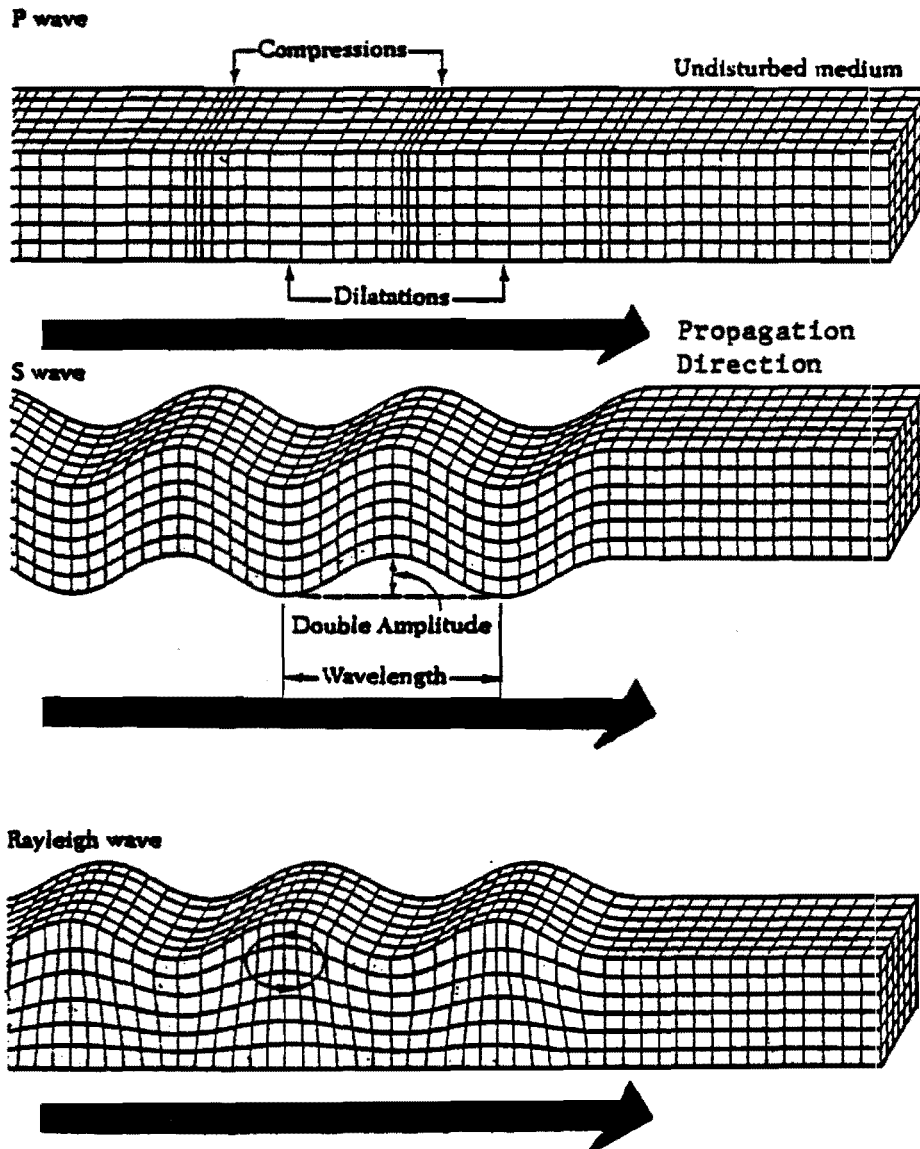


Fig 2.1. Characteristic motions of seismic waves (Ref 5).

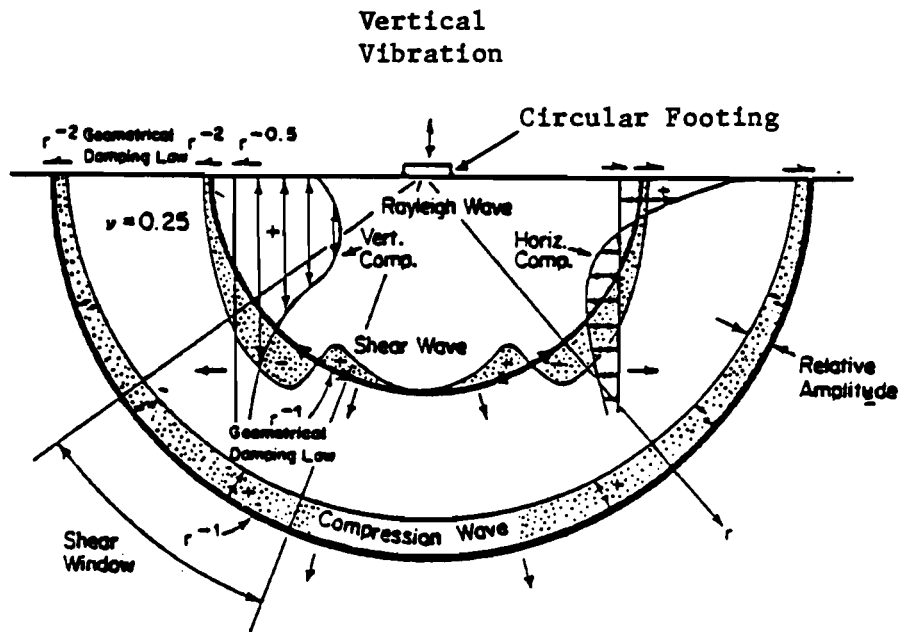


Fig 2.2. Distribution of Rayleigh, shear, and compression waves from a circular footing on a homogeneous, isotropic, elastic half-space (Ref 8).

surface of an elastic half-space, body waves (P- and S-waves) attenuate in proportion to $1/r^2$ (where r is the distance from the source), whereas surface wave amplitude decreases in proportion to $1/\sqrt{r}$. P-, S-, and R-wave velocities depend upon Poisson's ratio of the medium. The propagation velocities of all these waves relative to the shear wave velocity are shown as a function of Poisson's ratio in Fig 2.3.

In a layered medium, the problem becomes more complicated due to reflection and refraction of the wave front at the boundaries. For example, an incident P-wave can reflect back to the medium as both P- and S-waves.

For more detail on this subject the reader is referred to Ewing et al (Ref 7) and Richart et al (Ref 8).

EVALUATION OF ELASTIC PROPERTIES FROM PROPAGATION VELOCITY

The P-wave velocity can be defined as

$$v_p = \sqrt{\frac{\lambda + 2G}{\rho}} \quad (2.1)$$

where

$$\lambda(\text{Lame's constant}) = \nu E / \left[(1 + \nu)(1 - 2\nu) \right] \quad (2.2)$$

and

$$G(\text{Shear modulus}) = E/2(1 + \nu) \quad (2.3)$$

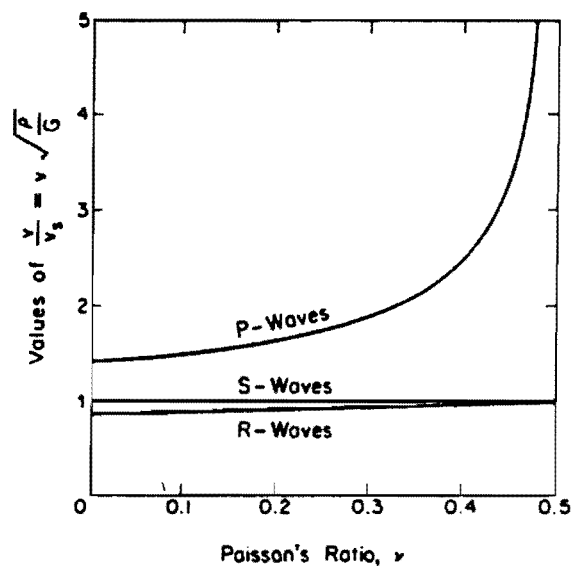


Fig 2.3. Relationship between Poisson's ratio and wave velocities in an elastic half-space (Ref 8).

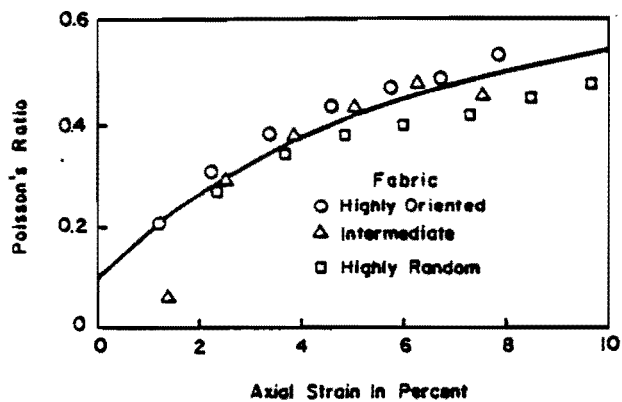


Fig 2.4. Poisson's ratio of sedimented kaolinite from unconfined compression tests (Ref 10).

and E , ν , and ρ are Young's modulus, Poisson's ratio, and mass density, respectively. In Eq 2.1, the numerator represents the constrained modulus, M , so that

$$M = \lambda + 2G = (1 - \nu)E / \left[(1 + \nu)(1 - 2\nu) \right] \quad (2.4)$$

Young's modulus and shear modulus can then be written as

$$E = \rho(1 + \nu)(1 - 2\nu)V_p^2 / (1 - \nu) \quad (2.5)$$

and

$$G = \rho(1 - 2\nu)V_s^2 / \left[2(1 - \nu) \right] \quad (2.6)$$

which gives each modulus in terms of Poisson's ratio and the compression wave velocity. Shear wave velocity and shear modulus are related by

$$G = \rho V_s^2 \quad (2.7)$$

Therefore, Young's modulus can be written in terms of V_s and ν as

$$E = 2(1 + \nu)\rho V_s^2 \quad (2.8)$$

From Eqs 2.5 through 2.8, Young's modulus and/or the shear modulus of the medium can be easily evaluated once the body wave velocities of the medium have been determined. P- and S-wave velocities are inter-related by Poisson's ratio by

$$V_p / V_s = \left[(1 - \nu) / (0.5 - \nu) \right]^{1/2} \quad (2.9)$$

or

$$v = \left[0.5(v_p/v_s)^2 - 1 \right] / \left[(v_p/v_s)^2 - 1 \right] \quad (2.10)$$

Rayleigh wave velocity is constant in a homogeneous half-space and is independent of frequency. Each frequency has a corresponding wavelength according to

$$V_R = fL_R \quad (2.11)$$

where

$$\begin{aligned} V_R &= \text{Rayleigh wave velocity,} \\ f &= \text{frequency of excitation, and} \\ L_R &= \text{wavelength of R-wave.} \end{aligned}$$

As mentioned earlier, R-wave and S-wave velocities are related by Poisson's ratio. Although the ratio of the R-wave and S-wave velocities increases as Poisson's ratio increases (see Fig 2.3), the change in this ratio is not significant, and it can be assumed that it is approximately equal to 0.90 without introducing an error larger than about 5 percent.

An important point in evaluating elastic properties from measurement of only one wave velocity is selection of the appropriate Poisson's ratio. Elastic and shear moduli are strain dependent. Up to a shearing strain level of about 0.01 percent, moduli are nearly constant, with only a slight decrease in the range from 0.001 to 0.01 percent. However, above a strain level of 0.01 percent, the moduli decrease significantly. Several studies which have been performed on Poisson's ratios of different materials show that they are quite small in the low-strain range. Chen (Ref 9) reported

Poisson's ratios as low as 0.1 for small strains on sands. Krizek (Ref 10) reported the variation of Poisson's ratio with strain measured in unconfined compression tests. His data are shown in Fig 2.4. The range of Poisson's ratio in Fig 2.4 is from 0.10 for near zero strain to 0.50 for 10 percent strain. Drained triaxial and plane strain tests of a sensitive Canadian clay by Wong and Mitchell (Ref 11) gave values of Poisson's ratio of about 0.10 to 0.15 for the first stage of loading. Hardin (Ref 12) recommends values for Poisson's ratio between zero and 0.20 for low-strain tests, with a mean value of 0.12.

Most conventional static laboratory tests do not involve measurements in the low-strain range, even at the start of loading. Therefore, high values of Poisson's ratio are determined from the tests. Although lower values of Poisson's ratio should be used in the analysis of tests such as the static deflection and steady-state dynamic deflection tests (e.g., Dynaflect), the final results are fortuitously insensitive to Poisson's ratio. However, for dynamic tests such as the wave propagation methods, this point must be considered.

IN SITU WAVE PROPAGATION METHODS

In situ wave propagation methods involve applying a transient or steady-state excitation at one point in the pavement system and detecting the response in two or more locations. Wave velocity is determined from the recorded response, and moduli are calculated using Eqs 2.5 through 2.8. Basically, all methods employing seismic wave propagation are performed at low-amplitude strains.

In situ measurement of soil properties by wave propagation can be summarized in the following six steps:

- (1) set up the receivers at known distances,
- (2) generate an impulse,
- (3) measure the travel time of the wave front between receivers (directly or indirectly),
- (4) calculate the wave velocity (distance/time),
- (5) calculate the elastic soil properties, and then
- (6) repeat steps 1 to 5 for different receiver locations (directly or indirectly).

In situ wave propagation methods can be categorized into two main groups: (1) borehole seismic methods and (2) surface seismic methods.

Borehole Seismic Methods

In these methods one or more boreholes are utilized as illustrated in Fig 2.5. Generally, P- and S-wave velocities are measured at different depths. The most common borehole seismic methods are

- (1) crosshole test, Hoar (Ref 4);
- (2) downhole test, Warrick (Ref 13);
- (3) uphole test, Meisner (Ref 14);
- (4) in-hole test, Ogura (Ref 15); and
- (5) bottom-hole test, Stokoe et al (Ref 16).

Except for the crosshole test, in which at least two boreholes are required, the tests can be performed with a single borehole. The ray paths in these tests are generally assumed to be directly between the source and receiver as shown in Fig 2.5.

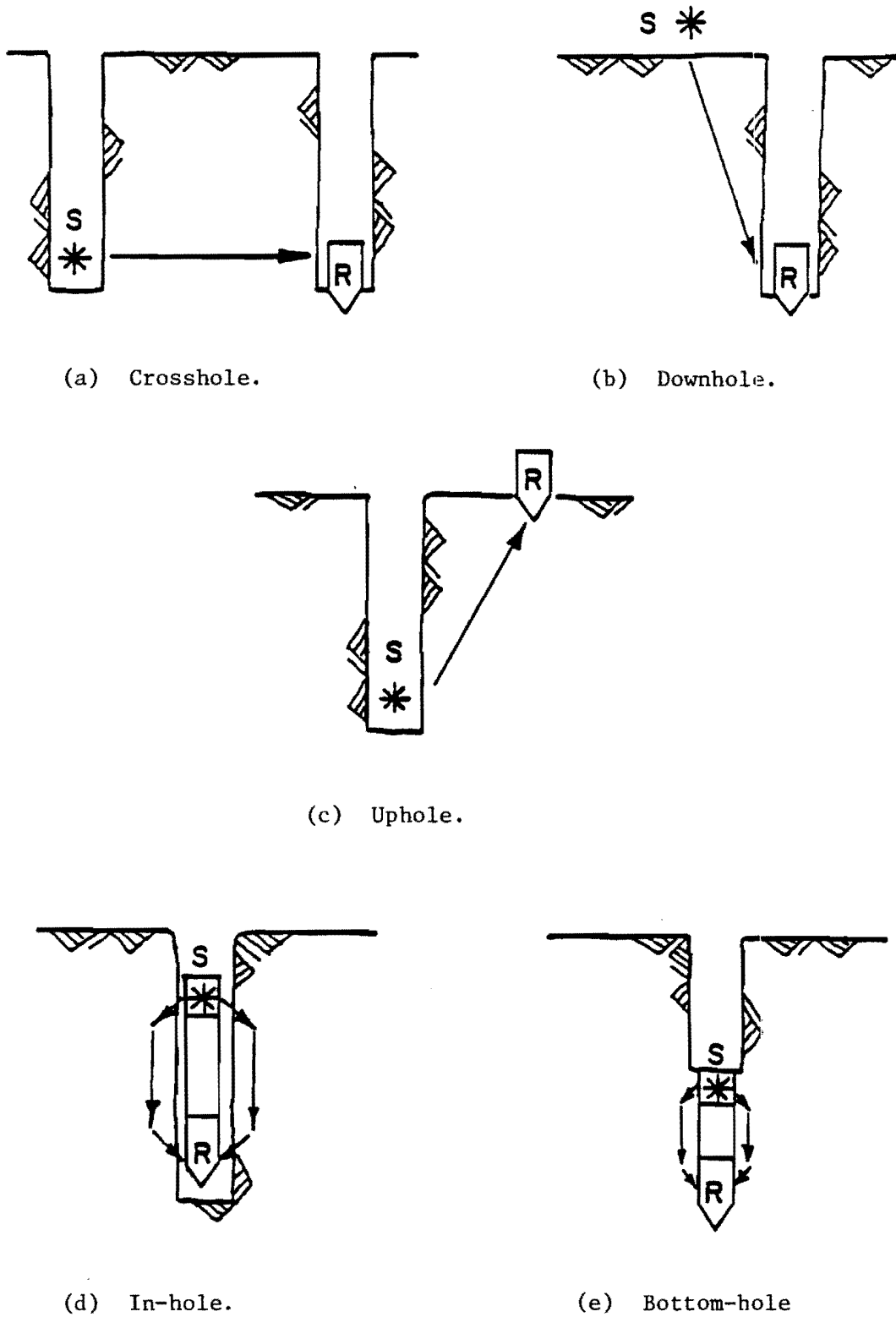


Fig 2.5. Schematic representation of borehole seismic methods (Ref 4).

To determine the variation in soil properties with depth in borehole seismic methods, the location of the source and/or the receiver is changed in the borehole, and the test is repeated.

Surface Seismic Methods

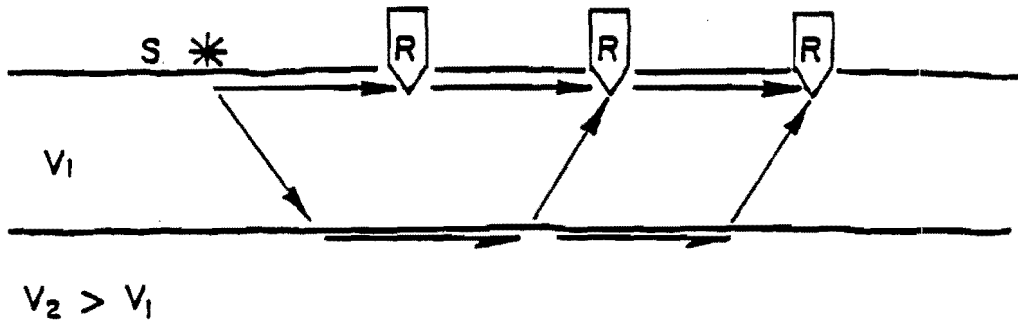
In these methods both the source and receivers are located at the surface. Thus, there is an economical advantage in these methods relative to the borehole seismic methods in that no boreholes are required. Common surface seismic methods are

- (1) surface refraction,
- (2) surface reflection,
- (3) steady-state Rayleigh wave, and
- (4) spectral analysis of Rayleigh waves.

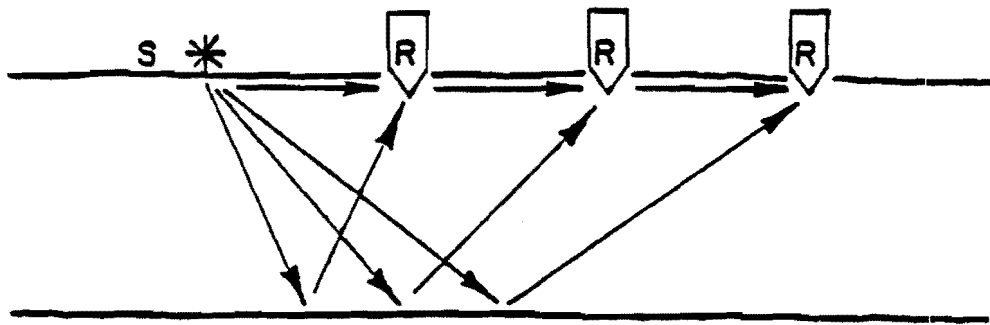
Figure 2.6 shows a simplified scheme of these different test methods.

The surface refraction method, Redpath (Ref 17), consists of measuring the travel times of body waves from a surface source to a linear array of receivers on the surface (see Fig 2.6a). The fastest path of the seismic waves depends upon the velocity distribution in the substructure, which is inferred from the time of first arrivals at each receiver. The main disadvantage of this method is that low-velocity layers beneath a high-velocity layer are not detected. As such, it is not appropriate for pavement systems.

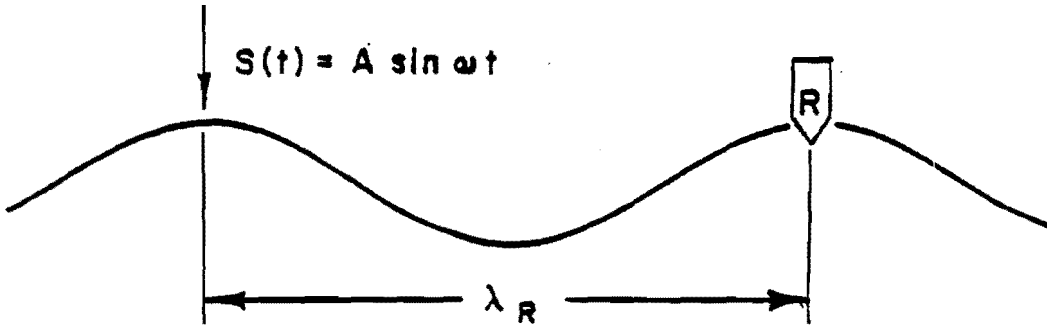
The surface reflection method, Borm (Ref 18), is very similar to the surface refraction method. The only difference is that measurement of waves reflected from different strata rather than waves refracted from the interface of the layers is the main objective. The main drawback of this method is that multiple reflections from one layer can obscure the detection



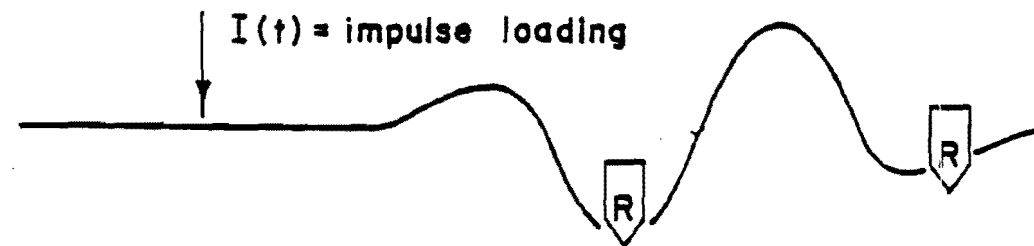
(a) Surface refraction.



(b) Surface reflection.



(c) Steady-state Rayleigh wave.



(d) Rayleigh wave dispersion.

Fig 2.6. Schematic representation of surface seismic methods (Ref 4).

of the primary reflected rays from other layers (see Fig 2.6b). In addition, the reflected ray is never the first arrival in the records detected by the receivers. Hence, analyzing of the data may be difficult and a great deal of judgement and interpretation is required.

A sinusoidal wave generator is used as the source in the steady-state Rayleigh wave method, and the wavelengths of waves with different frequencies are evaluated by means of the phase relationship between the surface waves monitored at different receivers. R-wave velocity is then determined by means of Eq 2.11. As a first approximation, it can be assumed that the effective sampling depth is equal to $1/2$ to $1/3$ of the wavelength. By varying the frequency of the source, an R-wave velocity profile can be constructed. As S- and R-wave velocities are related, as shown in Fig 2.3, S-wave velocities for different depths can be determined. By means of elastic theory, the elastic properties of the medium are then evaluated (Eqs 2.5 through 2.8).

Conceptually, the method involving spectral analysis of surface (Rayleigh) waves is identical to the steady-state method. The main difference is the excitation source, which is transient in the SASW method. One benefit of a transient impact is that it can excite a wide range of frequencies. Thus, with one impact, it is possible to record many different frequencies, and hence velocities and wavelengths, and eventually construct the complete profile. A detailed discussion of this method follows.

CHAPTER 3. SPECTRAL-ANALYSIS-OF-SURFACE-WAVES METHOD

The Spectral-Analysis-of-Surface-Waves (SASW) method is an economical and powerful method for evaluation of elastic properties of pavement systems as well as natural soil deposits. In addition, it can be used as a tool to control the quality of compaction during the construction of structures such as pavements and earth dams.

The SASW method is a nondestructive test method in which both the source and receivers are placed on the pavement surface, and Rayleigh waves at low strain levels are generated and detected. This method has the advantages of repeatability, high accuracy, no boreholes, and a simple set up of the equipment. Other advantages are

- (1) a continuous profile of the site properties, including modulus values and layer thicknesses, is produced;
- (2) there is a limited need for any engineering judgement to reduce the data gathered in the field and there is the possibility of fully automating the data reduction so that the results can be provided almost instantly; and
- (3) the test can be performed by a moderately skilled technician.

The main disadvantage at this point in the development is that testing is not rapid. For example, gathering the data for the asphalt shoulder section near Columbus, Texas, took about two hours.

Investigation of each site with the SASW method consists of the following three phases:

- (1) field testing,
- (2) determination of the R-wave dispersion curve, and
- (3) inversion of the R-wave dispersion curve.

Each phase is individually discussed in the following paragraphs.

FIELD TESTING

A simplified illustration of the test procedure is shown in Fig 3.1. Two or more vertical geophones (velocity transducers) are located on the surface at the site. A transient signal is generated by an appropriate source. The generated wave front is detected by the geophones as it propagates past them and is recorded on the appropriate device.

Source

The source should be able to generate Rayleigh waves over a wide range in frequencies with adequate amplitude so that they can be detected by the geophones. Simultaneously, the source should generate minimal P- and S-wave energy. Near the surface P- and S- waves (body waves) attenuate much more rapidly than surface waves, as discussed earlier. Thus, the distance between the first geophone (receiver closer to the source) and the source should be enough so that a significant amount of the energy associated with the body waves dies out before arrival at the first receiver. On the other hand, if the source is too far from the first receiver or the distance between the geophones is relatively large (relative to the wavelengths of the recorded waves), another problem arises. As the wavelet has to go through several cycles in the medium, the energy (amplitude) associated with different frequencies is not sufficient to be detected by the receivers, and background

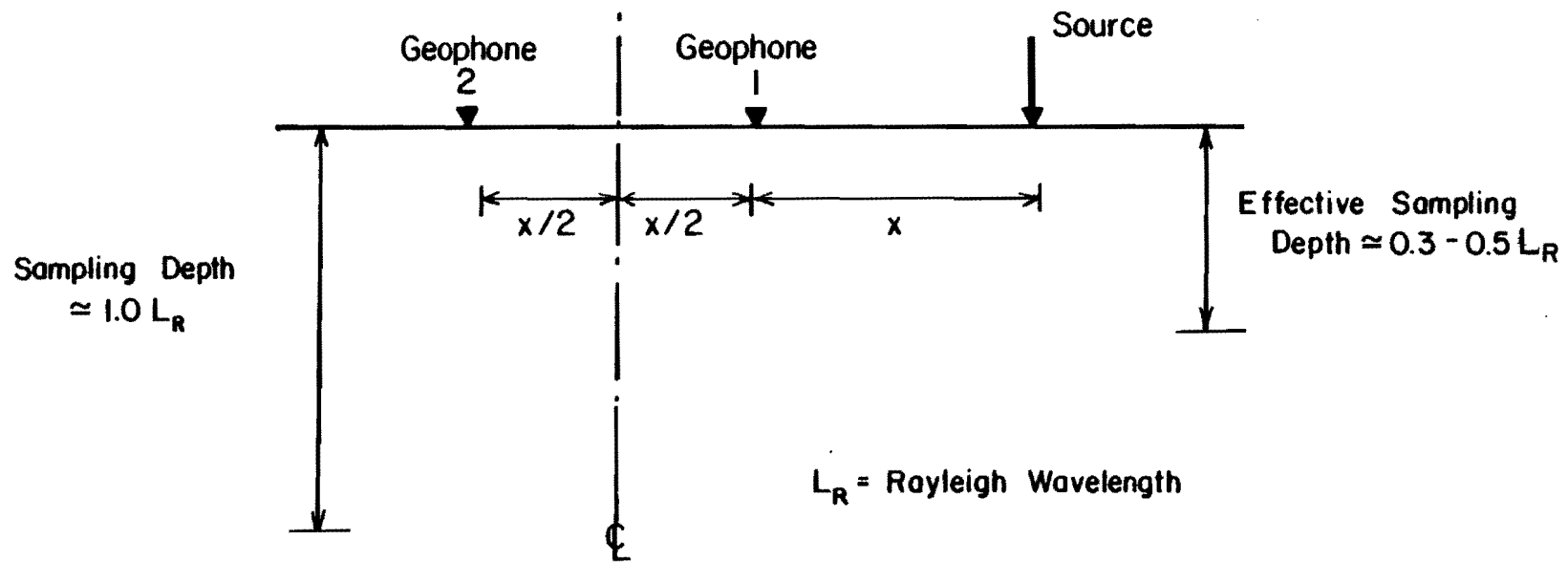


Fig 3.1. Schematic of Spectral-Analysis-of-Surface-Waves method.

noise dominates the record. The optimum distance between the source and first geophone is now under study.

As in any seismic experiment, elimination of background noise is one of the most important factors for achieving a good record and eventually a reliable result. Great care should be taken to minimize this undesirable element in any in situ test. One of the preferred methods of decreasing the effect of noise is averaging. In this method several records are gathered under constant conditions, and the arithmetic average of these records is determined. That part of the records which is associated with the experimental input from the source will be reasonably identical in each test, whereas the noise portion will vary. If a series of records at one point is summed and divided by the number of records, it will average to its so-called exact value, since the actual signal has been repeated. However, the noise is different in each record (because of its random nature), and the resulting average will tend to be zero. Theoretically, the more records that are averaged together, the more refined the final result will be. However, practically speaking, after a few averages this process will not appreciably improve the record. In Fig 3.2, the phases of cross power spectra for 5 and 25 averages are shown. The difference between the two records is negligible. Heisey (Ref 3) suggests that five averages is generally sufficient for the soil sites.

For sampling shallow depths the maximum frequency excited is of most importance. For shallow sampling the receivers and source are placed close to one another, so it is not necessary to transfer much energy to the medium (by the source). High frequencies translate to short wavelengths, which correspond to shallower depths of sampling. The highest frequency required in an experiment depends directly on the properties of the material near the

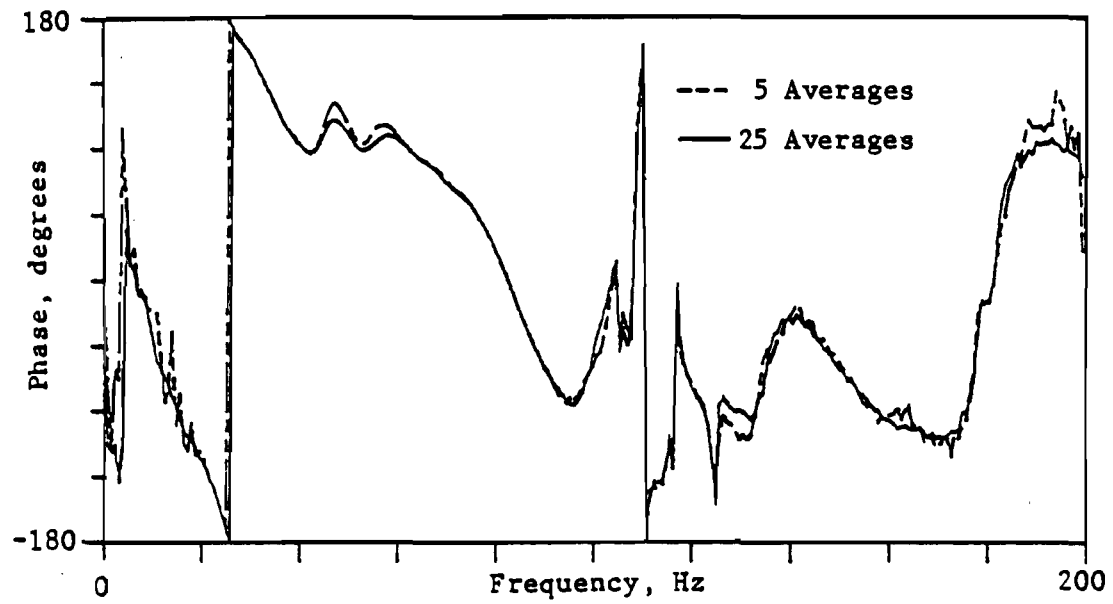


Fig 3.2. Comparison of phase information for 5 and 25 averages at a soil site (Ref 1).

surface. The product of the frequency and wavelength corresponding to that frequency in a layer is constant and equal to the R-wave velocity of that layer (Eq 2.11). For a constant wavelength, the maximum frequency required in testing will increase as the velocity of the layer increases. For a typical soil deposit, the highest frequency necessary is around 400 Hz, but, for an asphalt layer, the source should generate frequencies up to 3000 Hz, and, for a concrete layer, this upper bound is about 6000 Hz.

For determination of properties of relatively deep layers, the energy coupled into the medium is of greater importance. Excitation of low frequencies is relatively simple; however, the amplitude of these low frequency waves should be high enough so that they can be detectable by the receivers. In evaluation of the properties of pavement systems, the lowest frequency which should be excited is in the range of 5 to 10 Hz (depending upon the properties of the natural soil underlying the system). The source can be anything from a chisel and hammer, to a drop hammer, to a sledge hammer.

In summary, for experiments in which the properties of the shallow layers are of primary concern, a light weight source capable of exciting high frequencies is desirable; whereas for deep layers a relatively heavy source is preferable. The optimum range of frequencies generated at different sites is under study.

Location of Receivers (Geophone Array)

The factors that affect appropriate spacing of the geophones have been studied by Heisey (Ref 3). These factors include

- (1) velocity of the material,
- (2) depth of investigation,

- (3) range of frequencies,
- (4) attenuation properties of the medium, and
- (5) sensitivity of the instrumentation.

On the basis of the studies on several soil sites, Heisey (Ref 3) suggested that the distance between the receivers, X , should be less than two wavelengths and greater than one-third of a wavelength. This relationship can be expressed as

$$L_R/3 < X < 2L_R \quad (3.1)$$

As the velocities of different layers are unknown before testing, it is difficult to know if these limits are satisfied. Practically speaking, it is more appropriate to test with various distances between the receivers in the field and then to evaluate the range of wavelengths over which reliable measurements were made for that spacing. The relationship can then be expressed as

$$X/2 < L_R < 3X \quad (3.2)$$

The procedure is then to select a spacing between geophones, perform the test, and reduce the data to determine the wavelengths and velocities. The next step is to eliminate the points that do not satisfy Eq 3.2.

Theoretically, one seismic experiment in seismic testing is enough to evaluate the properties of the medium. For a more precise measurement, several tests are generally required. Different tests are performed with different geometries of the set up. The two most common types of geometrical arrangement for the source and receivers are the Common Source/Receiver and

the Common Midpoint geometries, Diebold and Stoffa (Ref 19).

In the common source/receiver (CSR) geometry, either the source or receivers are fixed in one location and the other is moved for different experiments in each test. In the common midpoint (CMP) geometry, both the source and receivers are moved the same distance about an imaginary centerline. For a medium consisting of a stack of horizontal layers with lateral homogeneity, the results of the tests performed with both methods should theoretically be identical. If the layers are not horizontal or the elastic properties of any layer varies laterally, the CMP geometry is preferred. In the CMP arrangement, the velocities are averaged in the range over which the test is extended. There is a trade-off, however; in a single CMP experiment there is no way to determine the dip of the layers. To compare the effect of the geometry of the set-up on the quality of the dispersion curves, a series of tests were performed at a soil site near the Walnut Creek sewerage plant, located east of Austin, Texas, and the results are discussed in Appendix A.

In the SASW method, the area between the two receivers is important, and the properties of the materials between the source and the near geophone have little effect on the test. Thus, the imaginary centerline in the CMP method is selected between the receivers. The two receivers are moved away from the imaginary centerline at an equal pace, and the source is moved such that the distance between the source and near geophone is equal to the distance between the two receivers. This geometry of source and receivers is called Common Receivers Midpoint (CRMP) geometry, hereafter.

Another advantage of the CRMP geometry is that, by reversing the location of the source and by averaging the records from direct and reversed

tests, the effect of any internal phase between the two geophones can be eliminated.

Recording Device

The records of wave arrivals at different receivers are easily recorded on magnetic tape. These measurements are thus performed in real time; that is, in the time domain. By means of the fast-Fourier-transform algorithm which is readily available, the results can then be converted to the frequency domain, and the data can be reduced to develop the R-wave dispersion curve.

A more convenient device for spectral analysis of surface waves is a Fourier Spectral Analyzer. A Fourier analyzer is a digital oscilloscope that by means of a microprocessor attached to it has the ability to perform directly in either the time or frequency domain. Fourier analysis is a powerful tool in decomposition of complicated transient waveforms into a group of simple harmonic waveforms. An in-depth review of Fourier transform and spectral analysis is presented in Appendix B, which is taken directly from Research Report 256-2, by Heisey et al (Ref 1).

The analyzer used in this study is a Hewlett-Packard 5423A structural dynamic analyzer which belongs to the Civil Engineering Department at the University of Texas at Austin. This model is the state-of-the-art in small, portable spectral analyzers today. The HP 5423A, shown in Fig 3.3, consists of three portable components which stack together vertically during operation and are connected by means of appropriate cables. These three units are



1. Oscilloscope and Microprocessor
2. Control Panel
3. Analog-to-Digital Converter

Fig 3.3. Hewlett-Packard 5423A Structural Dynamics Analyzer

- (1) oscilloscope and microprocessor,
- (2) control panel, and
- (3) analog-to-digital converter.

This analyzer is a hardwired, dual-channel analyzer with which two receivers can be recorded simultaneously. Several types of measurements can be performed in both the time and frequency domains. These measurements are extensively discussed in Appendix B.

DETERMINATION OF R-WAVE DISPERSION CURVE

The variation of wave velocity with frequency (wavelength) is known as dispersion. A dispersive wave, in which different wavelengths travel with different speeds, will appear as a train of events in which successive cycles have increasing or decreasing periods in the time domain. A plot of velocity versus wavelength is called a dispersion curve.

As mentioned in Appendix B, the phase information of the cross power spectrum provides the relative phase between the two signals (two-channel recorder) at each frequency in the range of frequencies excited in the experiment. For a travel time equal to the period of the wave, the phase difference is 360 degrees. Thus, for each frequency the travel time between receivers can be calculated by

$$t(f) = T \cdot \phi(f) / 360 \quad (3.3)$$

where

$$f = \text{frequency,}$$

$t(f)$ = travel time for a given frequency,
 $T = 1/f$ = period associated with a certain frequency, and
 $\phi(f)$ = phase difference in degrees of a given frequency.

As frequency is the reciprocal of period, Eq 3.3 can be written as

$$t(f) = \phi(f) / (360f) \quad (3.4)$$

The distance between the geophones, X , is a known parameter. Therefore, R-wave velocity, V_R , is calculated by

$$V_R(f) = X/t(f) \quad (3.5)$$

and the wavelength of the R-wave (L_R) is equal to

$$L_R(f) = V_R(f) / f \quad (3.6)$$

By repeating the procedure outlined by Eqs 3.4 through 3.6 for each frequency, the R-wave velocity corresponding to each wavelength is evaluated, and the dispersion curve is determined.

Rayleigh wave velocities determined by this method are not actual velocities of the layers but are apparent R-wave velocities. Existence of a layer with very high or very low velocity at the surface of the medium affects measurement of the velocities of the underlying layers. In the next section a method for evaluating of actual R-wave velocities from apparent R-wave velocities is presented.

INVERSION OF R-WAVE DISPERSION CURVE

Inversion of the Rayleigh-wave dispersion curve, or (in short) inversion, is the procedure of determination of actual propagation velocities at different depths from the dispersion curve. Inversion consists of determination of the depth of each layer and the actual R-wave velocity of

In a layered medium in which no significant contrast in the velocities of the layers exists, the apparent and actual R-wave velocities are approximately equal. But, if one or more layers have significantly different properties, apparent and actual R-wave velocities will be substantially different. This is especially true in a pavement system in which the stiffness of the materials can differ greatly. For example, in the case of a concrete pavement system consisting of layers of concrete, base, subbase and natural soil, the elastic properties of the concrete are typically several times higher than those of other materials. For this system, the apparent velocities of these underlying layers are falsely high. Conversely, at a soil site where there may be significant seasonal precipitation, the first few feet of the ground is softer in the wet season, and the apparent velocities of the underlying layers are too low.

To demonstrate this effect, the dispersion curves for an asphaltic concrete pavement (ACP) section and a continuously reinforced concrete pavement (CRCP) section are shown in Fig 3.4. Although the properties of the upper portions of the two pavement systems are different, the natural soils beneath the pavements are presumably the same since the systems are within a few feet of each other. However, the two dispersion curves for the deposits beneath the subgrade do not converge, and the apparent R-wave velocities associated with the natural soil beneath the CRCP section are consistently

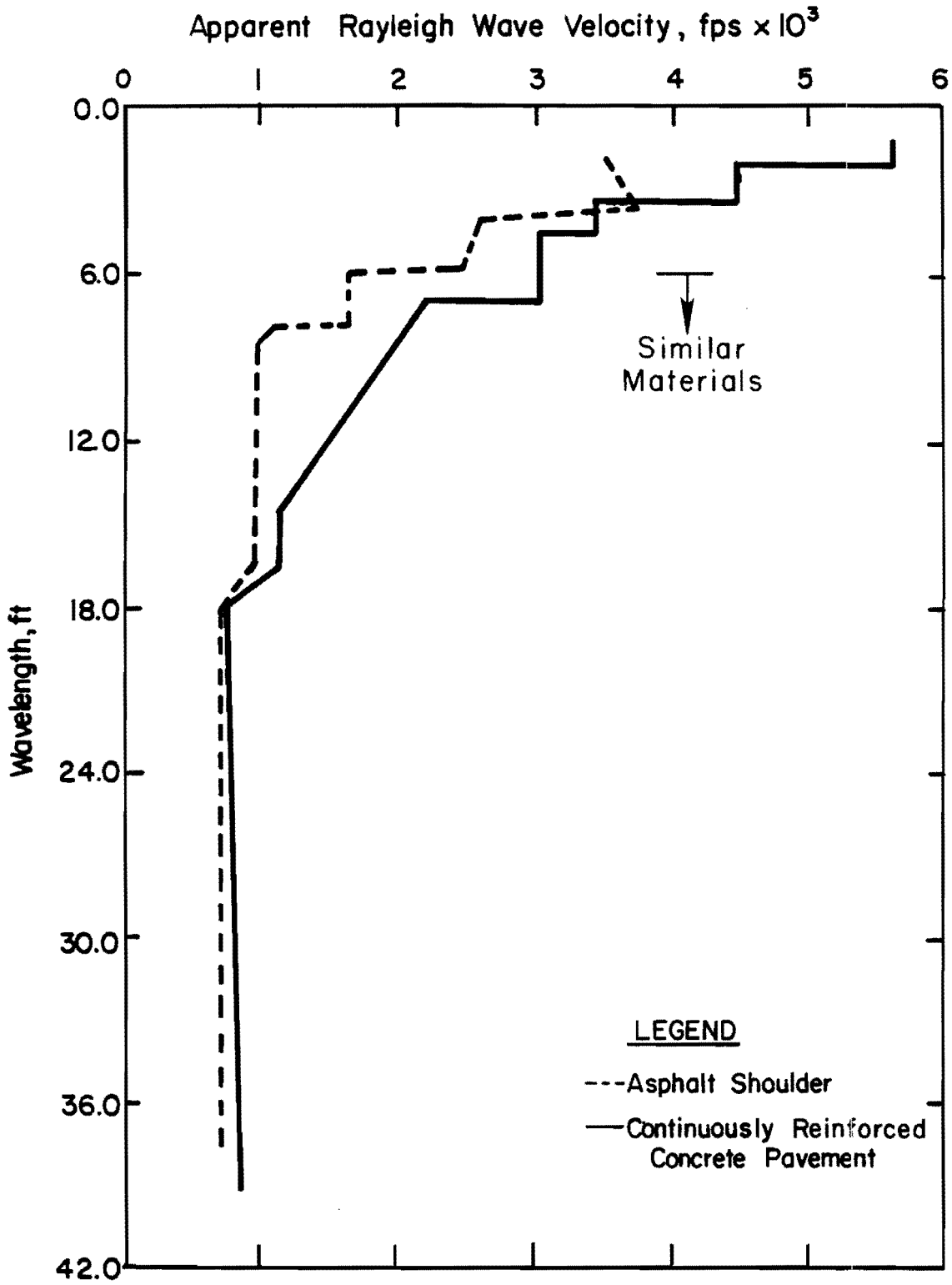


Fig 3.4. Comparison of dispersion curves under ACP and CRCP sections.

higher than those beneath the ACP section at wavelengths greater than about 4 ft. However, as the wavelength increases, this effect seems to become less significant.

In the preliminary investigation of the SASW method, Heisey et al (Ref 1) considered that the effective depth of sampling is equal to one third of a wavelength. In addition, he assumed that apparent and actual R-wave velocities for each wavelength are equal. This crude inversion method is applicable to soil sites with relatively uniform layers with no fine stratification, and Heisey (Ref 3) successfully applied this method to several soil sites.

A refinement in the inversion process has been developed herein. This refinement is based upon Haskell's (Ref 21) matrix for elastic surface waves in a multilayered solid media and is given in Appendix C. To simplify the process of inversion, some additional assumptions were made. These assumptions include:

- (1) the layers are horizontal,
- (2) the velocity of each layer is constant and does not vary with depth,
- (3) the layers are homogeneous and linearly elastic,
- (4) the effective sampling depth is equal to one third of the wavelength, and
- (5) the apparent and actual velocities of the top layer are equal.

From item 4, the depths of all layers are known, and, from item 5, the actual R-wave velocity of the top layer is available. By assuming that the wavefront passes through the overlying layers with the velocities of those layers, the R-wave velocity profile can be constructed from the top to the bottom sequentially.

The theory behind this refinement is presented in Appendix C, due to the complexity and excessive amount of mathematical operations. Because of the simplifying assumptions used, this refined inversion process does not accurately function under certain conditions. The process is not capable of handling

- (1) relatively thin layers (relative to the thickness of the other layers) with considerable variation in the properties of the thin layers and
- (2) layers with variable velocity with depth.

A more elaborate inversion program is under study, and it is hoped that this will be available in the near future.

CHAPTER 4. EXPERIMENT NEAR COLUMBUS, TEXAS

The SASW method was used on three sections with different layerings near Columbus, Texas. These tests are particularly important because, by means of the SASW method, the elastic properties of a continuously reinforced concrete pavement system have been evaluated for the first time.

DESCRIPTION OF SITE

The selected site was located near Columbus, Texas, on State Highway 71 at station 1279+75, about half a mile south of the SH 71 overpass on US 90. Figure 4.1 shows this location. The longitudinal section of SH 71 along which testing was performed is illustrated in more detail in Fig 4.2. The highway consists of two continuously reinforced concrete pavement (CRCP) lanes, each 12 ft wide, a 4-ft-wide asphaltic-concrete pavement (ACP) shoulder, and a median (natural soil).

In August, 1981, a preliminary set of SASW tests was conducted on all the three sections (CRCP, ACP, and median) by S. Heisey. In March, 1982, a second set of tests was performed at approximately the same location. In conjunction with these tests, a series of crosshole seismic tests was performed under the ACP shoulder and median. Unfortunately, due to lack of appropriate drilling equipment, no crosshole tests could be conducted under the concrete section. As there were no crosshole test results available on the CRCP section, a third set of SASW tests was performed on this section in May, 1982, to study the reproducibility of the results.

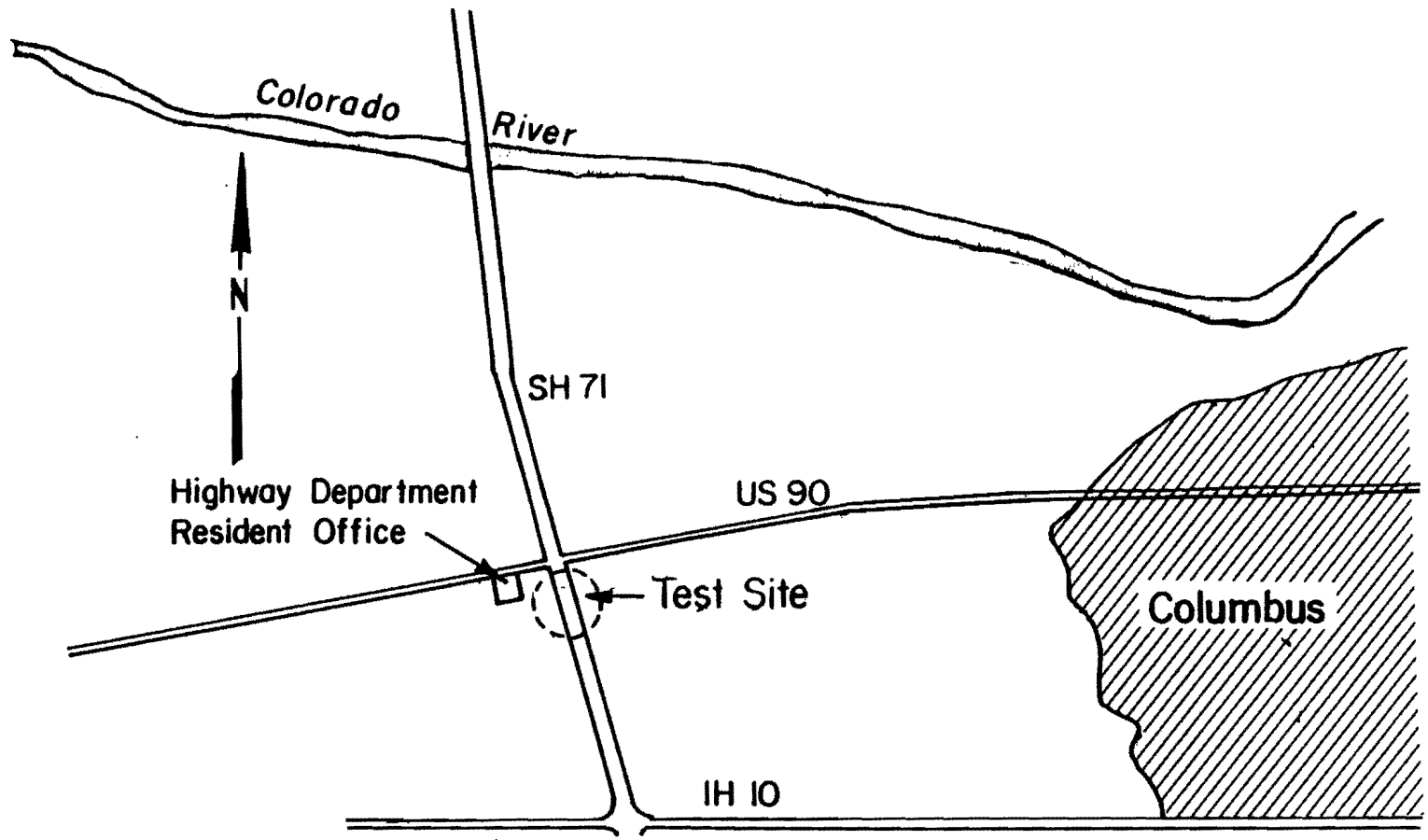


Fig 4.1. Location of test site near Columbus, Texas.

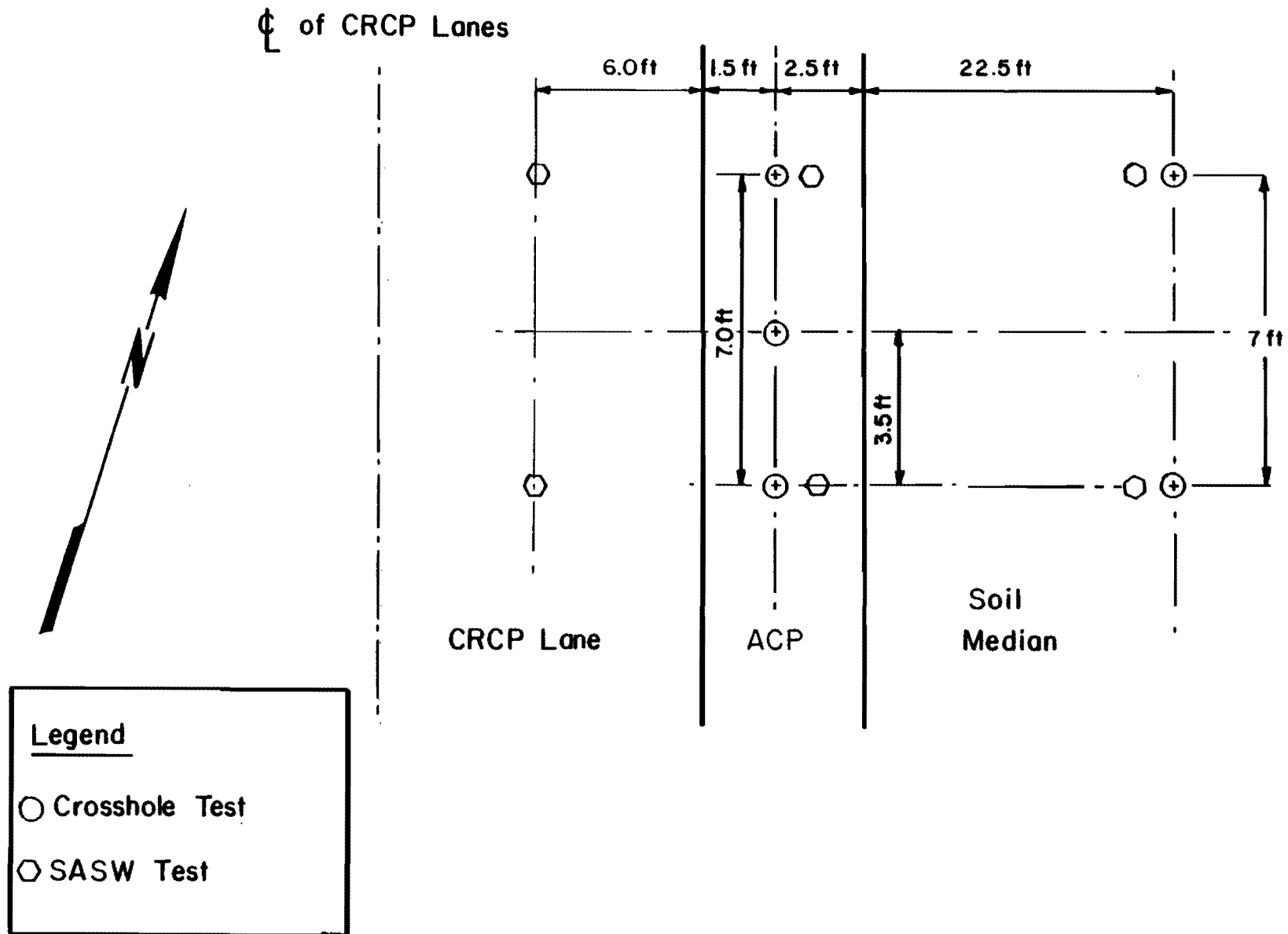


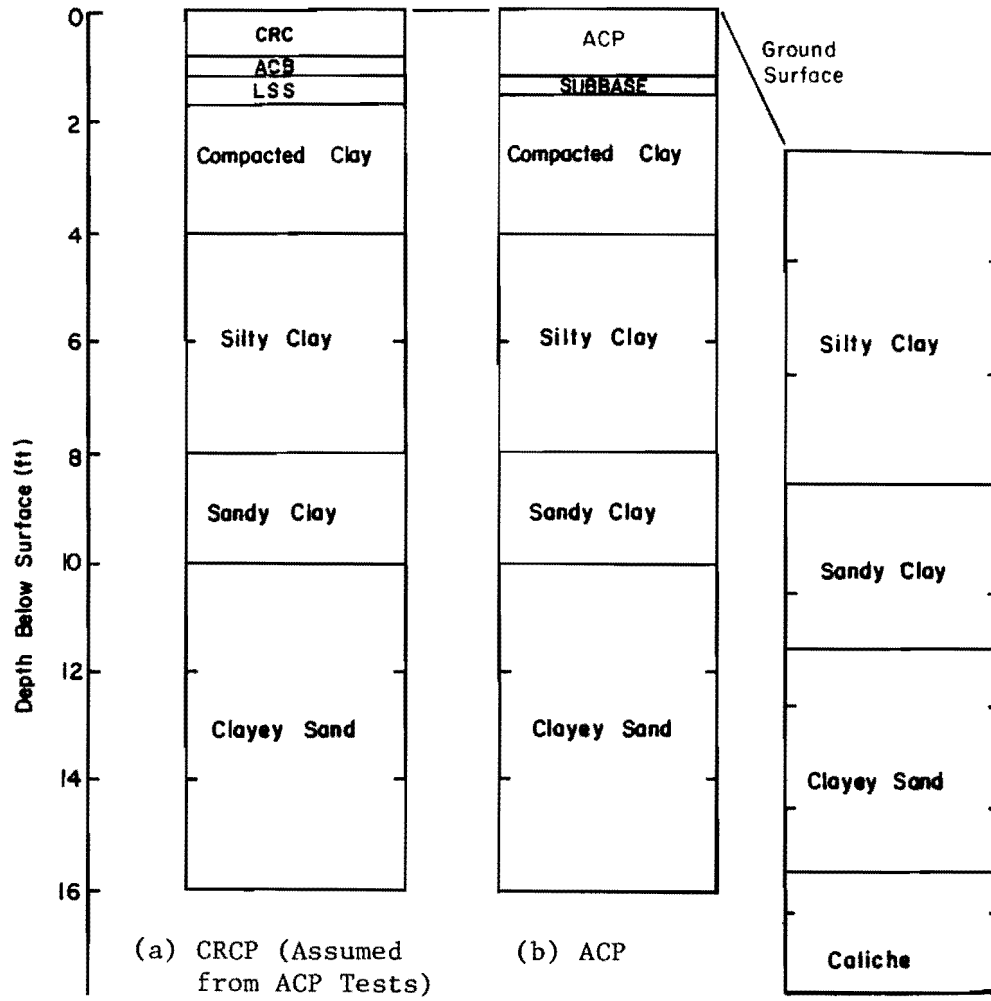
Fig 4.2. Plane view of testing locations.

The soil profiles under the asphalt shoulder and median determined from the boreholes drilled for the crosshole tests are shown in Fig 4.3. It is assumed that the soil profiles under the CRCP and ACP sections are identical below the subbase. The assumed profile for the CRCP section is also shown in Fig 4.3.

SET-UP AND PROCEDURE

The general configuration of the source, receivers, and recording equipment is shown in Fig 4.4. Vertical geophones with a natural frequency of about 8 Hz were used as receivers. The distance between the two geophones was doubled in each test about an imaginary centerline (CRMP method) as shown in Fig 4.5. The distance between geophones ranged from 1 ft to 16 ft. The distance between the source and near receiver was always equal to the distance between the two geophones. In addition, the location of the source relative to the geophones was reversed for each test (i.e., the location of the source was changed without changing the position of the geophones so that the far receiver in the first test functioned as the near receiver in the second test).

The pattern of SASW testing on each section is illustrated in Fig 4.5. The closer spacings are appropriate for determining the properties of the shallower depths and the larger spacings for deeper layers. This set up is representative of the CRMP geometry. However, a common source geometry was used in August, 1981, as shown in Fig 4.6.



CRC = Continuously Reinforced Concrete
 ACB = Asphaltic-Concrete Base
 LSS = Lime-stabilized Subbase
 ACP = Asphaltic-Concrete Pavement

Fig 4.3. Soil profiles under different test sections.

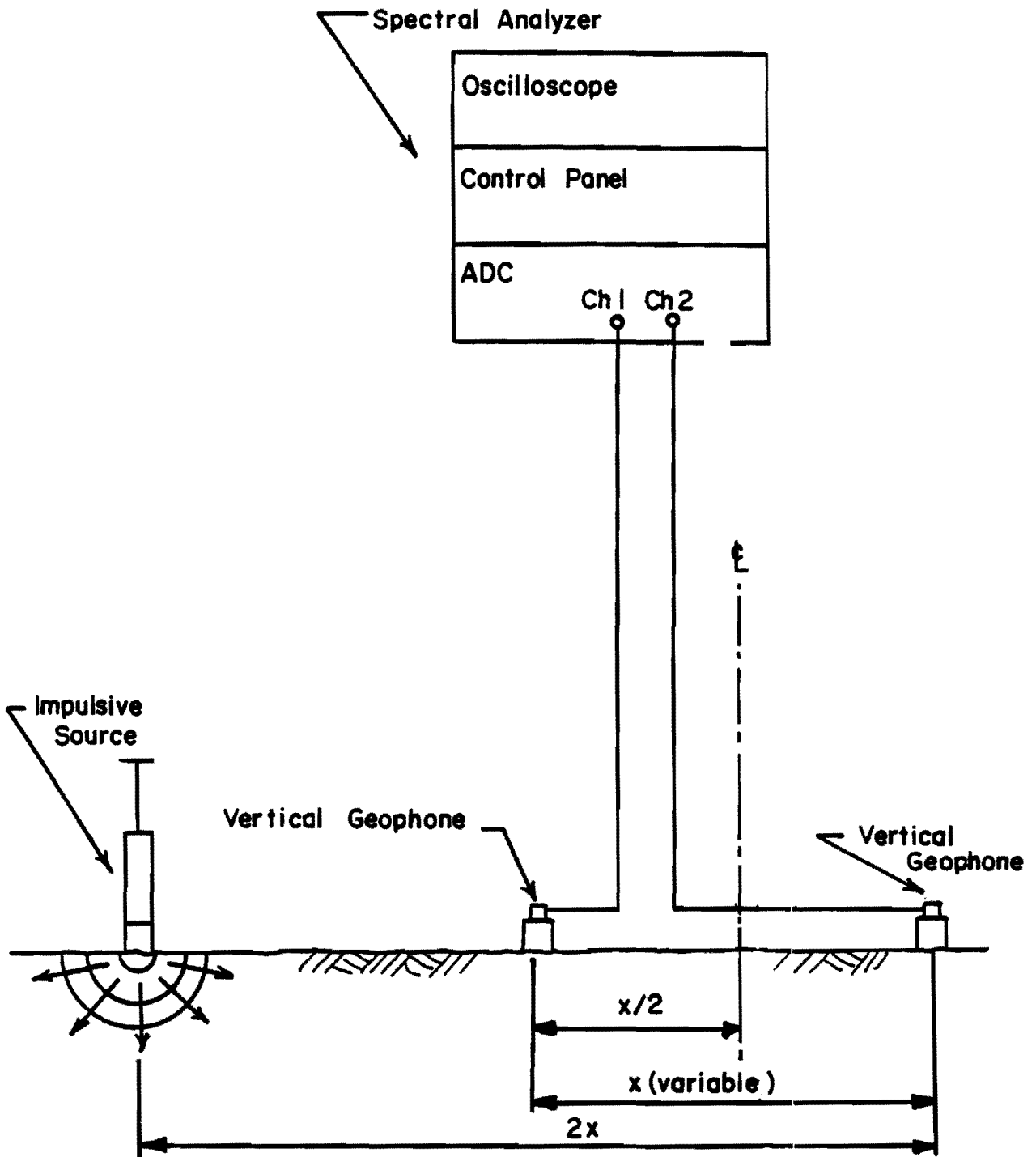
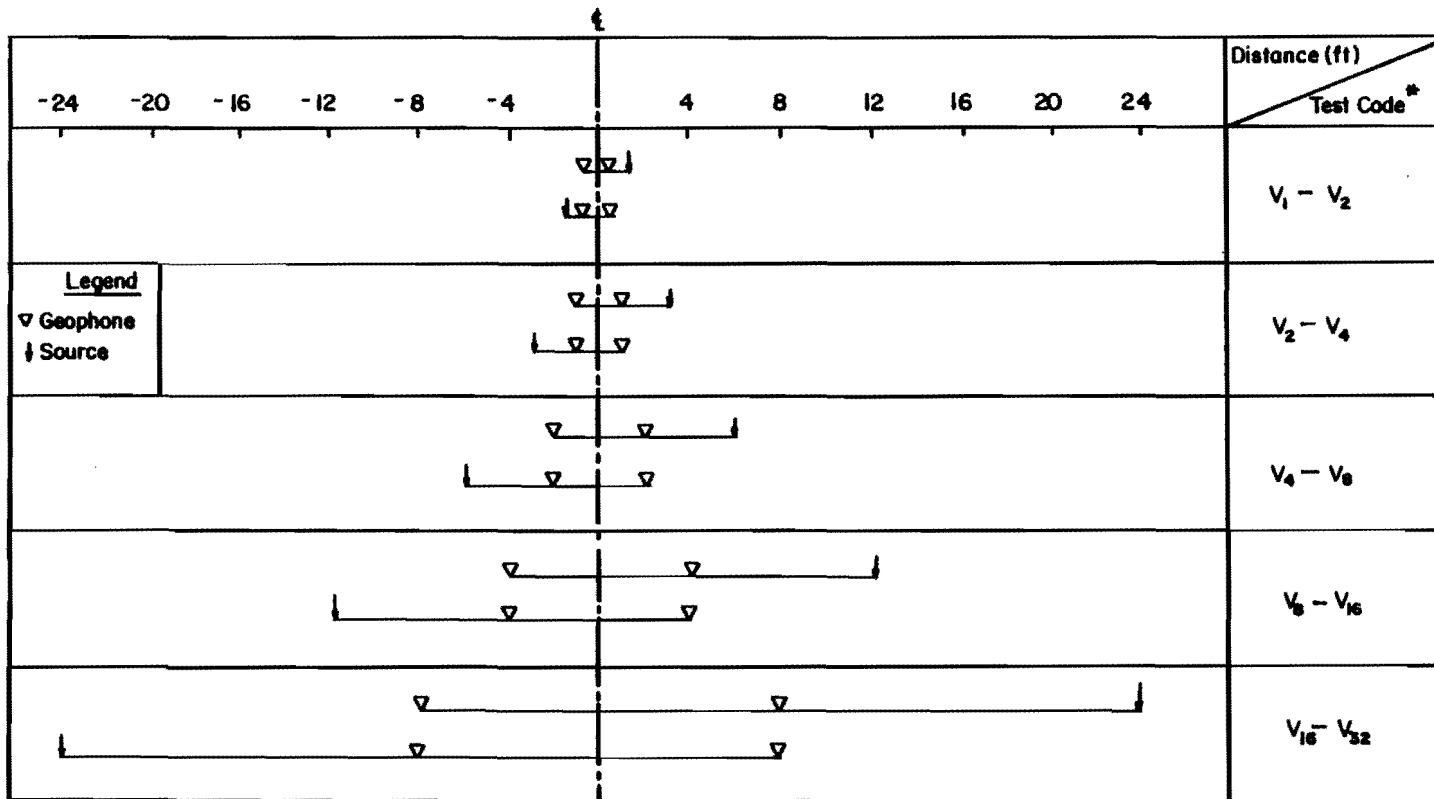


Fig 4.4. Schematic of experimental arrangement for the SASW tests.



* $V_n - V_m$ means that the distance between the source and near vertical geophone is equal to n and the distance between the source and far vertical geophone is equal to m.

Fig 4.5. Pattern of the SASW tests used in March and May, 1982.

		Distance(ft)	Test Code *
		32 28 24 20 16 12 8 4 0	
			$V_1 - V_2$
			$V_2 - V_4$
Legend ▽ Geophone ↓ Source			$V_4 - V_2$
			$V_6 - V_8$
			$V_{16} - V_{32}$

* See Fig 4.5

Fig 4.6. Pattern of the SASW tests used in August, 1981.

CHAPTER 5. PRESENTATION OF RESULTS

Two different methods of wave propagation testing were used at the Columbus site: crosshole seismic tests and spectral-analysis-of-surface waves tests. Shear wave velocities and elastic properties determined from the two methods are presented in the following sections.

CROSSHOLE SEISMIC TEST

The crosshole testing method is briefly reviewed in an earlier section (see Fig 2.5). This method has been under study by Hoar (Ref 4) for many years, and several experiments on different sites have proven the versatility and precision of this method.

Crosshole tests were performed under the median and the asphalt shoulder in March, 1982. The exact procedure used is discussed in Appendix D.

Soil Section (Median)

The location of the crosshole tests in the median is shown in Fig 4.2. Testing was performed to a depth of 15 ft at 2.5-ft intervals. A center-to-center spacing between the boreholes of about 7 ft was used. At each measurement depth, shear and compression wave velocities were determined. By means of Eq 2.10, Poisson's ratio at each depth was then determined. Values of Poisson's ratio evaluated by this method are at low-strain levels and are consistently less than Values of S- and P-wave velocities and Poisson's ratio at the different depths are presented in Table 5.1 and Fig 5.1.

TABLE 5.1. PROPERTIES OF THE MEDIAN FROM CROSSHOLE TESTS

Depth (ft)	S-Wave Velocity (fps)	P-Wave Velocity (fps)	Poisson's Ratio
(1)	(2)	(3)	(4)
2.5	660	820	0.27
5.0	820	1520	0.38
7.5	930	1910	0.33
10.0	1080	1430	0.26
12.5	1070	1540	0.27
15.0	1020	1550	0.30

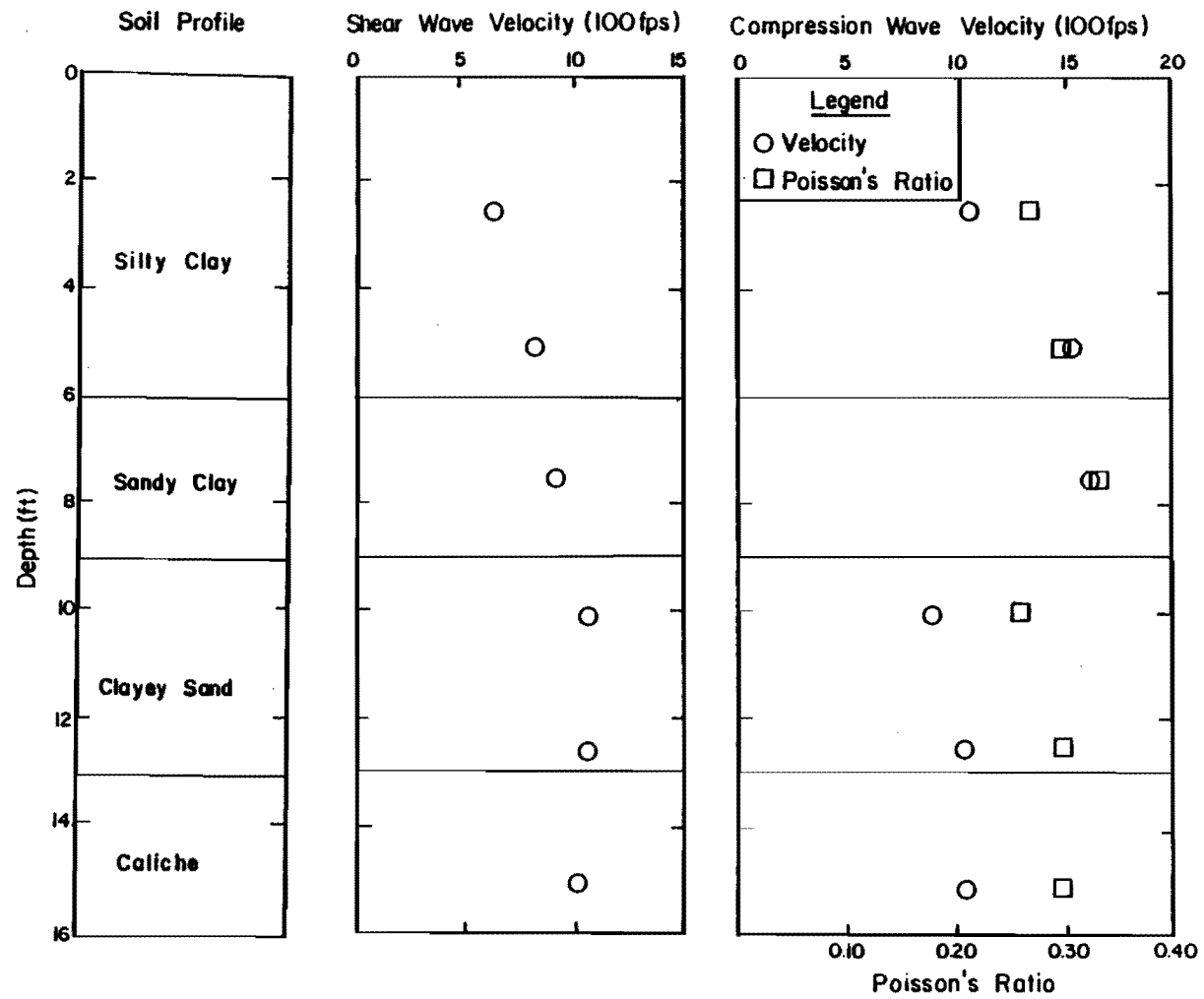


Fig 5.1. Composite profile of median.

Asphalt (ACP) Section

Two series of tests were performed on this section (see Fig 4.2). The distance between the boreholes in the first series was approximately 3.5 ft. This close spacing was used in an attempt to eliminate or minimize undesirable reflected and refracted ray paths in the high-velocity layers at the top of the section (i.e., asphalt layer and subbase). The S- and P-wave velocities were measured at depths of 7 inches (asphalt layer); 16.5 and 20 inches (subbase); 30 and 40 inches (fill); and 50 inches, 5 ft and 7.5 ft (natural soil). Testing was terminated at the depth of 7.5 ft with the 3.5-ft borehole spacing.

In the second set of crosshole tests, the two boreholes were approximately 7 ft apart. This test was extended to the depth of 15 ft. These tests were performed at the same depths as those with the 3.5-ft borehole spacing to a depth of 7.5 ft, and then at 2.5-ft intervals to a depth of 15 ft.

The profiles of P- and S-wave velocities determined from these tests are shown in Fig 5.2 and Table 5.2, along with the resulting profile of Poisson's ratio.

SPECTRAL-ANALYSIS-OF-SURFACE-WAVES METHOD

The primary objective of the tests performed by the SASW method was to evaluate the elastic properties of the different layers of the ACP and CRCP sections. As this method has been used very little on pavement sections, the reproducibility of the results by different operators and for different attempts was of concern. Therefore, the first series of tests was conducted by S. Heisey in August, 1981, and the next two series were performed by the

TABLE 5.2. PROPERTIES OF THE ACP SECTION FROM CROSSHOLE TESTS

Depth (ft)	S-Wave Velocity (fps)		P-Wave Velocity (fps)		Poisson's Ratio	
	Borehole Spacing (ft)		Borehole Spacing (ft)		Borehole Spacing (ft)	
	3.5	7.0	3.5	7.0	3.5	7.0
(1)	(2)	(3)	(4)	(5)	(6)	(7)
0.58	2630	2960	3910	3960	0.07	0.07
1.38	1590	-	-	-	-	-
1.68	1530	1690	2510	-	0.20	-
2.50	970	1400*	1130	1830*	0.16	0.21*
3.33	790	1030*	1430	1550	0.18	0.21*
5.0	830	870	1490	1470	0.27	0.23
7.5	1000	980	1910	1930	0.27	0.28
10.0	-	1010	-	1820	-	0.28
12.5	-	1010	-	1780	-	0.27
15.0	-	1030	-	1870	-	0.28

* Probably involved refracted waves.

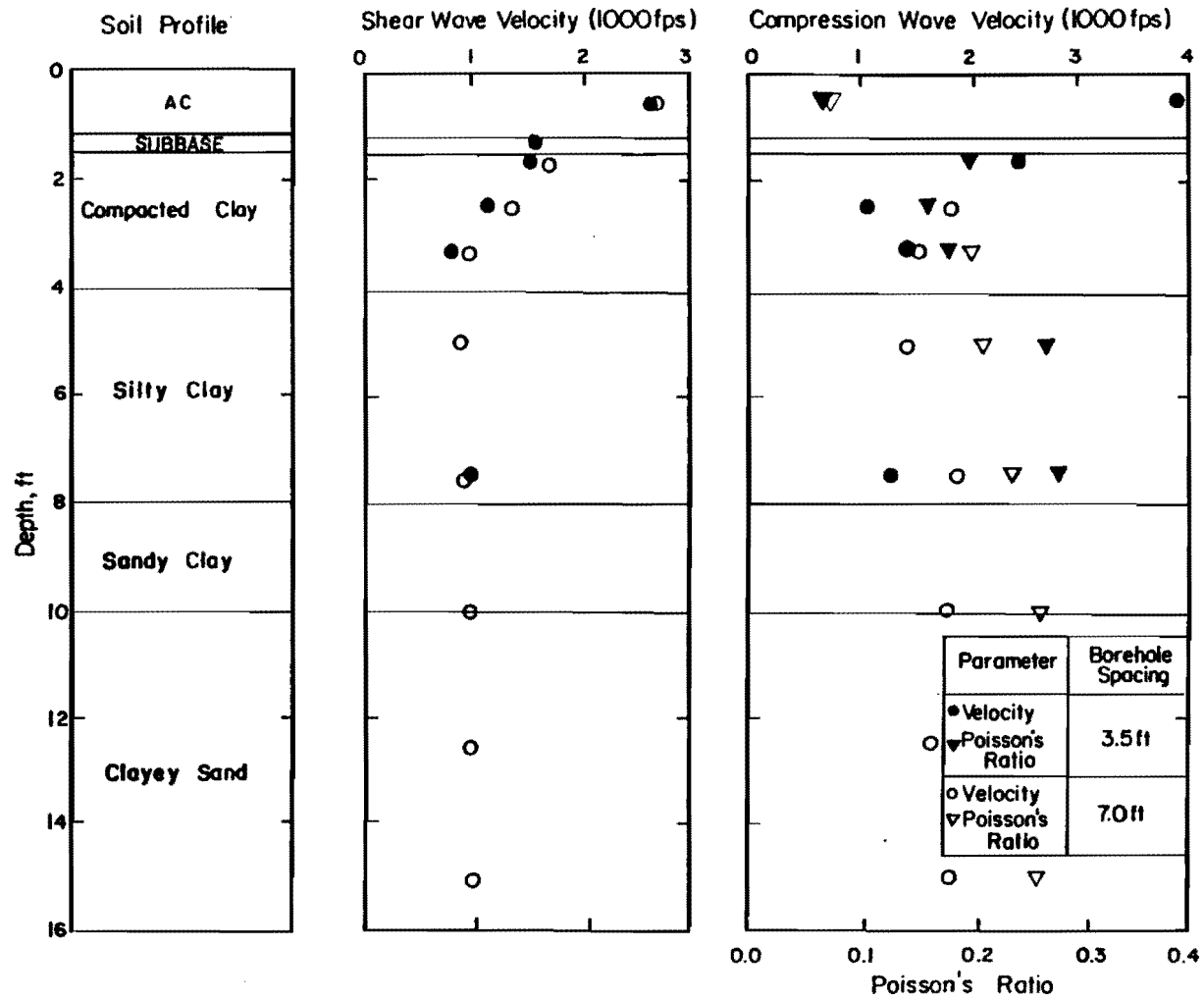


Fig 5.2. Composite profile of ACP section.

authors. In addition, the SASW test was tried for the first time on a concrete pavement.

Soil Section (Median)

The dispersion curves for tests performed at this site in August, 1981, are shown in Fig 5.3. could be due to lateral inhomogeneity of soil properties. At low frequencies, scatter could also be due to the insensitivity of the receivers at these low frequencies. Overall, the maximum scatter is less than 15 percent.

The tests performed in August, 1981, were done using the common source geometry method. The pattern of common source geometry used in this series of tests is demonstrated in Fig 4.6. It is assumed that the dispersion curve is representative of the average soil properties of the area located between the two receivers. As there is no overlap between the area covered by the geophones in different tests, each dispersion curve corresponds to a different location in CSR geometry (although these locations are very close to one another) which can contribute to the scatter as shown in Appendix A.

In Fig 5.4 the dispersion curves for different tests in March, 1982, are presented. Scatter in the data is less in these tests, probably because the CRMP geometry was used. As mentioned before, this set-up has the advantage of averaging the effect of lateral inhomogeneity in the soil profile. In addition, as the spacing between the geophones becomes larger, the area covered by the earlier test is always included in the present test. Thus the precision of the tests in the CRMP geometry is relatively improved (relative to CSR set-up). In the March tests, the sampling depth was also extended to shallower depths by exciting higher frequencies.

The average dispersion curves for the tests performed in August, 1981, and March, 1982, are shown in Fig 5.5. Upon comparing these curves, it can

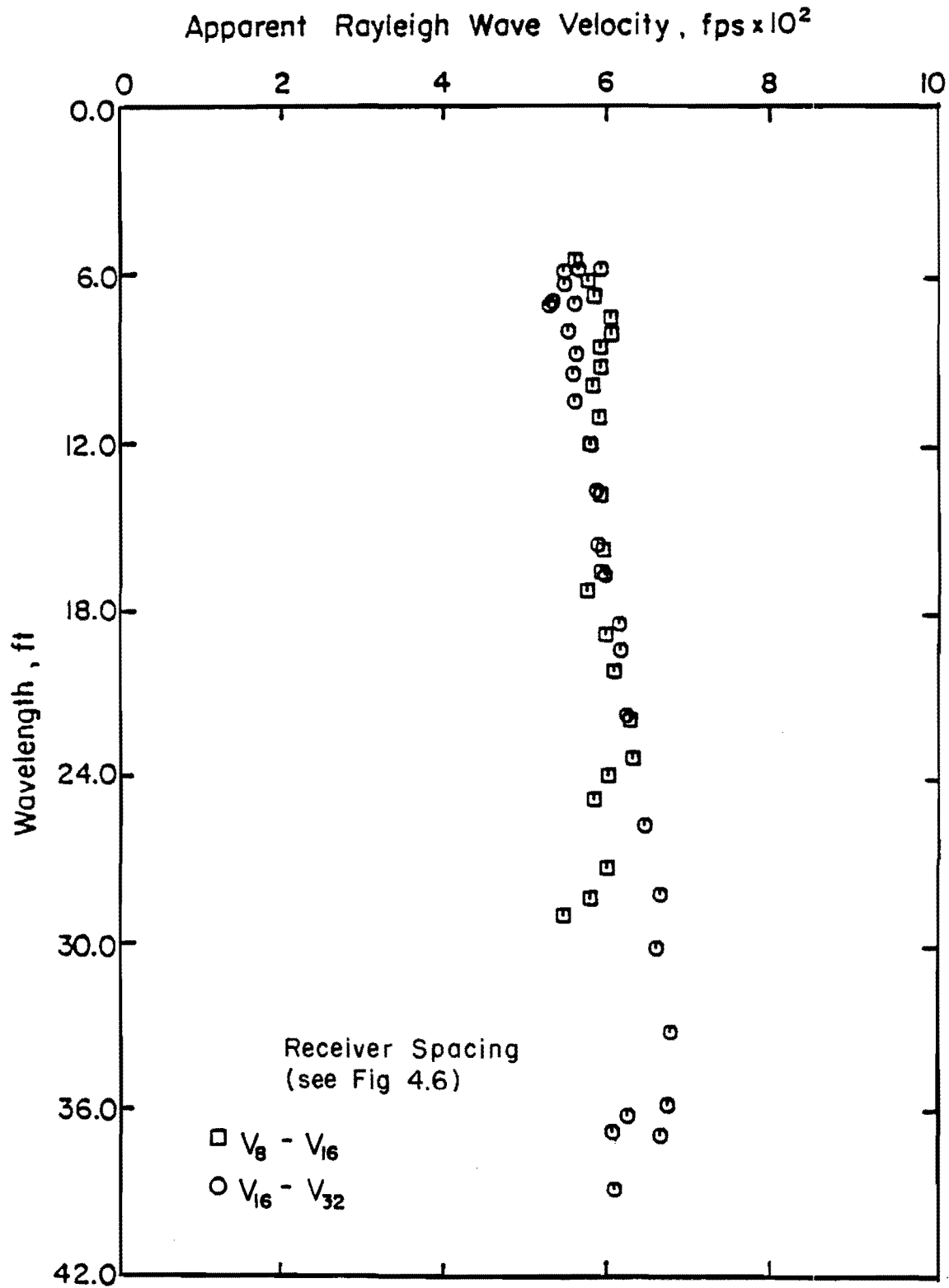


Fig 5.3. Dispersion curves for median from SASW tests performed in August, 1981, using common source geometry.

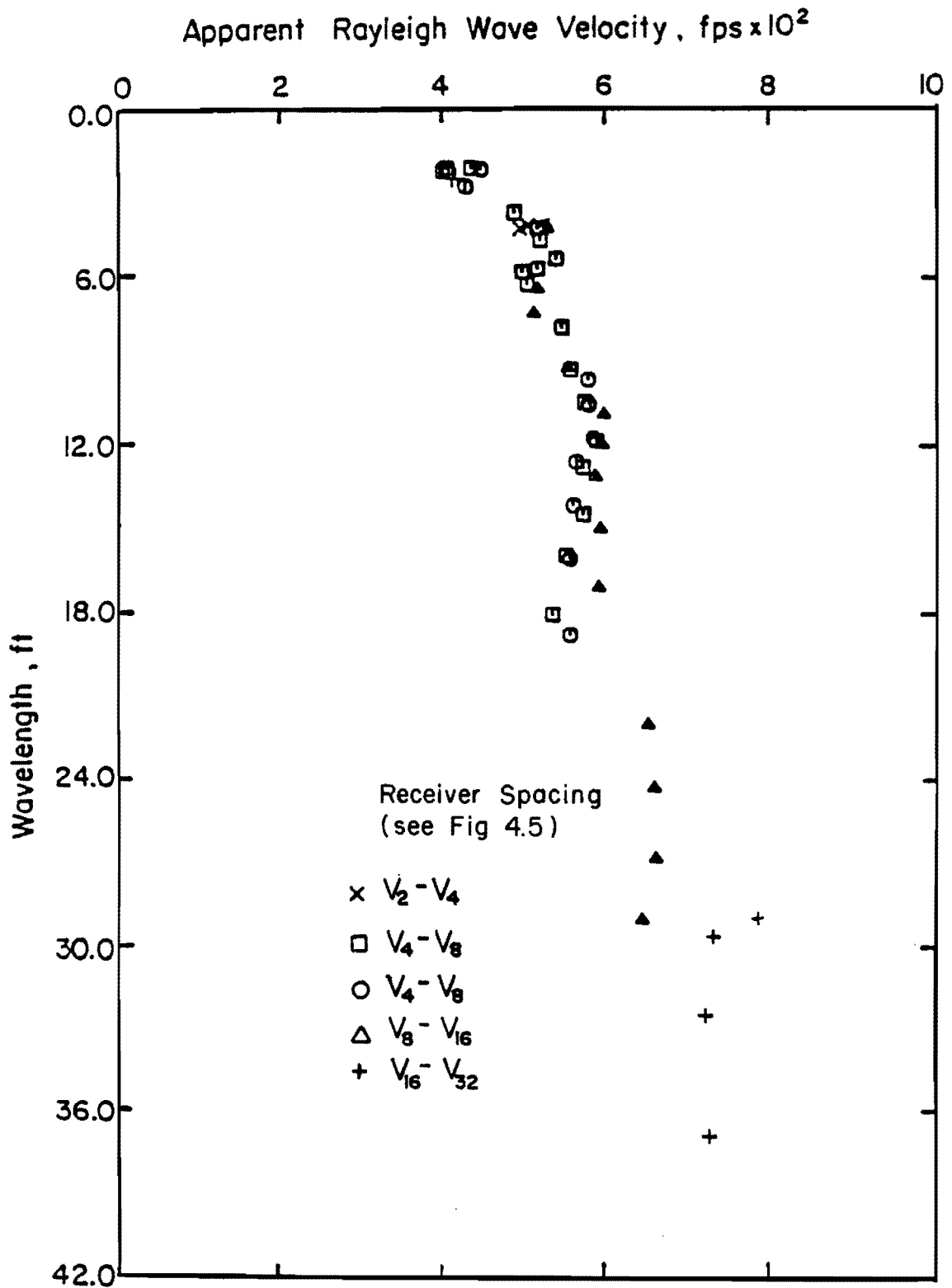


Fig 5.4. Dispersion curves for median from SASW tests performed in March, 1982, using common receivers midpoint geometry.

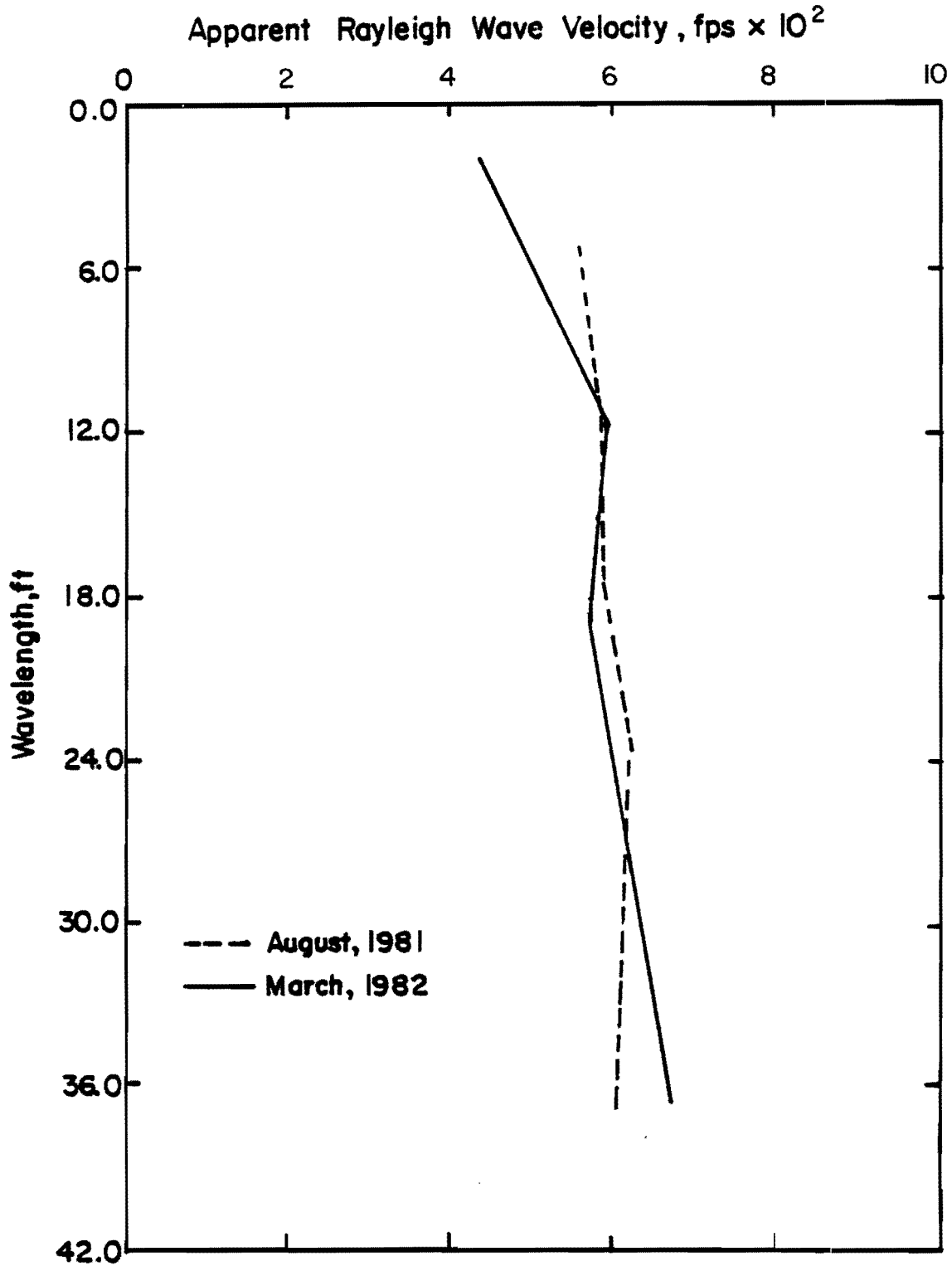


Fig 5.5. Average dispersion curves for median from SASW tests performed in August, 1981, and March, 1982.

be seen that there is no major difference in the results for wavelengths longer than 10 ft, with a maximum difference of 8 percent at a wavelength of about 36 ft. Determination of the average dispersion curve for the data from August, 1981, was difficult because of scatter in the data. Due to extensive precipitation on the day before the tests were performed, in March, 1982, the first few feet of the median was very soft, causing a significant drop in the elastic properties of the near-surface material. Thus, R-wave velocities of the near-surface layer are low, as shown in Fig 5.4.

It should be mentioned that all of the dispersion curves were filtered according to the criteria presented by Eq 3.2.

Asphalt (ACP) Section

In the first attempt on the asphalt section in 1981, only two sets of data were gathered (geophone spacings of 2 ft and 8 ft) due to a malfunction of the equipment. These results are shown in Fig 5.6.

The dispersion curves for the experiments conducted on this section in March, 1982, are shown in Fig 5.7. The thicknesses and apparent R-wave velocities for different layers from the 1981 and 1982 tests are in good agreement, and no significant differences can be detected in the average dispersion curves from these attempts, as shown by the average curves presented in Fig 5.8. The relative difference between the two curves does not exceed 6 percent. Adequate high frequencies were not generated in the tests performed in 1981. Therefore, no sampling was made in the asphaltic concrete layer in this series.

Concrete (CRCP) Section

The most critical section studied was the concrete section. Fine layering in the pavement system and a great contrast in the velocities of the

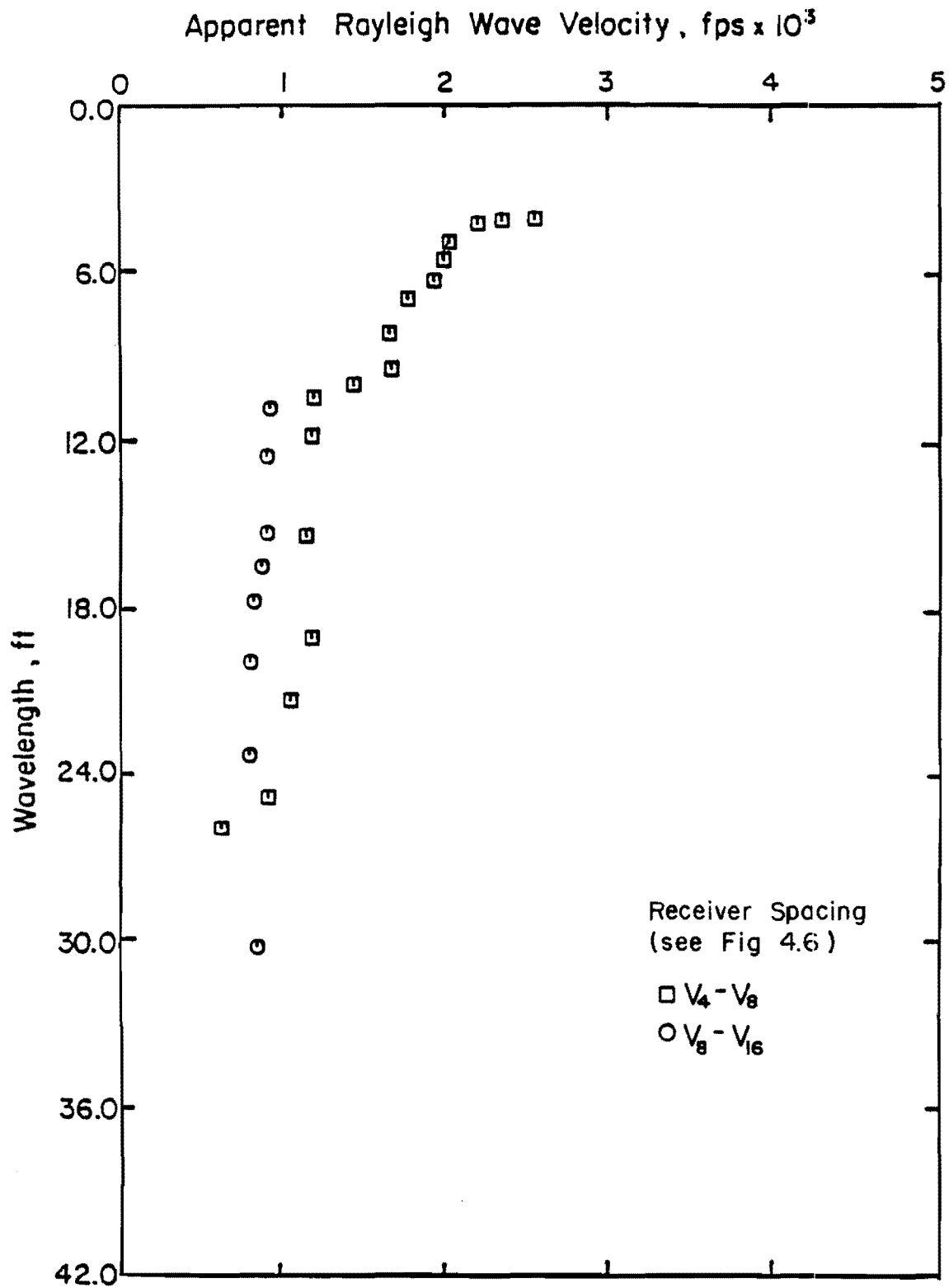


Fig 5.6. Dispersion curves for ACP section from SASW tests performed in August, 1981 using common source geometry.

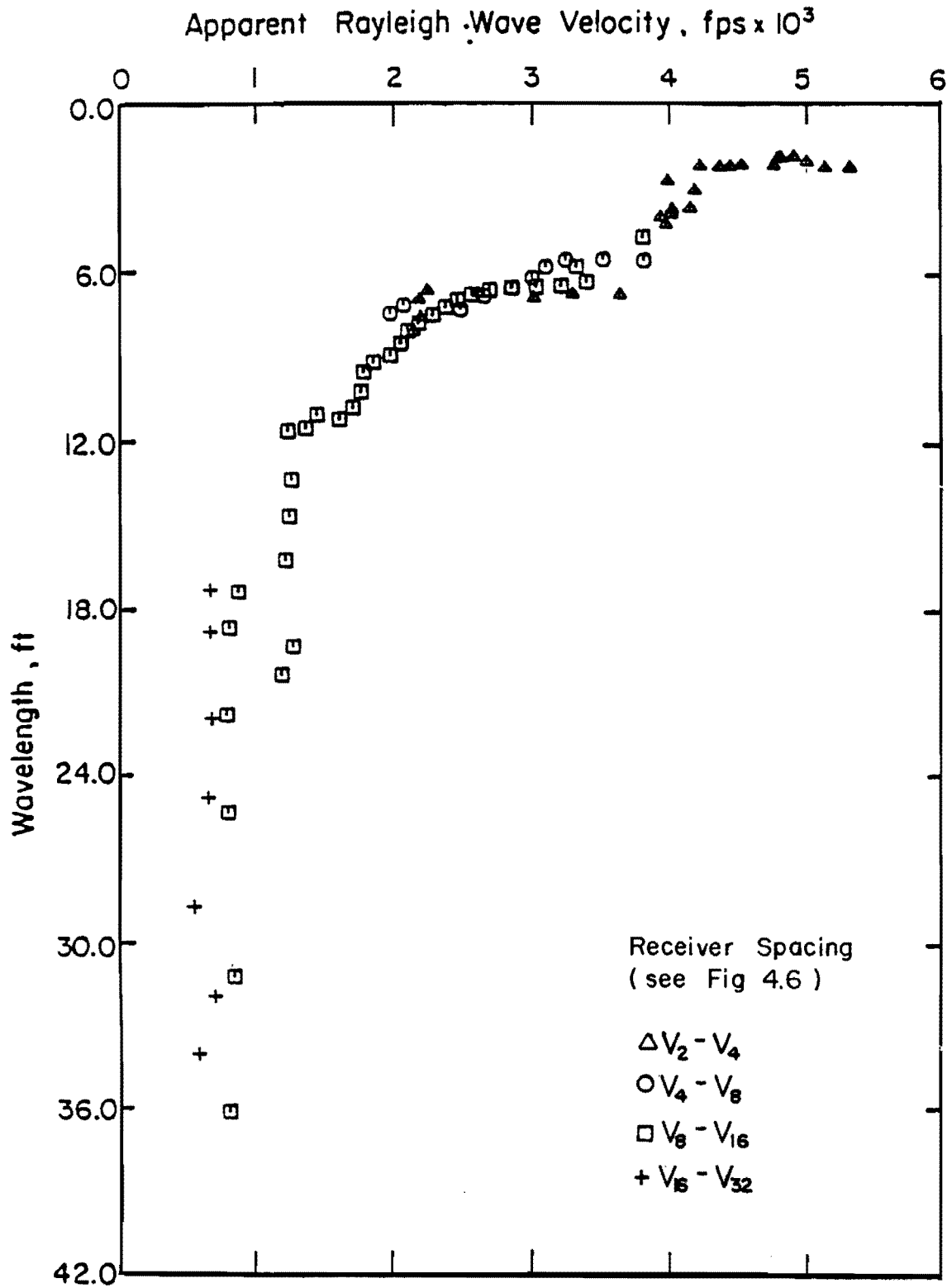


Fig 5.7. Dispersion curves for ACP section from SASW tests performed in March, 1982, using common receivers midpoint geometry.

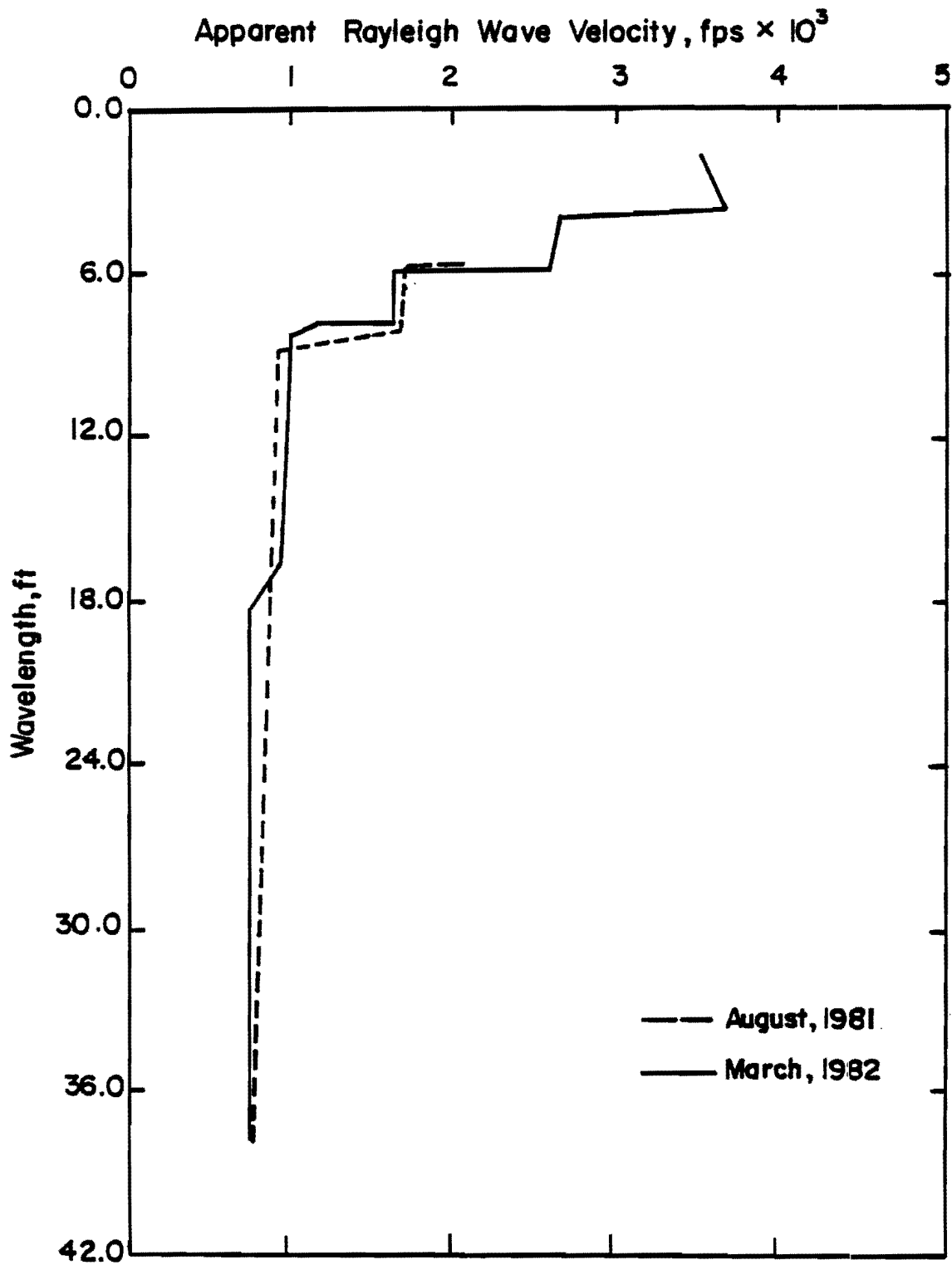


Fig 5.8. Average dispersion curves for ACP section from SASW tests performed in August, 1981, and March, 1982.

layers in a depth of less than 3 ft required special considerations. Use of a source capable of generating high-frequency waves was essential. In addition, good coupling between the concrete and geophones was necessary to monitor correctly the high frequencies.

The dispersion curves for the first attempt on a CRCP section in 1981 are shown in Fig 5.9. As high-frequency waves were not excited, no information on the properties of the concrete and base layers could be obtained. Use of the CRS geometry may have contributed to the scatter in the range of wavelengths equal to 10 ft to 15 ft (corresponding to the fill layer). Dispersion curves of the tests performed in March, 1982, are presented in Fig 5.10. The number of tests performed on this site in this set of tests was less than those of August, 1981, due to time limitations. The two sets of dispersion curves compare closely in layering and R-wave velocities. The shortest wavelength obtained in the second attempt was approximately one ft (equivalent to a sampling depth of 4 in.).

The primary concerns in the May, 1982, testing at the CRCP section were to sample even shallower depths as well as to check the reproducibility of the results. Figure 5.11 shows the dispersion curves from these tests. Several tests with close spacings (spacing between the geophones equal to one ft and two ft) were performed, which resulted in decreasing the minimum in depth of sampling to 3 inches. It should be mentioned that the highest frequency excited in this set was 3900 Hz, whereas in the earlier attempt it was 3100 Hz. The 800-Hz increase in the upper bond of the frequency content of the impact only decreased the depth of sampling by about one inch.

Average dispersion curves obtained from the three attempts on the CRCP section are illustrated in Fig 5.12. Except for the range of wavelengths from 5 to 8 ft, in which there is some scatter, these curves agree with less

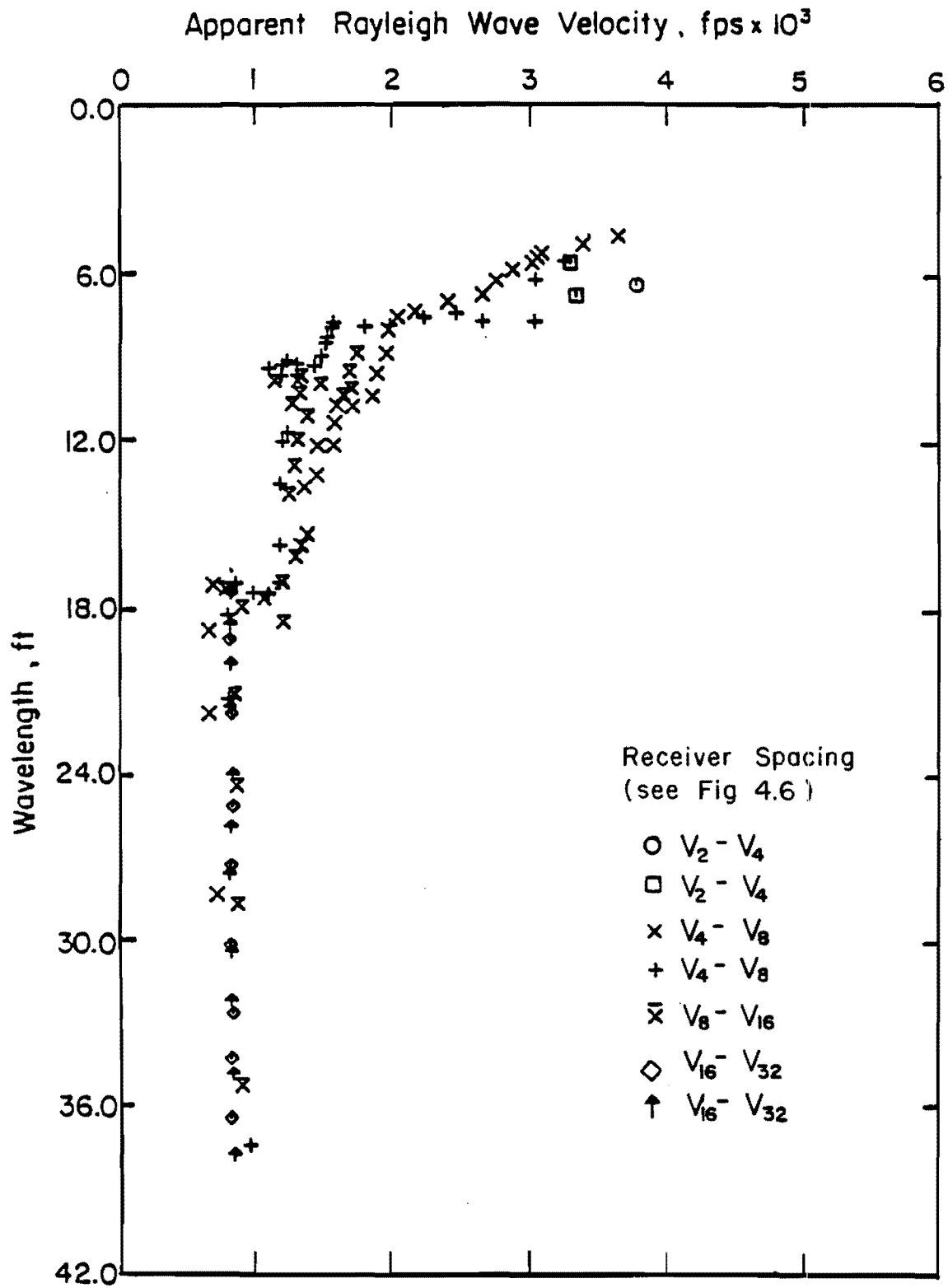


Fig 5.9. Dispersion curves for CRCP section from SASW tests performed in August, 1981, using common source geometry.

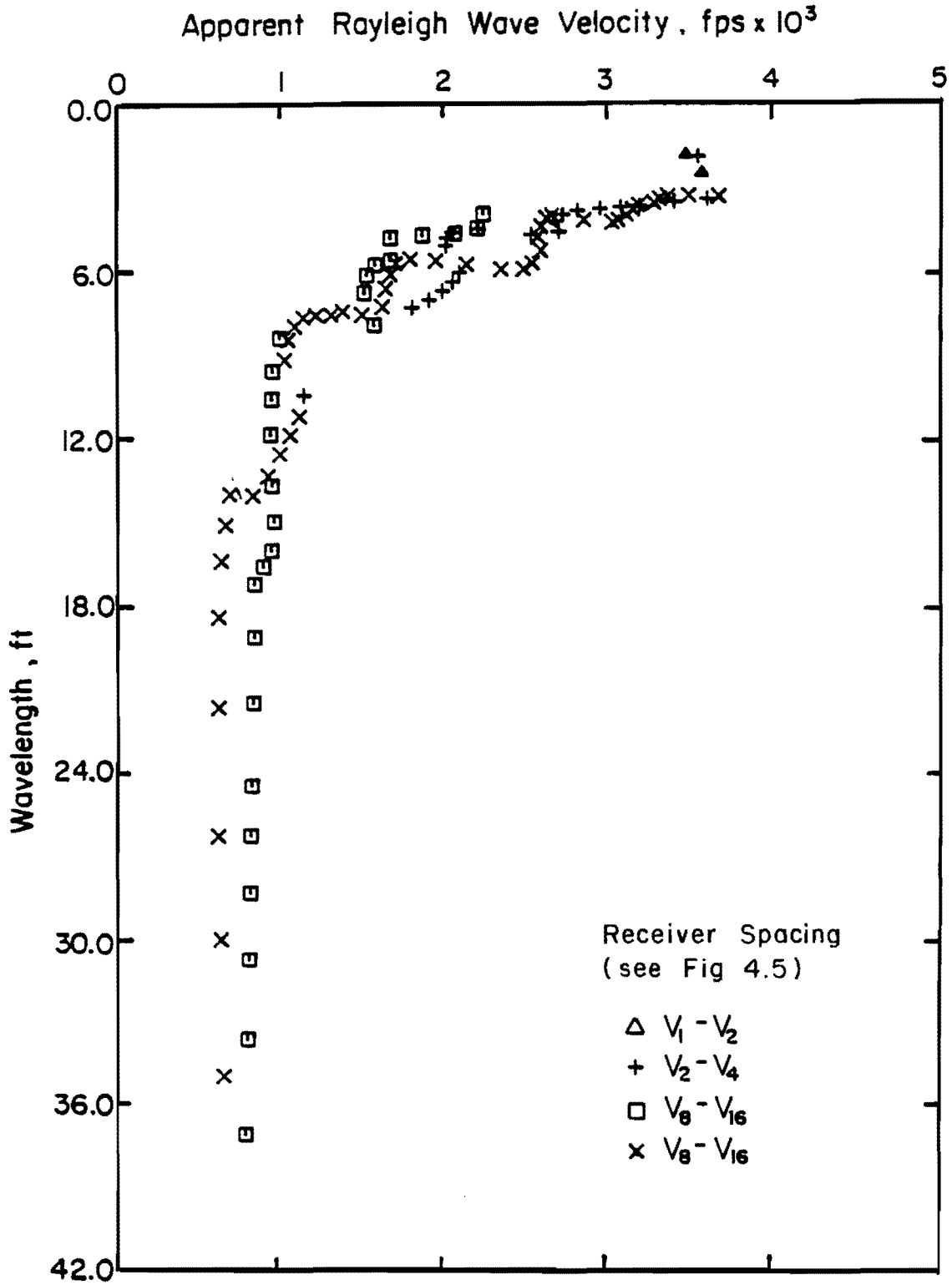


Fig 5.10. Dispersion curves for CRCP sections from SASW tests performed in March, 1982 using common receivers midpoint geometry.

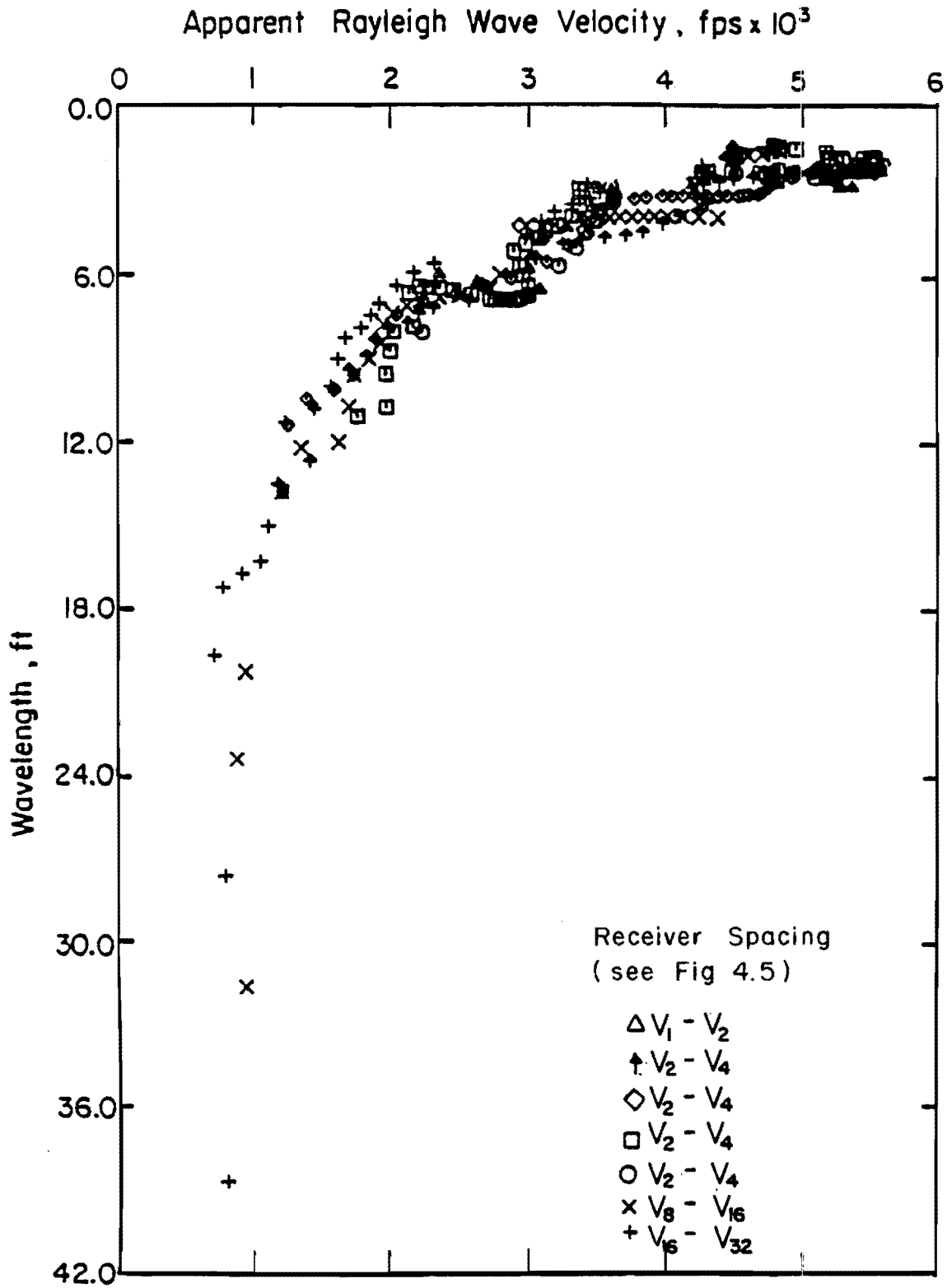


Fig 5.11. Dispersion curves for CRCP section from SASW tests performed in May, 1982, using common receivers midpoint geometry.

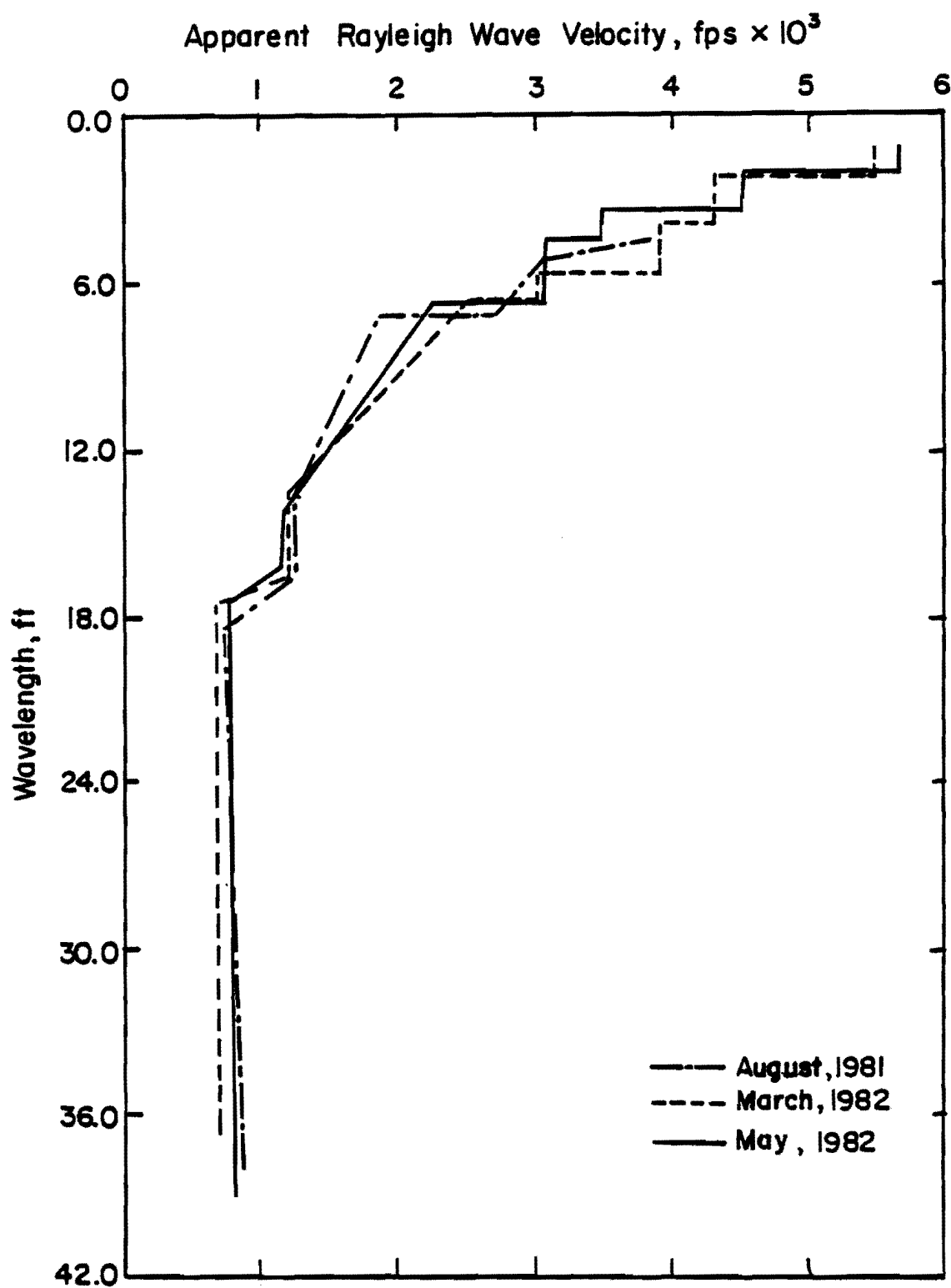


Fig 5.12. Average dispersion curves for CRCP section from SASW tests performed in August, 1981, March, 1982, and May, 1982.

than a 9 percent difference. This deviation that corresponds to the few inches above and below the boundary between the subbase and compacted fill (wavelengths in 5 to 8 ft range) may be due to inaccuracy in leveling the fill before placement of the subbase during construction along the distance covered by the geophones. However, as great emphasis was placed on measurement of the pavement reliable. The reproducibility of the tests is very good, as shown in Fig 5.12.

EVALUATION OF ELASTIC PROPERTIES

The principles of evaluation of the elastic soil properties from Rayleigh wave velocities are discussed earlier. By means of Eqs 2.5 to 2.8, Young's modulus of each layer can be readily determined from the SASW tests. Based upon the average dispersion curves for the median and ACP section from March, 1982 (Figs 5.5 and 5.8), and the average dispersion curve for the CRCP section from May, 1982 (Fig 5.12), R-wave and S-wave velocities at each depth were evaluated. Shear wave velocities determined from the SASW and crosshole seismic tests are compared in Figs 5.13, 5.14 and 5.15 for the median, ACP, and CRCP sections, respectively. These velocities are discussed in the following chapter.

In crosshole tests, Young's moduli were calculated from P-wave velocities measured in situ (Eq 2.5). In the case of the SASW tests, shear moduli were first determined from the shear wave velocities (Eq 2.7). Then, with values of Poisson's ratio evaluated from the crosshole tests (Eq 2.10), Young's moduli were calculated. Once again, it should be mentioned that these Poisson's ratios were lower than those generally found in static tests, because of the stress dependence of Poisson's ratio.

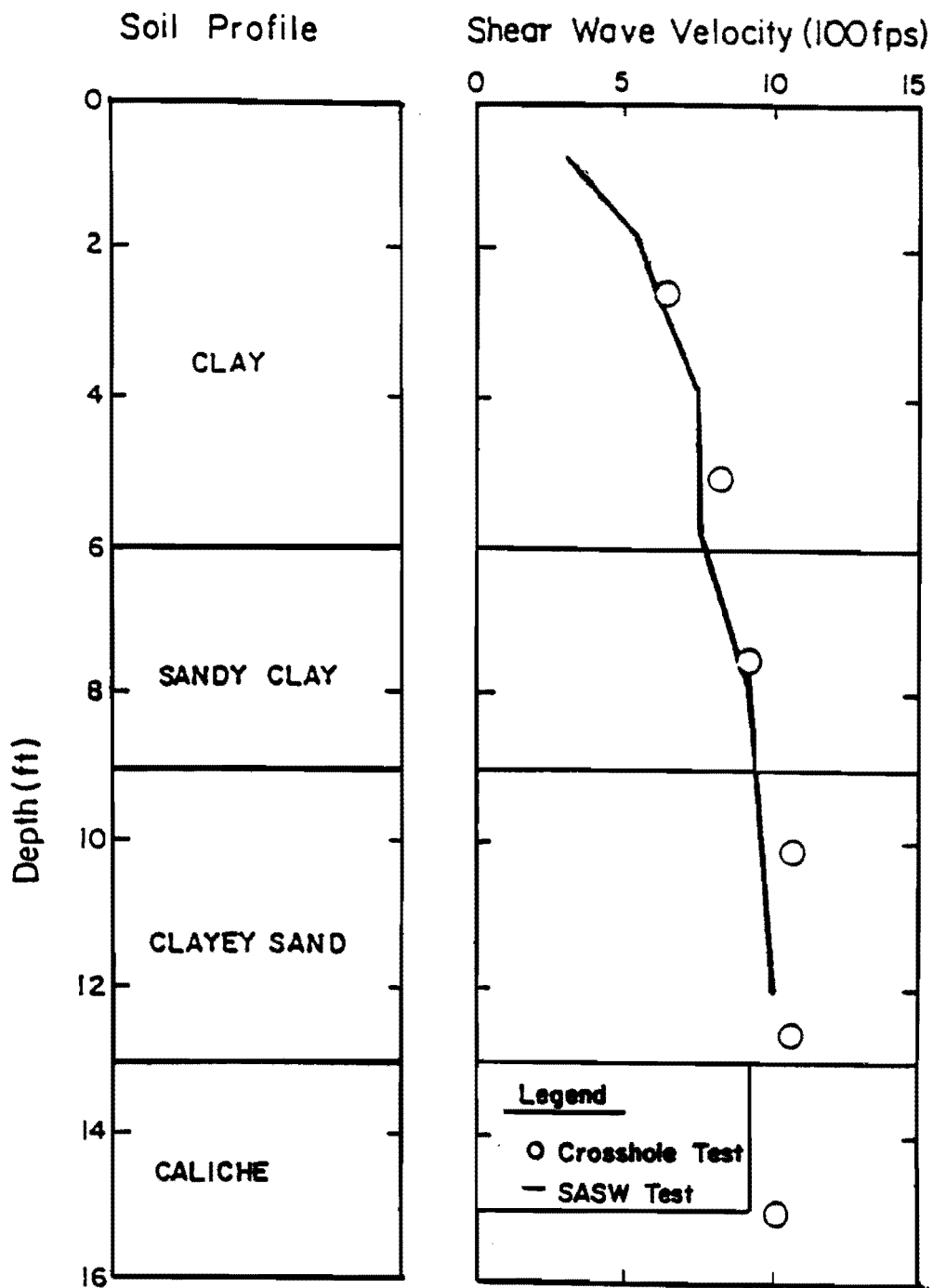


Fig 5.13. Comparison of shear wave velocities determined by crosshole and SASW tests at the median.

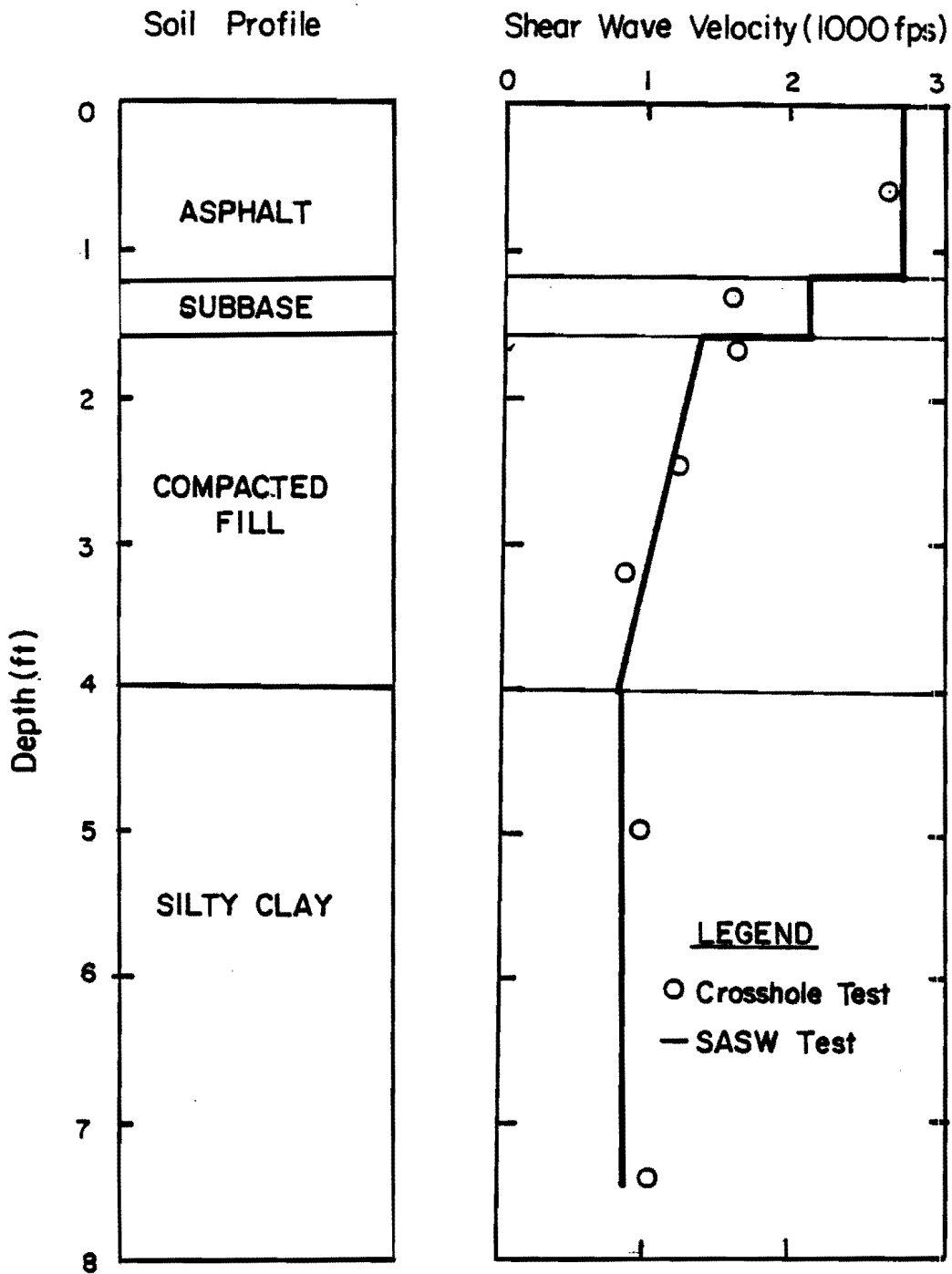


Fig 5.14. Comparison of shear wave velocities determined by crosshole and SASW tests at ACP section.

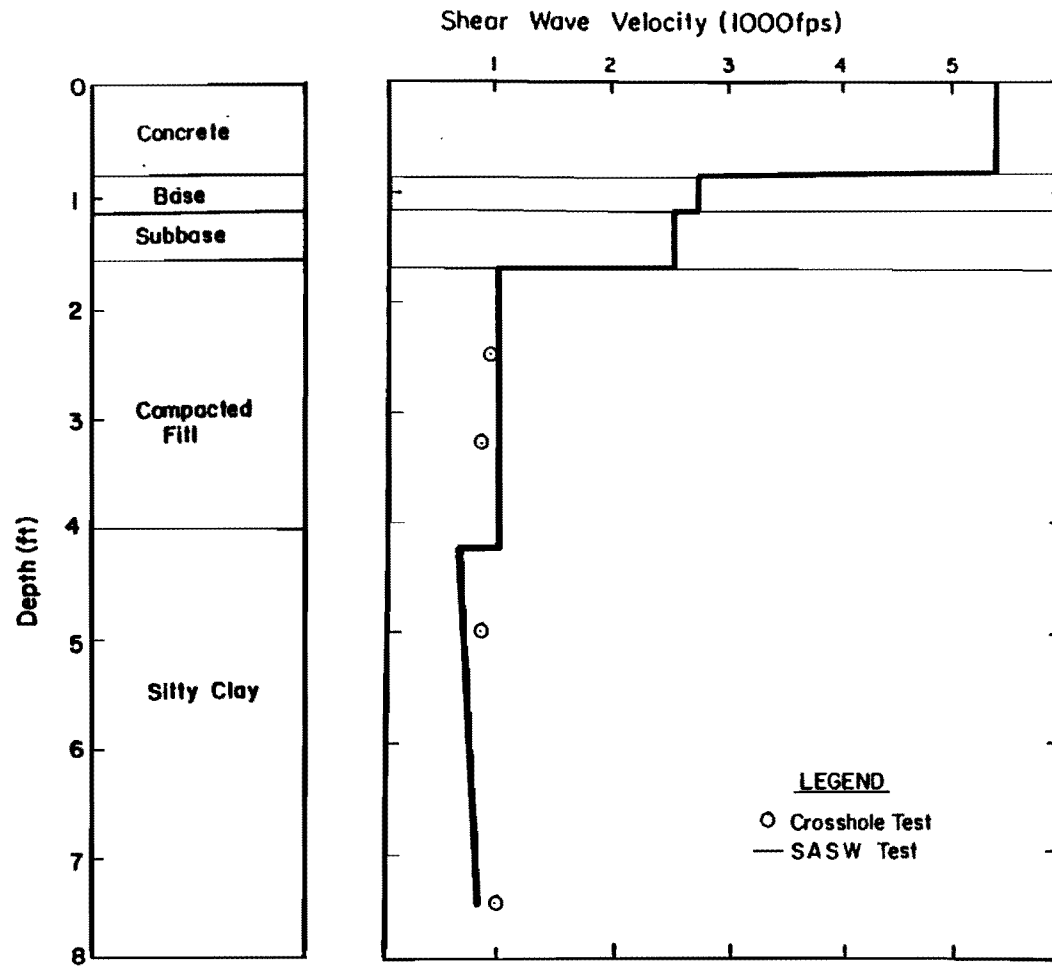


Fig 5.15. Comparison of shear wave velocities determined by SASW tests and assumed from the crosshole tests (performed at the ACP section) at CRCP section.

CHAPTER 6. COMPARISON OF CROSSHOLE SEISMIC AND SASW RESULTS

Plots of S-wave velocity versus depth after application of the inversion technique presented in Appendix C are shown in Figs 5.13 to 5.15 for the three sections tested. Also presented in the same figures are results from the crosshole tests performed at the same locations. The velocities determined by these two methods are in good agreement, especially for the soil site. Deviation of shear wave velocities under the median from these two methods of testing is less than 7 percent, except at a depth of about 5 ft where the difference equals 14.3 percent (Fig 5.13).

As mentioned before, the preliminary inversion method used herein is not able to handle sudden changes in velocity for a thin layer. Thus for the paved sections, there are still some differences between the results determined by the two methods, as shown in Fig 5.14. These are especially evident in the subbase in the ACP section. Ignoring this substantial difference in S-wave velocities from the two types of tests due to the problem just mentioned, the remainder of the profile differs by less than 9 percent for the ACP section (Fig 5.14).

As no crosshole tests could be performed at the CRCP section, it was assumed that the S-wave velocity profile below the pavement system (i.e., below the depth of 5 ft) from a crosshole test performed under the ACP section is also representative of the CRCP section. The two profiles (crosshole and SASW profile) of S-wave velocity agree within 10 percent.

Young's moduli evaluated from the crosshole and SASW tests are shown in Tables 6.1, 6.2 and 6.3, and Figs 6.1, 6.2 and 6.3 for the median, ACP, and

TABLE 6.1. COMPARISON OF YOUNG'S MODULI FROM CROSSHOLE AND SASW TESTS AT MEDIAN

Depth (ft)	Young's Modulus (psi)		Difference $\frac{(3)-(2)}{(3)}$ (percent)
	Crosshole	SASW	
(1)	(2)	(3)	(4)
2.5	10180	11230	+9.3
5.0	33150	25540	-29.8
7.5	34810*	31480	-10.5
10.0	30230	31880	+5.2
12.5	35050	-	-
15.0	35510	-	-

* Evaluated from S-wave velocity.

TABLE 6.2. COMPARISON OF YOUNG'S MODULI FROM CROSSHOLE AND SASW TESTS AT ACP SECTION

Layer	Depth (ft)	Young's Modulus (psi)		Difference $\frac{(4)-(3)}{(4)}$ (percent)
		Crosshole	SASW	
(1)	(2)	(3)	(4)	(5)
Asphalt	0.58	467500	453200	-3.2
Subbase	1.38	110000	198310	+44.5
Compacted Fill	1.67	49500	45610	-8.5
	2.50	32850	37430	+12.2
	3.33	32350	36900	+11.5
Sandy Clay	5.0	42050	38820	-8.3
	7.5	40250	39340	-2.3

TABLE 6.3. COMPARISON OF YOUNG'S MODULI FROM CROSSHOLE AND SASW TESTS AT CRCP SECTION

Layer	Depth (ft)	Young's Modulus (psi)		Difference $\frac{(4)-(3)}{(4)}$ (percent)
		Crosshole*	SASW	
(1)	(2)	(3)	(4)	(5)
CRC ¹	0.83	-	3928000	-
ACB ²	1.17	-	462380	-
LSS ³	1.67	-	223380	-
Compacted Fill	2.50	32850	41450	-20.8
Sandy	5.00	42050	34740	-21.0
	7.50	40250	37960	-6.0

* Beneath ACP Shoulder

1 Continuously Reinforce Concrete

2 Asphaltic Concrete Base

3 Lime-Stabilized Subbase

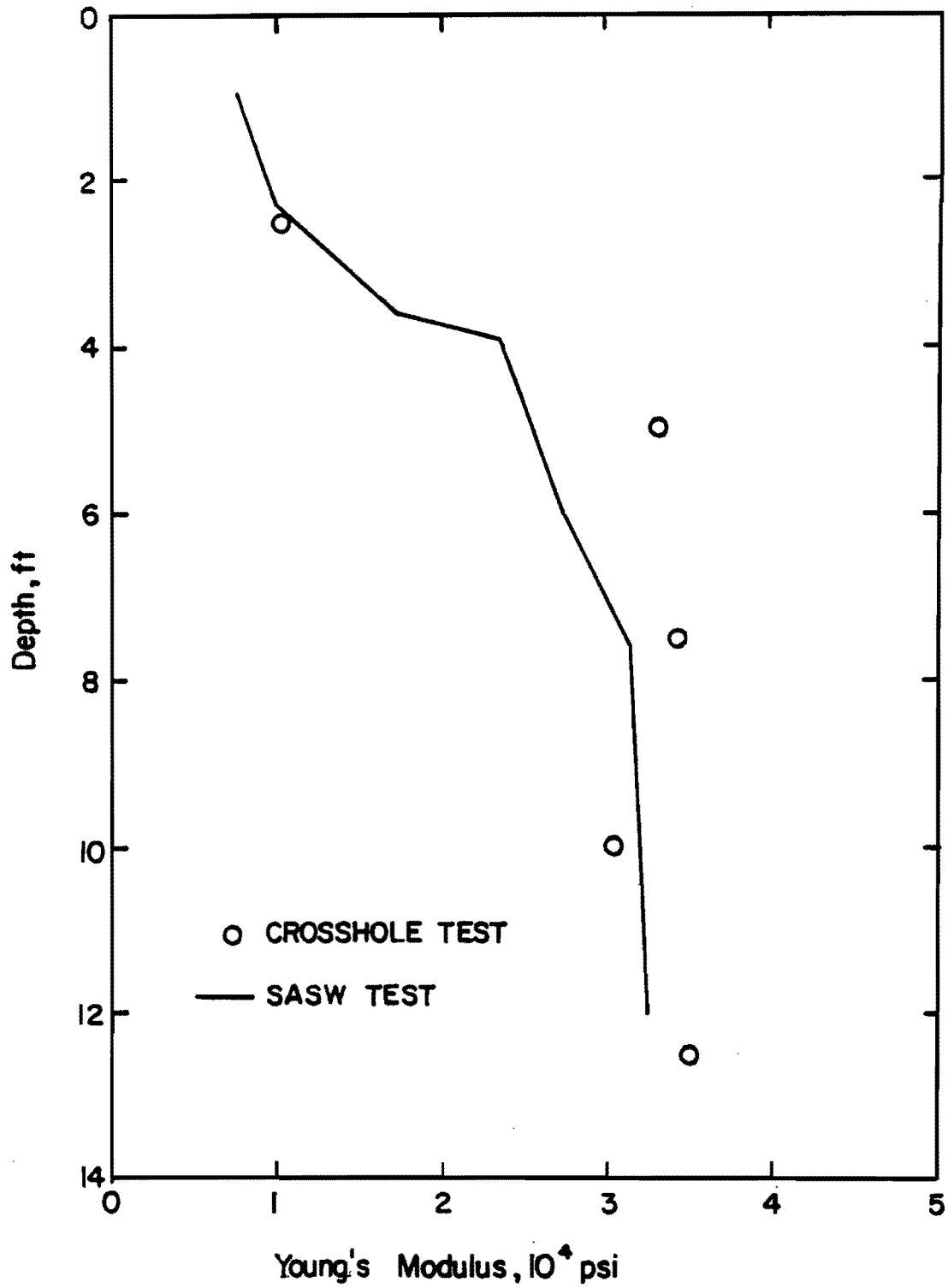


Fig 6.1. Young's modulus profile from crosshole and SASW tests at the median.

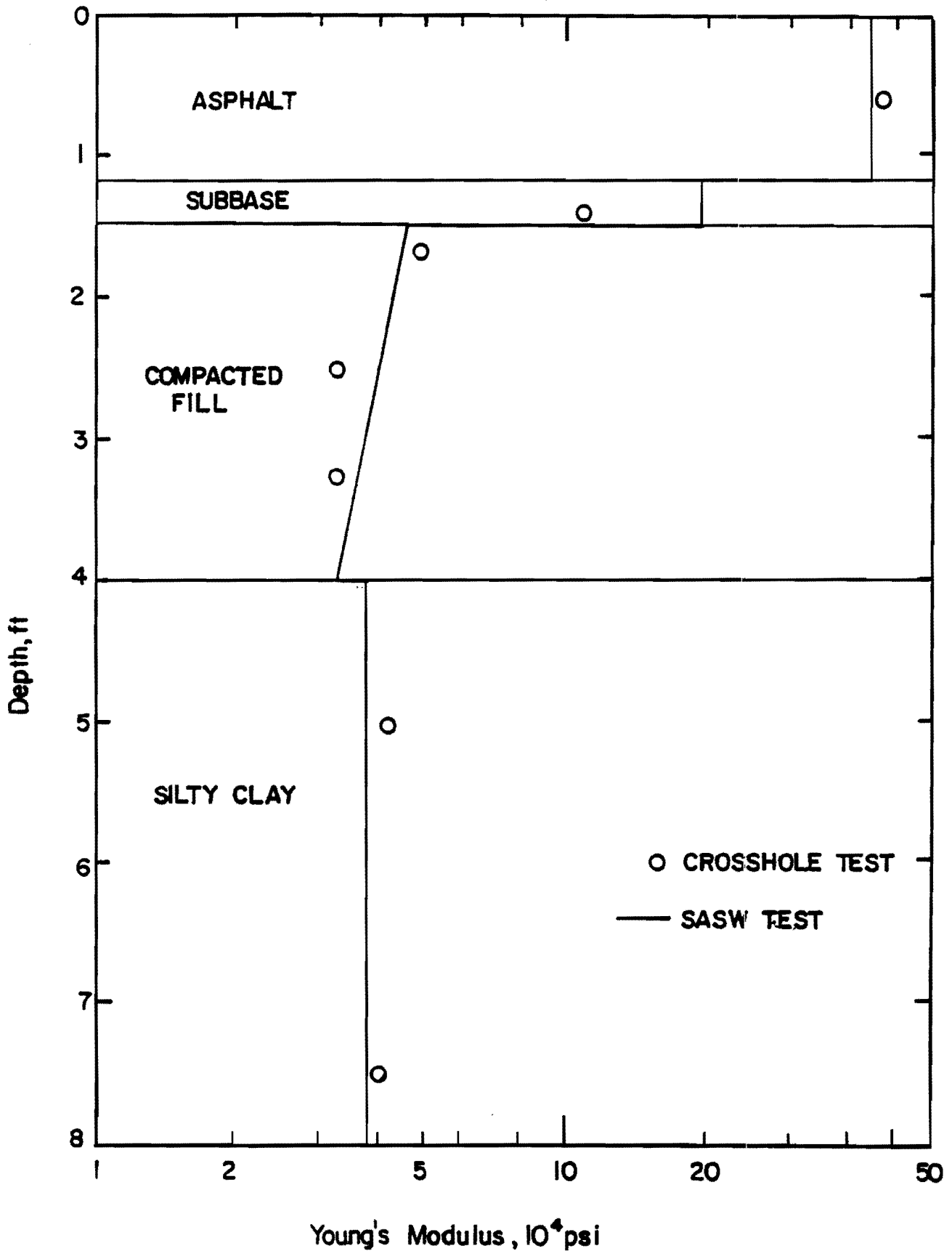


Fig 6.2. Young's modulus profile from crosshole and SASW tests at ACP section.

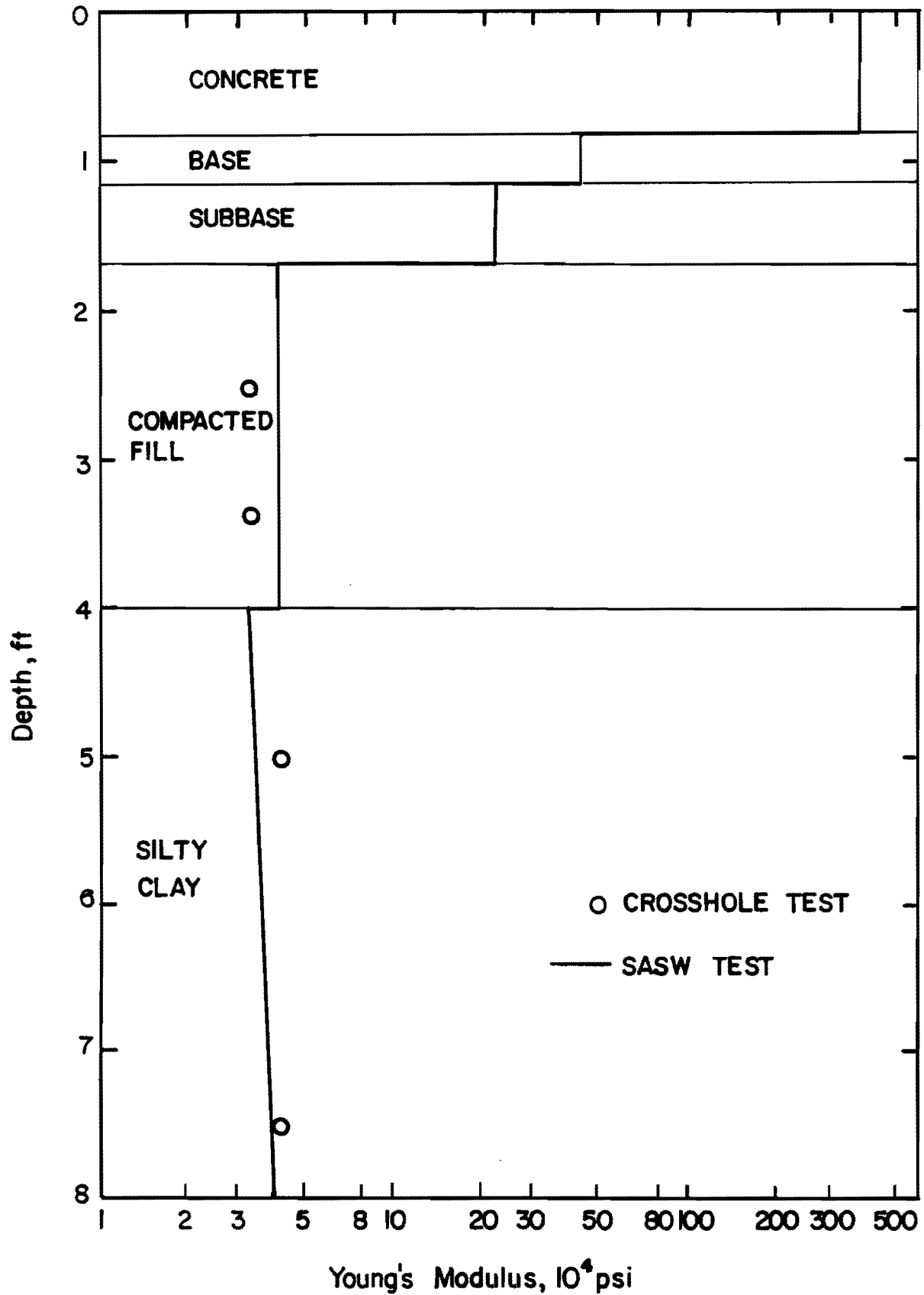


Fig 6.3. Young's modulus profile from crosshole and SASW tests at CRCP section.

CRCP sections, respectively. Deviation in elastic moduli from these two methods are proportional to the square of the S-wave velocity, given constant mass density and Poisson's ratio (Eqs 2.5 to 2.8). For the median, Young's moduli from the two methods differ by less than 11 percent, except for a depth of 5 ft, at which moduli from the two methods differ by about 34 percent.

In the case of the ACP and CRCP sections, variations in elastic moduli are less than 13 and 21 percent, respectively. However, for the subbase beneath the ACP and the base beneath the CRCP, these moduli are significantly different. To solve this problem, a more refined and sophisticated inversion process is essential.

It should be mentioned that the percentage deviations presented above are the maximum differences and over most of the profiles these numbers are significantly less, as shown in Tables 6.1, 6.2 and 6.3.

Layering at each site was compared with boring logs determined during the crosshole seismic tests, and the thicknesses of different layers are in good agreement with the logs (typically within an inch).

CHAPTER 7. SUMMARY, CONCLUSIONS, AND RECOMMENDATIONS

SUMMARY

The spectral-analysis-of-surface-waves method is described in this report. By means of a transient impact on the surface of a pavement system or soil deposit, a group of waves with different frequencies is transmitted to the medium. By analysis of the phase information for each frequency determined between two receivers located at the surface, R-wave velocity, S-wave velocity, and eventually the elastic moduli of the pavement system at different depths are determined. The method has the advantages of being

- (1) fast and economical,
- (2) nondestructive, and
- (3) capable of full automation.

CONCLUSIONS

Preliminary studies of the feasibility and testing procedure were conducted by Heisey et al (Ref 1) and are discussed in Report No. 256-2. This initial work has been expanded and improved in the following areas

- (1) The testing set-up has been modified. Instead of the common source geometry which was used, the tests are now performed using a common receiver midpoint geometry. Also, the direction of testing is reversed to eliminate the effect of a possible internal phase between the receivers and to average the effect of dipping layers.
- (2) A simple, approximate inversion method for elimination of the effect of high- or low-velocity shallow layers has been developed.

Three series of tests were performed on SH 71 near Columbus, Texas, and the results are presented herein. Elastic moduli determined from the SASW method are compared with the crosshole test. Deviation between moduli determined by the two methods is on the average less than 10, 13, and 21 percent in the median, ACP, and CRCP sections, respectively. The layering determined with the boring logs (drilled for the crosshole seismic test) and the SASW method compare closely.

RECOMMENDATIONS FOR FUTURE STUDIES

Further work is needed to substantiate the universality of this method and to refine further the technique developed on this project. Additional development is required in the following areas.

- (1) Various types of sites should be tested to establish the versatility and precision of the method. Investigation should include different types and depths of pavement layering. In conjunction with SASW tests, other types of tests such as Dynaflect, Texas cone penetrometer and crosshole seismic tests should be performed in situ. In addition, undisturbed samples from different layers should be taken for laboratory testing. These different tests would provide a check on moduli determined from the surface measurements.
- (2) The second phase of the analytical technique to invert R-wave dispersion curves should be developed to eliminate problems involved with the present inversion process. The second phase of the inversion method is under preliminary study.
- (3) To evaluate the properties of the thin layers for depths less than one foot, a source capable of generating high frequencies is essential. A simple sledge hammer with a pointed edge is able to generate frequencies of 3900 Hz on concrete pavements. However, development of a source capable of generating frequencies up to 6000 Hz is desirable.
- (4) Sampling deeper layers (more than 15 ft) is possible with this method, but velocity transducers with lower natural frequencies than the ones used in this study are required. These transducers are under construction and will be available in the near future.

- (5) The SASW method has the potential of full automation. Preliminary studies of adequate hardware required for this process should be made and equipment purchased so that testing time can be significantly decreased in the future.

REFERENCES

1. Heisey, S., K. H. Stokoe, II, W. R. Hudson, and A. H. Meyer, "Determination of In Situ Shear Wave Velocities From Spectral Analysis of Surface Waves," Research Report 256-2, Center for Transportation Research, The University of Texas at Austin, November 1982.
2. Lytton, R. L., W. M. Moore, and J. P. Mahoney, "Pavement Evaluation: Phase I, Pavement Evaluation Equipment," Report FHWA-RD-75-78, Federal Highway Administration, Washington, D. C., 1975.
3. Heisey, S., "Determination of In Situ Shear Wave Velocity from Spectral Analysis of Surface Waves," Master's Thesis, The University of Texas at Austin, 1981.
4. Hoar, R. J., "Field Measurement of Seismic Wave Velocity and Attenuation for Dynamic Analysis," Doctoral Thesis, The University of Texas at Austin, 1982.
5. Bolt, B. A., Nuclear Explosions and Earthquakes, W. H. Foreman and Company, San Francisco, California, 1976.
6. Miller, G. G., and H. Pursey, "On the Partition of Energy Between Elastic Waves in a Semi-Infinite Solid," Proceedings, Royal Society, London, Vol 223, 1955.
7. Ewing, W. M., W. S. Jardetzky, and F. Press, Elastic Waves in Layered Media, McGraw-Hill Book Co., Inc., 1957.
8. Richart, R. F., Jr., J. R. Hall, Jr., and R. D. Woods, Vibration of Soils and Foundations, Prentice-Hall, Englewood Cliffs, NJ, 1970.
9. Chen, L. S., "An Investigation of Stress-Strain and Strength Characteristics of Cohesionless Soils by Triaxial Compression Tests," Proceedings, 2nd International Conference on Soil Mechanics and Foundation Engineering, Rotterdam, Vol 5, 1948.
10. Krizek, R. J., "Fabric Effects on Strength and Deformation of Kaolin Clay," Proceedings, 9th International Conference on Soil Mechanics and Foundation Engineering, Tokyo, Vol 1, 1977.
11. Wong, P. K. K., and R. J. Mitchell, "Yielding and Plastic Flow of Sensitive Cemented Clay," Geotechnique, Vol 25, No. 4, December 1975.

12. Hardin, B. O., "The Nature of Stress-Strain Behavior in Soils," Proceedings, Earthquake and Soil Dynamics Conference, ASCE, Pasadena, California, Vol 1, 1978.
13. Warrick, R. E., "Seismic Investigation of a San Francisco Bay Mud Site," Bulletin of Seismological Society of America, Vol 64, No. 2, 1974.
14. Meisner, R., "Wave-Front Diagrams from Up-Hole Shootings," Geophysical Prospecting, Vol 9, No. 4, 1961.
15. Ogura, K., "Development of a Suspension Type S-Wave Log System," OYO Technical Note TN 34, OYO Corporation, Tokyo, 1979.
16. Stokoe, K. H., II, E. J. Arnold, R. J. Hoar, D. J. Shirley, and D. G. Anderson, "Development of a Bottom-Hole Device for Offshore Shear Wave Velocity Measurement," Proceedings, 10th Annual Offshore Technology Conference, Paper No. OTC 3210, 1978.
17. Redpath, B. B., "Seismic Refraction Exploration for Engineering Site Investigation," Technical Report TRE-73-4, Waterways Experimental Station, U. S. Army Corps of Engineers, Vicksburg, MS, 1973.
18. Borm, G. W., "Methods for Exploration Seismology: Reflection, Refraction, and Borehole Prospecting," Proceedings, Conference on Dynamical Methods in Soil and Rock Mechanics, Germany, Vol III, 1978.
19. Diebold, J. B., and P. L. Stoffa, "The Travel Time Equation, Tau-P Mapping, and Inversion of Common Midpoint Data," Geophysics, Vol 46, No. 3, 1981.
20. Hewlett Packard Company, "Digital Signal Analysis: Time and Frequency Domain Measurements," Application Note 240-0, Hewlett Packard, 1977.
21. Haskell, N. A., "The Dispersion of Surface Waves on Multilayered Media," Bulletin of the Seismological Society of America, Vol 43, No. 1, 1953.
22. Brigham, E. O., The Fast Fourier Transform, Prentice-Hall, Englewood Cliffs, NJ, 1974.
23. Newland, D. E., Random Vibration and Spectral Analysis, Longman, London, 1975.

APPENDIX A

EFFECT OF SET-UP CONFIGURATION ON DISPERSION
CURVES IN SASW METHOD

APPENDIX A. EFFECT OF SET-UP CONFIGURATION ON DISPERSION CURVES
IN SASW METHOD

To study the effect of set-up configuration during SASW testing, a series of tests was performed at a soil site located at the Walnut Creek Treatment Plant, 5 miles east of the campus of The University of Texas at Austin. This is the same site used by Heisey et al (Ref 3) in some of their testing, as well as Hoar (Ref 4) in some of his testing. Two geometries were selected; Common Source/Receiver (CSR) and Common Receiver Midpoint (CRMP). Schematics of these two approaches are shown in Figs 4.6 and 4.5, respectively.

The dispersion curves obtained from these two set-ups are shown in Figs A.1 and A.2 for CSR and CRMP geometries, respectively. Also shown on each figure is the range in velocities from the other figure. It can be concluded that scatter in the dispersion curves is much less in the CRMP approach. As such, the average dispersion curve obtained from the CRMP geometry is more reliable and more representative of the nature of the sub-surface material.

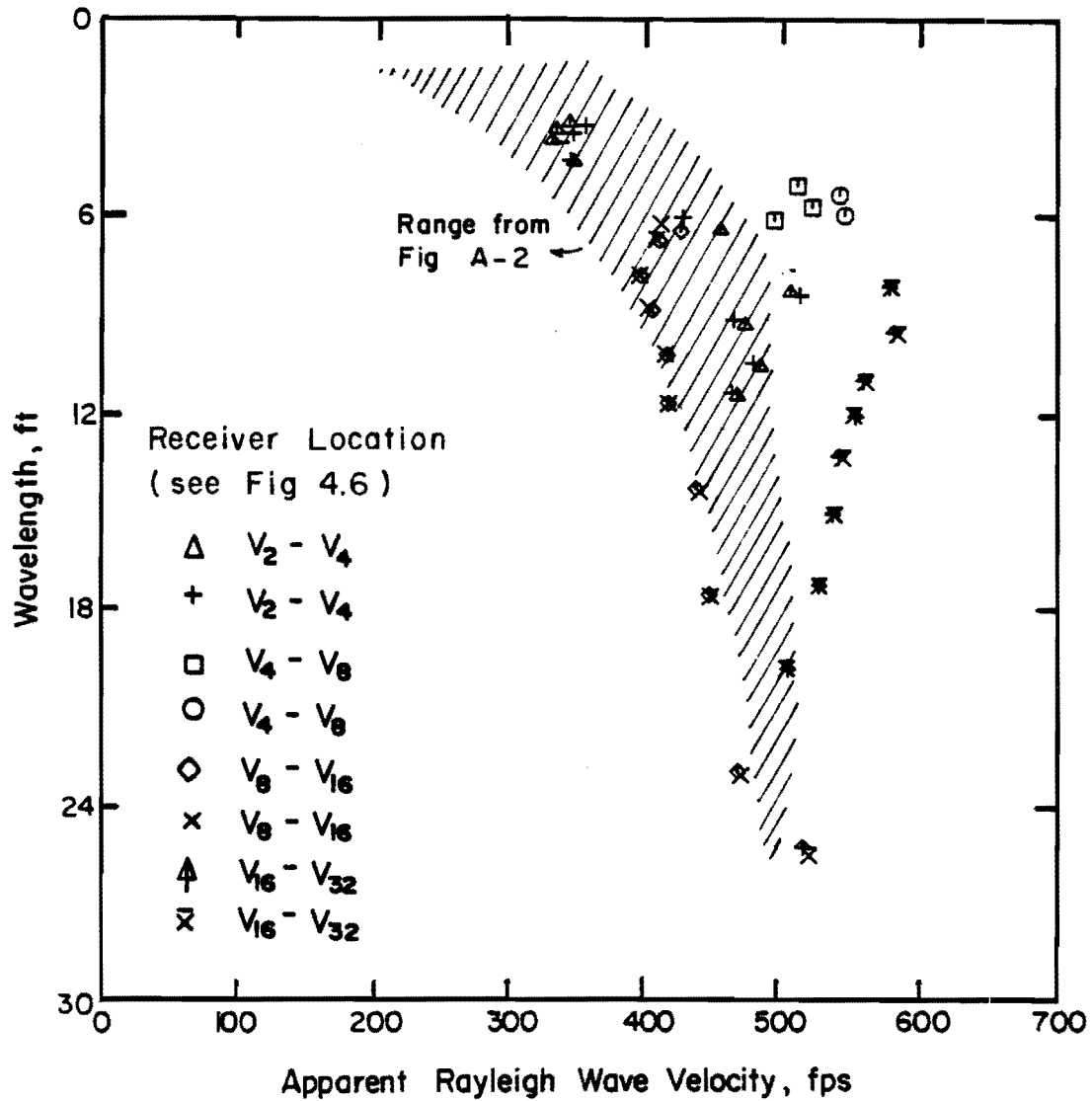


Fig A.1. Dispersion curves from SASW tests performed using common source geometry at Walnut Creek site.

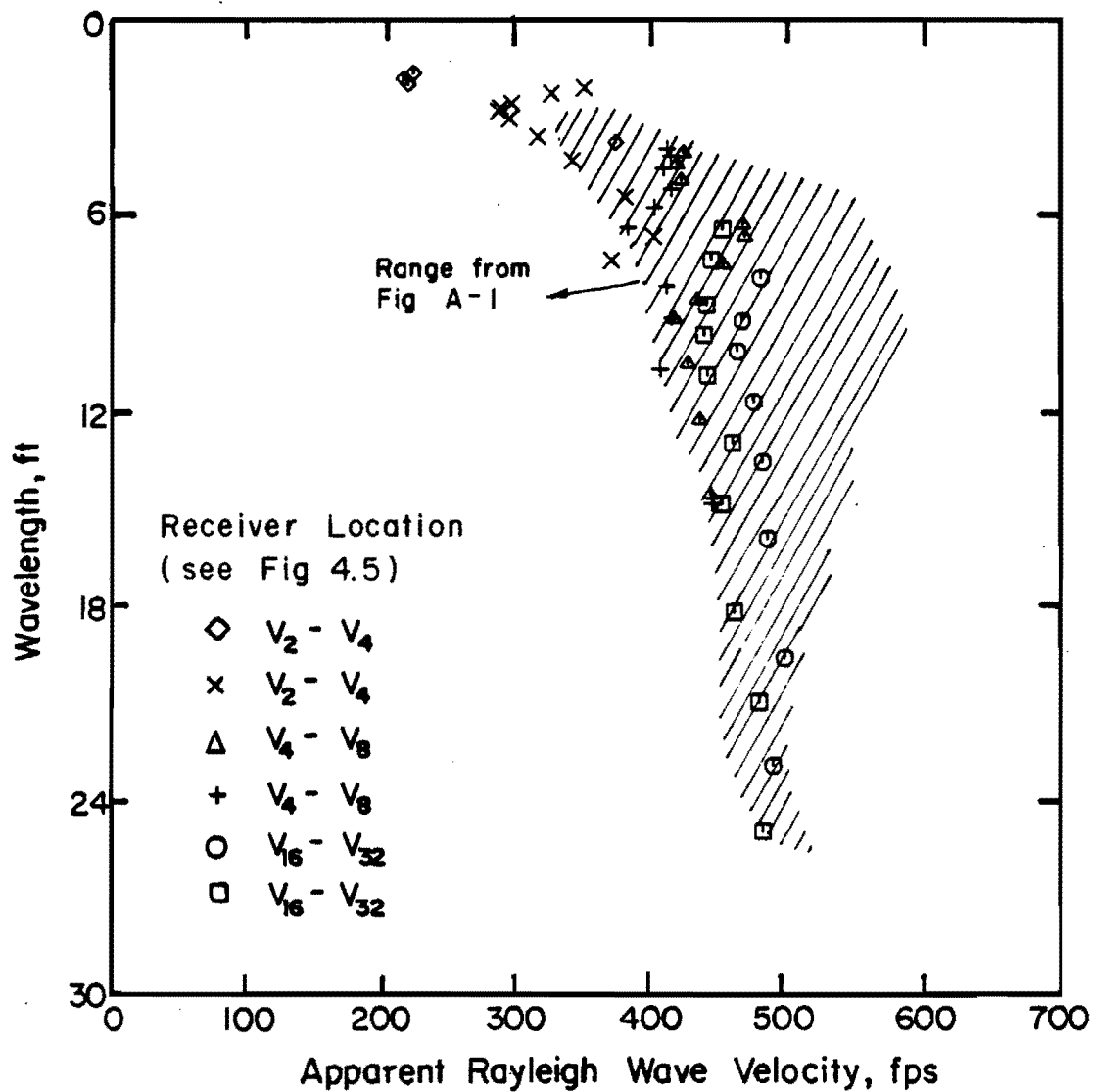


Fig A.2. Dispersion curves from SASW tests performed using common receivers midpoint geometry at Walnut Creek site.

APPENDIX B

FOURIER TRANSFORM AND SPECTRAL ANALYSIS

APPENDIX B. FOURIER TRANSFORM AND SPECTRAL ANALYSIS

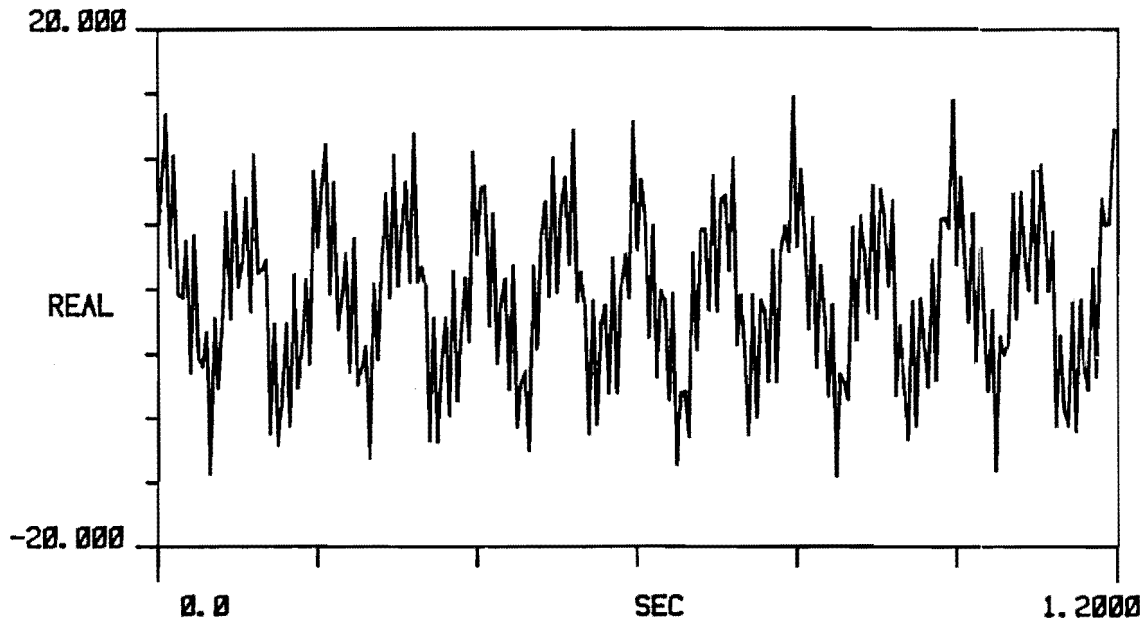
INTRODUCTION

In the past ten to fifteen years, the development of microprocessors and the Fast Fourier Transform (FFT) algorithm has greatly extended the capability to measure and analyze dynamic systems in the frequency domain. Instrumentation now exists that rapidly filters and converts an analog signal to a digitized signal, transforms the signal from its representation in the time domain into its frequency components, and analyzes the data in various formats. Consequently, frequency spectral analysis provides a quick and feasible approach to evaluating the propagation of elastic waves through layered systems.

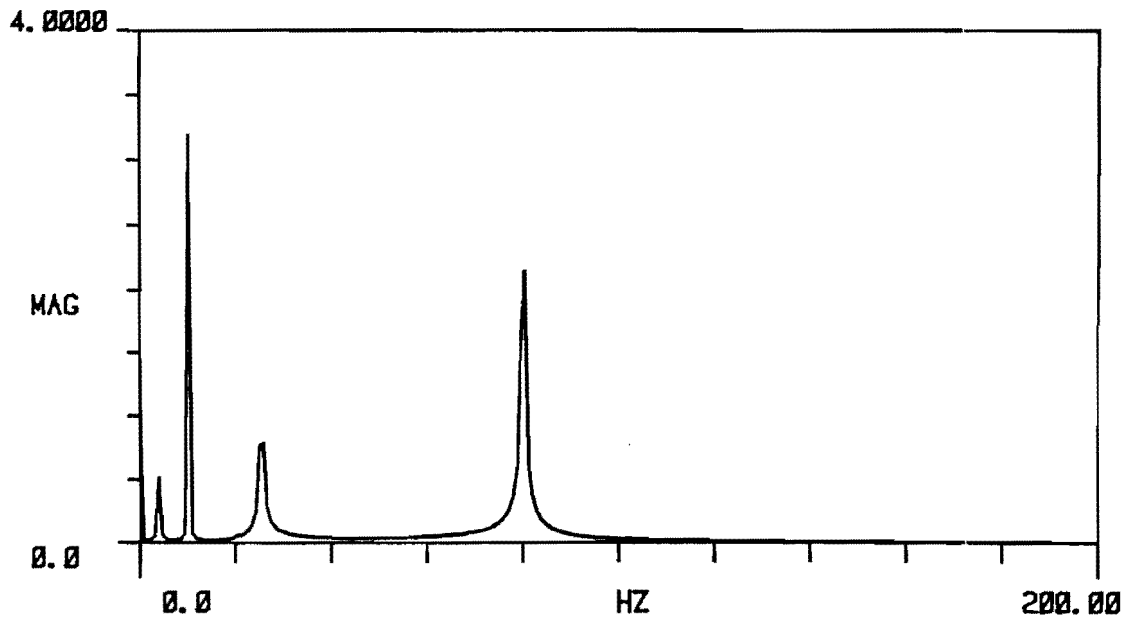
ADVANTAGES OF SPECTRAL ANALYSIS

The primary reason for utilizing spectral analysis is that information can be extracted from the data that was not apparent from the time domain representation of the signal. For example, the components of the signal in Fig B.1a are indistinguishable in the time record, but each wave and its relative contribution to the overall waveform are easily observed in the frequency spectrum shown in Fig B.1b. The amplitude and phase of each frequency component in the waveform can be determined. In addition, relationships between two signals can be easily identified.

Second, handling of data in the frequency domain permits ease of operations. For example, integration of a signal in the time domain



(a) Signal in the time domain.



(b) Signal in the frequency domain.

Fig B.1. Representation of a complex time signal by its frequency spectrum (Ref 1).

simplifies to just one division of the corresponding spectrum in the frequency domain. The advantage of spectral analysis is similar to that of using logarithms to solve a problem involving noninteger exponents.

Last, most of the measurements made in the frequency domain do not require a synchronized signal. As such, a trigger condition for averaging signals is not necessarily required. Unknown trigger delays that can affect time domain measurements are not a factor in most spectral analyses.

THE FOURIER TRANSFORM

Fourier analysis is central to the theory and mathematics involved in transforming a signal from a time record to its spectrum. The discussion that follows provides only a framework in which to introduce the types and usefulness of various spectral measurements. A more rigorous and complete presentation of the theory can be found in Brigham (Ref 5) or Newland (Ref 19).

The concept of the Fourier transform is an extension of the Fourier series representation of a periodic function. If $x(t)$ is a periodic function of time with period T , then that function can be represented by an infinite trigonometric series (Fourier series) of the form

$$x(t) = a_0 + \sum_{n=1}^{\infty} a_n \cos \frac{2\pi n t}{T} + \sum_{n=1}^{\infty} b_n \sin \frac{2\pi n t}{T} \quad (B.1)$$

where the a_n , a_n 's, and b_n 's are called Fourier coefficients. In the case where $T \rightarrow \infty$ (such as a waveform with no apparent periodicity), $x(t)$ is no longer periodic and cannot be represented by discrete frequency components. However, the approach of representing waveforms by frequency components is still valid for practically all engineering problems except that the discrete

Fourier series becomes a continuous Fourier integral and the discrete Fourier coefficients become a continuous function of frequency called the Fourier transform. The Fourier transform of $x(t)$ is then defined as

$$X(f) = \int_{-\infty}^{\infty} x(t) e^{-j2\pi ft} dt \quad (\text{B.2})$$

and the Fourier integral or inverse Fourier transform is

$$x(t) = \int_{-\infty}^{\infty} X(f) e^{j2\pi ft} df \quad (\text{B.3})$$

where $X(f)$ and $x(t)$ are called a transform pair. The "negative" frequencies are introduced solely for mathematical convenience.

The definition of $X(f)$ indicates that the Fourier transform exists in complex form. Using Euler's identity,

$$e^{j2\pi fnt} = \cos(2\pi fnt) + j\sin(2\pi fnt) \quad (\text{B.4})$$

yields

$$\cos(2\pi fnt) = \frac{e^{j2\pi fnt} + e^{-j2\pi fnt}}{2} \quad (\text{B.5})$$

and

$$\sin(2\pi fnt) = \frac{e^{j2\pi fnt} - e^{-j2\pi fnt}}{2} \quad (\text{B.6})$$

Substituting Eqs B5 and B6 into Eq B1, and rearranging, gives the form

$$a(t) = a_0 + \sum \frac{a_n - jb_n}{2} e^{j2\pi fnt} + \frac{a_n + jb_n}{2} e^{-j2\pi fnt} \quad (\text{B.7})$$

In this form, the a_n (or cosine) terms become the real part and the b_n (or sine) terms become the imaginary part in the representation of the spectrum. The amplitudes of these coefficients are half the amplitudes in Eq B.1 to allow for the previously introduced "negative" frequencies.

Using real and imaginary components, Fourier coefficients can be treated as rotating phasors in the complex plane. Such a representation is illustrated in Fig B.2. Each pair of coefficients (a_n , b_n) is represented by a phasor with magnitude A_n and phase θ_n , where

$$A_n = \sqrt{a_n^2 + b_n^2} \quad (\text{B.8})$$

and

$$\theta_n = \tan^{-1} \left(\frac{b_n}{a_n} \right) \quad (\text{B.9})$$

Magnitude and phase are often convenient ways to examine spectral data.

MEASUREMENT IN THE FREQUENCY DOMAIN

Several types of measurements can be made directly with most of the spectral analyzers that are currently available. The basic measurement is the linear spectrum, generally of both an "input" signal and an "output" signal. Other functions are defined using these two spectrums or their complex conjugates. The linear spectrum, denoted by $S_x(f)$, is simply the Fourier transform of the signal. From the previous definition

$$S_x(f) = F [x(t)] = \int_{-\infty}^{\infty} x(t) e^{-j2\pi ft} dt \quad (\text{B.10})$$

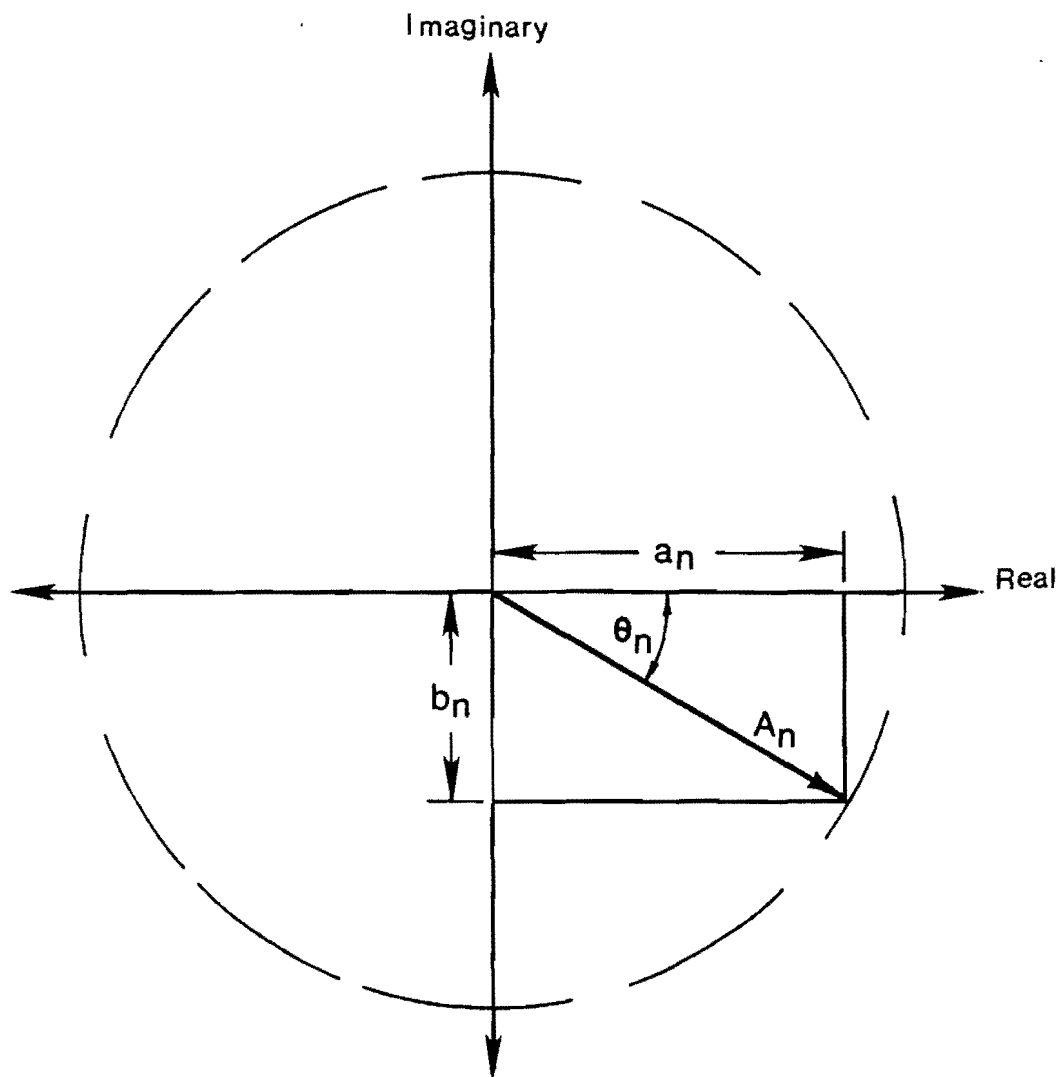


Fig B.2. Representation of Fourier coefficients by a rotating phasor in the complex plane (Ref 1).

The linear spectrum provides both magnitude and absolute phase information for all frequencies within the bandwidth for which the measurement was taken. Since the absolute phase is measured, a trigger is required to synchronize the signal for averaging. Linear spectrum averaging is useful for determining predominant frequencies of excitation, identifying fundamental modes and harmonics of a dynamic system, or extracting a "true" signal out of background noise.

The autospectral density function, $G_{xx}(f)$, commonly called the autospectrum, is defined as the linear spectrum, $S_x(f)$, multiplied by its own complex conjugate, $S_x^*(f)$. That is,

$$G_{xx} = S_x(f) \cdot S_x^*(f) \quad (\text{B.11})$$

The magnitude of the autospectrum is the magnitude squared of the linear spectrum. This magnitude can be thought of as the power (or energy of a transient, impulse signal) at each frequency in the measurement bandwidth. However, multiplication by the complex conjugate eliminates the imaginary components of the spectrum, so no phase information is provided by the autospectrum. The advantage of the autospectrum is that it provides information similar to that of the linear spectrum but does not require a trigger to synchronize the averaging of signals. The autospectrum is the Fourier transform of the autocorrelation function in the time domain.

The cross-spectral density function, $G_{yx}(f)$, or cross spectrum, is the Fourier transform of the cross correlation function between two different signals, $x(t)$ and $y(t)$. The cross spectrum is defined by

$$G_{yx}(f) = S_y(f) \cdot S_x^*(f) \quad (\text{B.12})$$

where $S_y(f)$ is the linear spectrum of the output and $S_x^*(f)$ is the complex conjugate of the linear spectrum of the input. The magnitude of $G_{yx}(f)$ is a measure of the mutual power between the two signals, making the cross spectrum an excellent means of identifying predominant frequencies that are present in both the input and output signals. The phase of $G_{yx}(f)$ is the relative phase between the signals at each frequency in the measurement bandwidth. Since the phase is a relative phase, the cross spectrum measurement can be made without a synchronizing trigger. The cross spectrum is used primarily to determine the phase relationships between two signals which may be caused by time delays, propagation delays or varying wave paths between receivers.

The transfer function, $H(f)$, or frequency response function, characterizes the input-output relationship of a dynamic system. The frequency response function is the ratio of the spectrum of the system's response (output) to the spectrum of the system's excitation (input):

$$H(f) = S_y(f)/S_x(f) \quad (B.13)$$

Due to statistical variance of $S_x(f)$ and $S_y(f)$ for certain systems, a better measure of $H(f)$ can be obtained by using the autospectrum and cross-spectrum functions. If both numerator and denominator are multiplied by $S_x^*(f)$,

$$H(f) = \frac{S_y(f) \cdot S_x^*(f)}{S_x(f) \cdot S_x^*(f)} \quad (B.14)$$

Thus, the transfer function is similar to the cross spectrum. Both provide the same information; the magnitude of the transfer function is normalized by the autospectrum of the input $G_{xx}(f)$ relative to the magnitude of the cross spectrum. Consequently, the transfer function of a given system should be

constant regardless of the input (if the system does not undergo nonlinear behavior). Generally, the input is a force measurement derived from the signal of a load cell mounted on the source of excitation. Depending on the quality which is measured as output, the transfer function may provide a measurement of impedance, dynamic stiffness, or one of several other system properties. The transfer function is frequently used to identify natural frequencies and damping coefficients of a dynamic system.

The coherence function, $\gamma^2(f)$, is a measurement made in conjunction with the transfer function. Coherence is defined as,

$$\gamma^2(f) = \frac{G_{yx}(f) \cdot G_{yx}^*(f)}{G_{xx}(f) \cdot G_{yy}(f)} \quad (\text{B.15})$$

The coherence is a real-valued function which is the ratio of the response (output) power caused by the measured input to the total measured response power. Therefore, $\gamma^2(f) = 1$, all of the output at the particular frequency of interest, is due to the measured inputs. The coherence function may be less than unity when

- (1) there are multiple input signals in the system which are not being measured,
- (2) background noise is present in the measurement,
- (3) the frequency response function is nonlinear for the system, or
- (4) there are closely spaced resonant peaks which cannot be detected with the given frequency resolution inherent in the digitization of the signal.

The coherence function is often used in the form of the signal-to-noise ratio (S/N):

$$\frac{S(f)}{N(f)} = \frac{\gamma^2(f)}{1 - \gamma^2(f)} \quad (\text{B.16})$$

In addition, the coherence function can be used to weigh the output autospectrum $G_{yy}(f)$ to reflect the output power caused only by the input. This weighted spectrum is called the coherent output power and is given by $G_{yy}(f) \cdot \gamma^2(f)$. The relative contributions of several inputs can be separated using the coherent output power function. In general, the coherence function indicates the "quality" of the measurement at each frequency. A low value of coherence does not necessarily indicate that the measurement is invalid for a particular frequency but may suggest that more averaging is required to improve the signal-to-noise ratio.

ADDITIONAL CONSIDERATIONS FOR DIGITAL SIGNAL ANALYSIS

Digital signal processes offer the advantages of quick and efficient data measurement, analysis, and storage. The capability to average a series of records enhances data measurement since noise and non-synchronized signals will approach a mean value of zero. Digitization also permits convenient manipulation of data for calculations and interpretation. However, the conversion of an analog signal to a digital signal includes some drawbacks.

First, to ensure that the digitized signal accurately represents the analog signal, the sampling rate of the "function" which converts the signal must be at least twice the frequency of the highest frequency present in the waveform being sampled. If the sampling rate is too low, higher frequencies will "alias", or appear as lower frequencies in the spectrum. This potential problem is demonstrated graphically for the time record shown in Fig B.3. Generally, the instrumentation is designed so that the selection of the bandwidth for the measurement automatically adjusts the necessary filtering and sampling rate.

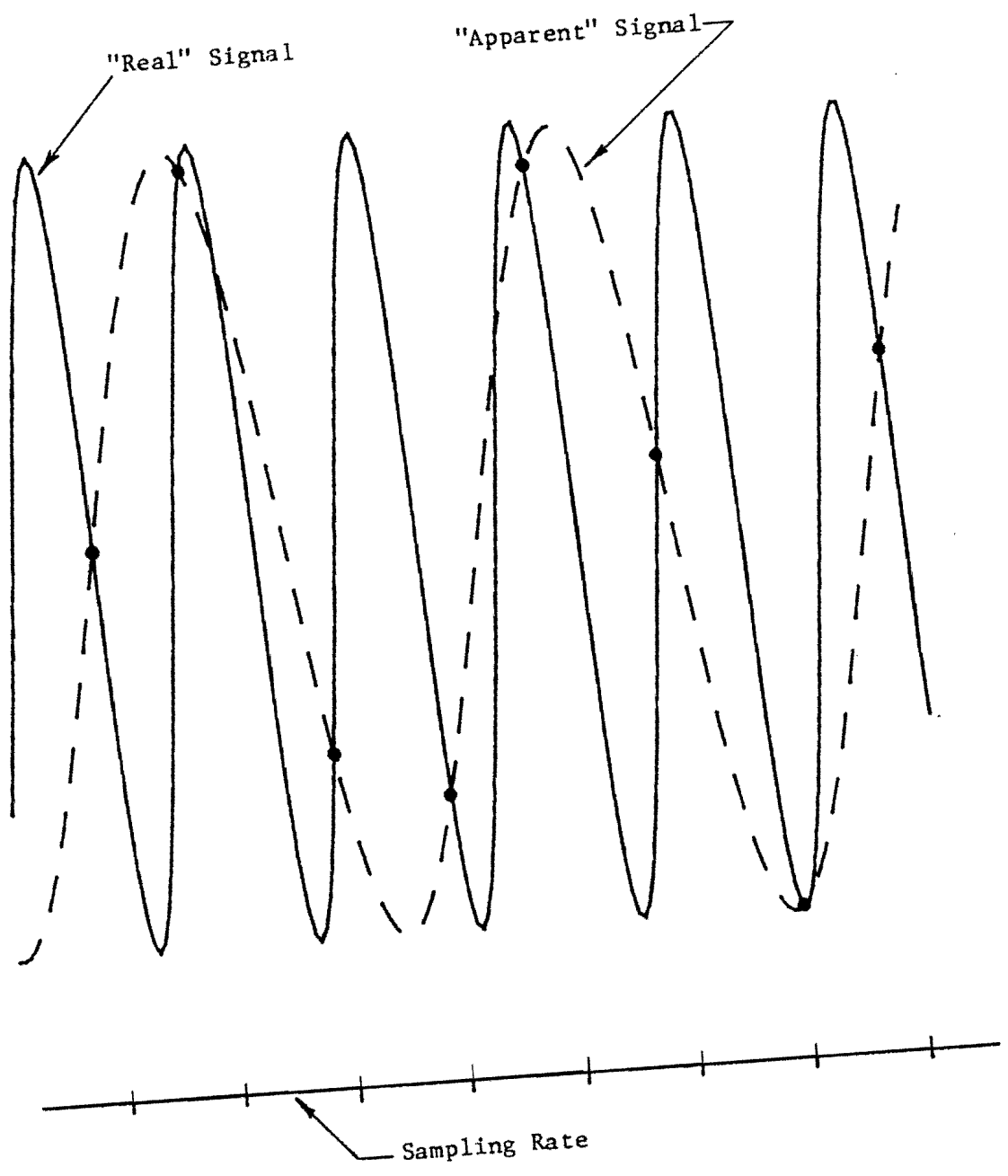


Fig B.3. Low-frequency alias resulting from insufficient sampling of a high-frequency signal (Ref 1).

Secondly, since computers or microprocessors can handle only a finite amount of data, the signal must be truncated. Truncation is accomplished with a function called a window. The simplest type of window is a rectangular box. When the window "examines" an exact integral number of cycles of all the frequency components, the resulting spectrum is accurate. If a noninteger number of cycles occurs in the window, some of the magnitude of a given frequency component may appear at adjacent frequencies. This phenomenon is known as leakage. Invariably, some leakage is going to occur for some frequencies in most signals. The type of signal (e.g., sinusoidal, random, or transient) governs the type of window employed to minimize the effects of leakage.

Lastly, the inherent inverse relationship between period, or length of the time signal, and frequency creates problems with resolution, particularly when the digital signal consists of a fixed number of data points. As the time length of the signal increases, the bandwidth of the measurement in the frequency domain narrows. Conversely, wider bandwidths require shorter time records and provide less frequency resolution. Some instruments include capabilities to overcome this dilemma. Rather than make a wide baseband measurement from zero to some high frequency, the measurement is centered about the high frequency with a narrow band. The band selectable analysis, or "zoom" measurement, allows high frequency resolution in a high frequency range.

APPENDIX C

INVERSION OF DISPERSION CURVES

APPENDIX C. INVERSION OF DISPERSION CURVES

The dispersion equation in a layered medium as shown in Fig C.1 can be written as (Ref 21):

$$KN - MN = 0 \quad (C.1)$$

where:

$$k = \gamma_n r_{\alpha n} A_{12} + (\gamma_n - 1)A_{22} - r_{\alpha n} A_{32}/\rho_n c^2 + A_{42}/\rho_n c^2 \quad (C.2)$$

$$L = \gamma_n r_{\alpha n} A_{11} + (\gamma_n - 1)A_{21} - r_{\alpha n} A_{31}/\rho_n c^2 + A_{41}/\rho_n c^2 \quad (C.3)$$

$$M = -(\gamma_n - 1)A_{12} + \gamma_n r_{\beta n} A_{22} + A_{32}/\rho_n c^2 + r_{\beta n} A_{42}/\rho_n c^2 \quad (C.4)$$

$$N = -(\gamma_n - 1)A_{11} + \gamma_n r_{\beta n} A_{21} + A_{31}/\rho_n c^2 + r_{\beta n} A_{41}/\rho_n c^2 \quad (C.5)$$

and

$$A_{ij} = \sum_{k=1}^n a_{ij,k} \quad (C.6)$$

$$\gamma_n = 2(V_{sn}/c)^2 \quad (C.7)$$

$$r_{\beta n} = -i[1 - (c/V_{sn})^2]^{1/2} \quad (C.8)$$

$$r_{\alpha n} = -i[1 - (c/V_{pn})^2]^{1/2} \quad (C.9)$$

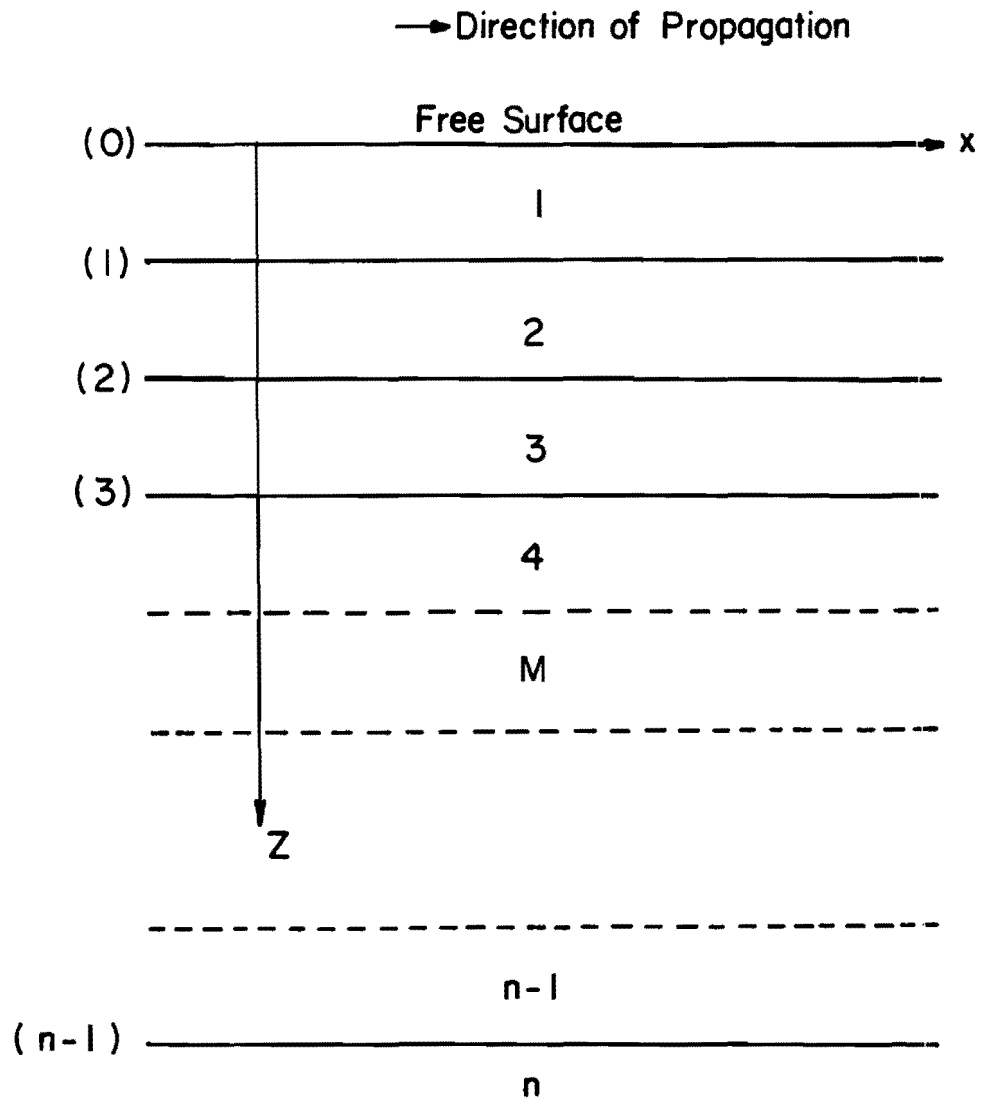


Fig C.1. Direction of axes and number of the layers and interfaces (Ref 21).

The elements of matrix a_{ij} for each layer are

$$(a_m)_{11} = \gamma_m \cos P_m - (\gamma_m - 1) \cos Q_m$$

$$(a_m)_{12} = i (\gamma_m - 1) r_{am}^{-1} \sin P_m + \gamma_m r_{\beta m} \sin Q_m$$

$$(a_m)_{13} = -(\rho_m c^2)^{-1} (\cos P_m - \cos Q_m)$$

$$(a_m)_{14} = i(\rho_m c^2)^{-1} (r_{am}^{-1} \sin P_m + r_{\beta m} \sin Q_m)$$

$$(a_m)_{21} = -i[\gamma_m r_{am} \sin P_m + (\gamma_m - 1) r_{\beta m}^{-1} \sin Q_m]$$

$$(a_m)_{22} = -(\gamma_m - 1) \cos P_m + \gamma_m \cos Q_m$$

$$(a_m)_{23} = i(\rho_m c^2)^{-1} (r_{am} \sin P_m + r_{\beta m}^{-1} \sin Q_m)$$

$$(a_m)_{24} = (a_m)_{13}$$

$$(a_m)_{31} = \rho_m c^2 \gamma_m (\gamma_m - 1) (\cos P_m - \cos Q_m)$$

$$(a_m)_{32} = i \rho_m c^2 [(\gamma_m - 1)^2 r_{am}^{-1} \sin P_m + \gamma_m^2 r_{\beta m} \sin Q_m]$$

$$(a_m)_{33} = (a_m)_{22}$$

$$(a_m)_{34} = (a_m)_{12}$$

$$(a_m)_{41} = i \rho_m c^2 [\gamma_m^2 r_{am} \sin P_m + (\gamma_m - 1)^2 r_{\beta m}^{-1} \sin Q_m]$$

$$(a_m)_{42} = (a_m)_{31}$$

$$(a_m)_{43} = (a_m)_{21}$$

$$(a_m)_{44} = (a_m)_{11}$$

In these equations, the nomenclature is as follows:

V_{sn} = shear wave velocity of n^{th} layer,

c = phase velocity,

V_{pn} = compressional wave velocity of n^{th} layer,

$i = \sqrt{-1}$

ρ_n = density of the n^{th} layer.

Parameters a_{ij} are the elements of a 4 x 4 matrix. If

$$P_n = kr_{\alpha n} h_n$$

and

$$Q_n = kr_{\beta n} h_n$$

in which h_n is the thickness of the n^{th} layer and

$$k = \frac{2\pi}{\text{wavelength}}$$

the elements a_{ij} can be readily calculated.

In addition,

$$\frac{V_{pn}}{V_{sn}} = \sqrt{\frac{1 - v_n}{0.5 - v_n}}$$

where ν_n is the Poisson's ratio for the n^{th} layer. Shear wave velocity is then used to determine R-wave velocity of each layer. So, by knowing the velocity and the depth of the first layer at the top and the depth of other layers, Eq C.1 can be solved for different layers by trial and error. This matter is discussed in full detail by Ewing et al (Ref 7).

APPENDIX D
CROSSHOLE SEISMIC TESTS

APPENDIX D. CROSSHOLE SEISMIC TESTS

INTRODUCTION

The basic concept of the crosshole seismic method involves propagating body waves through horizontal travel paths at different depths and measuring the propagation velocities at these depths. By means of elastic theory the moduli of each layer are then evaluated (as described in Chapter 2) and the thicknesses of different layers can be determined from the borings used to advance the boreholes.

TESTING PROCEDURE

A schematic of the testing procedure is shown in Fig D.1. One or more boreholes are drilled to the maximum depth at which testing is to be conducted. These boreholes function as holes in which receivers are placed. The boreholes are cased if there is any risk of caving during testing. Another borehole is then drilled to function as the source borehole. At each depth at which seismic testing is to be performed, the drilling operation is stopped, and a source is placed in the bottom of the hole. Simultaneously, the receivers are located at the same depth in the other holes. A vertical transient impulse which simultaneously activates the recording device is then applied to the source. The impulse is detected by receivers in the other holes as the body waves pass by.

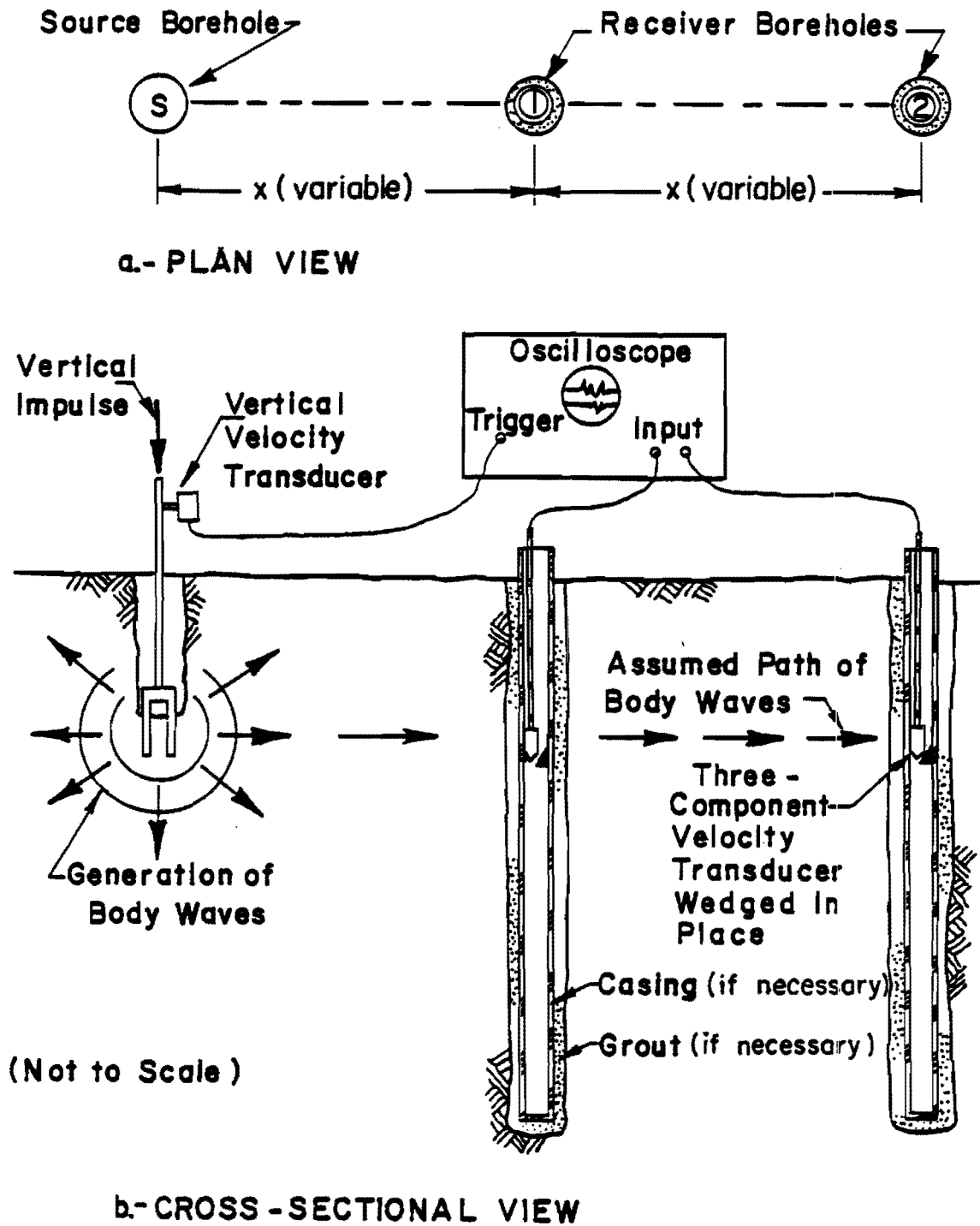


Fig D.1. Schematic of crosshole seismic testing (Ref 4).

Required equipment for a crosshole seismic test includes

- (1) a drilling rig,
- (2) a mechanical source,
- (3) three-dimensional receivers,
- (4) a recording device, and
- (5) a triggering system.

In Fig D.2 the drilling rig is shown advancing one of the boreholes at the Columbus site. Five-inch diameter boreholes were used, and care was taken during the drilling process to cause minimum disturbance in the soil deposit.

The source used in Columbus consisted of a sampling tube attached to a 1-inch diameter rod as shown in Fig D.3. A vertical velocity transducer was secured to the rod just above the sampling tube. This transducer served as the trigger for the recording device.

The receivers consisted of three-dimensional velocity transducers in which three transducers were oriented in three perpendicular directions (i.e., the vertical direction and two perpendicular horizontal directions). The receivers were secured at the desired depths by inflating bicycle tubes attached to the receivers (as shown in Fig D.4). The receivers were properly oriented with the orientation rods which extended from the receivers to the surface. The receivers and the transducer located on the source were connected to the recording device, a digital oscilloscope, through a switching box (see Fig D.5). By means of the switching box, the geophone with proper orientation for the wave motion to be measured was easily selected. The records were saved on magnetic diskette for future reference and in-house data reduction.

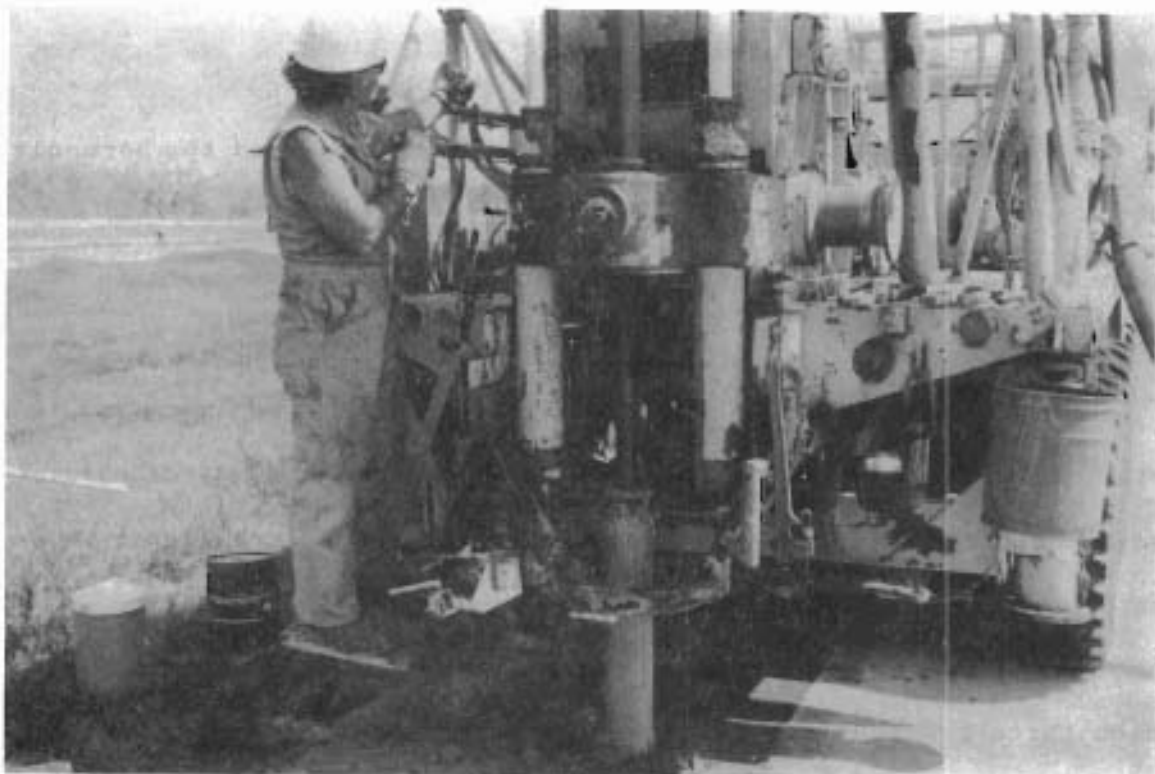


Fig D.2. Drilling operation for crosshole seismic tests at Columbus site.

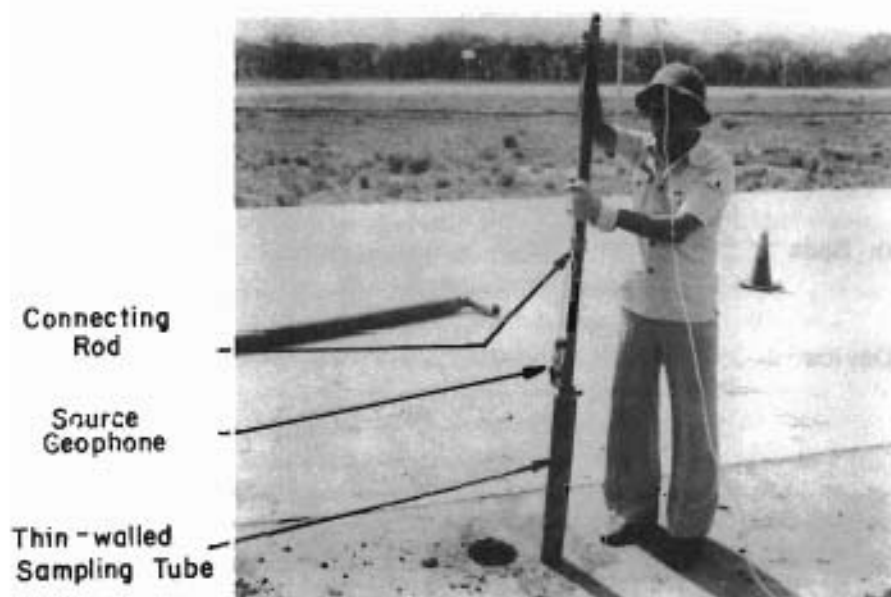


Fig D.3. Source used in crosshole seismic tests at Columbus site.

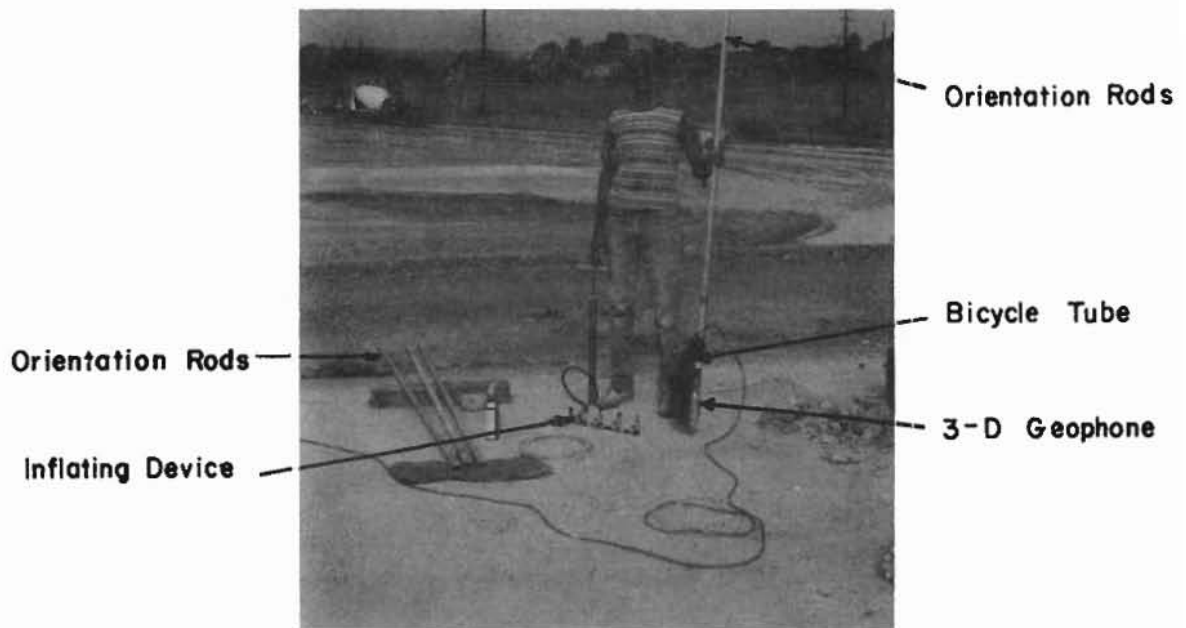


Fig D.4. Three-dimensional receiver used in crosshole seismic tests.

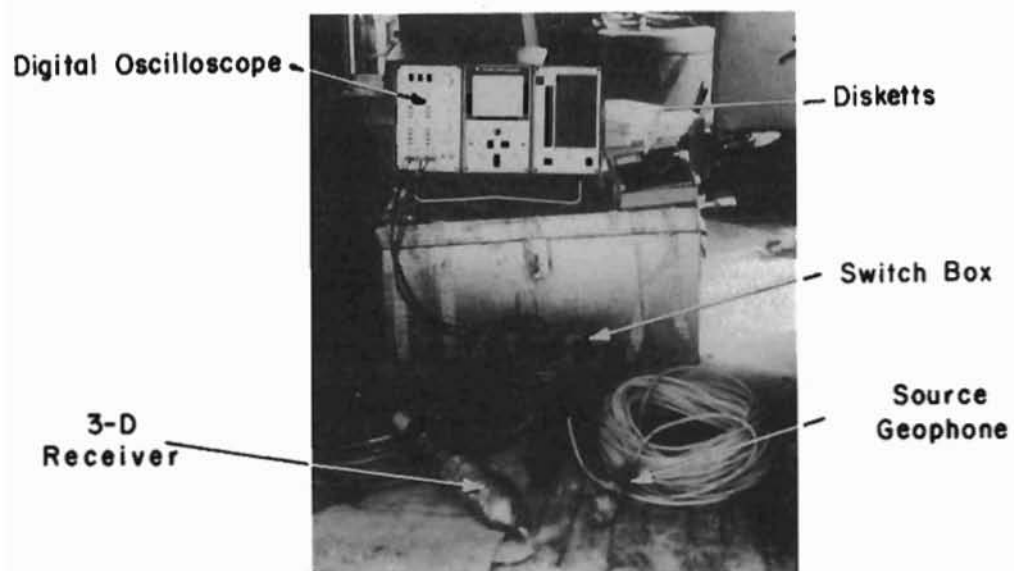


Fig D.5. Recording device used in crosshole seismic tests.

Figure D.6 shows a crosshole test being performed on the ACP shoulder on SH 71 near Columbus. The three boreholes can be clearly seen in this figure. The distance between the boreholes depends on the stiffness of the medium. Generally, this distance is on the order of 3 ft to 5 ft for paved sections and 7 ft to 10 ft for soil deposits. The reason for close spacing in paved sections is to minimize (undesirable) refracted ray paths. The vertical impulse to the rod is applied by an ordinary hammer. A vertical impulse transmitted to a medium generates P- and S-waves which can be detected by horizontal and vertical geophones, respectively.

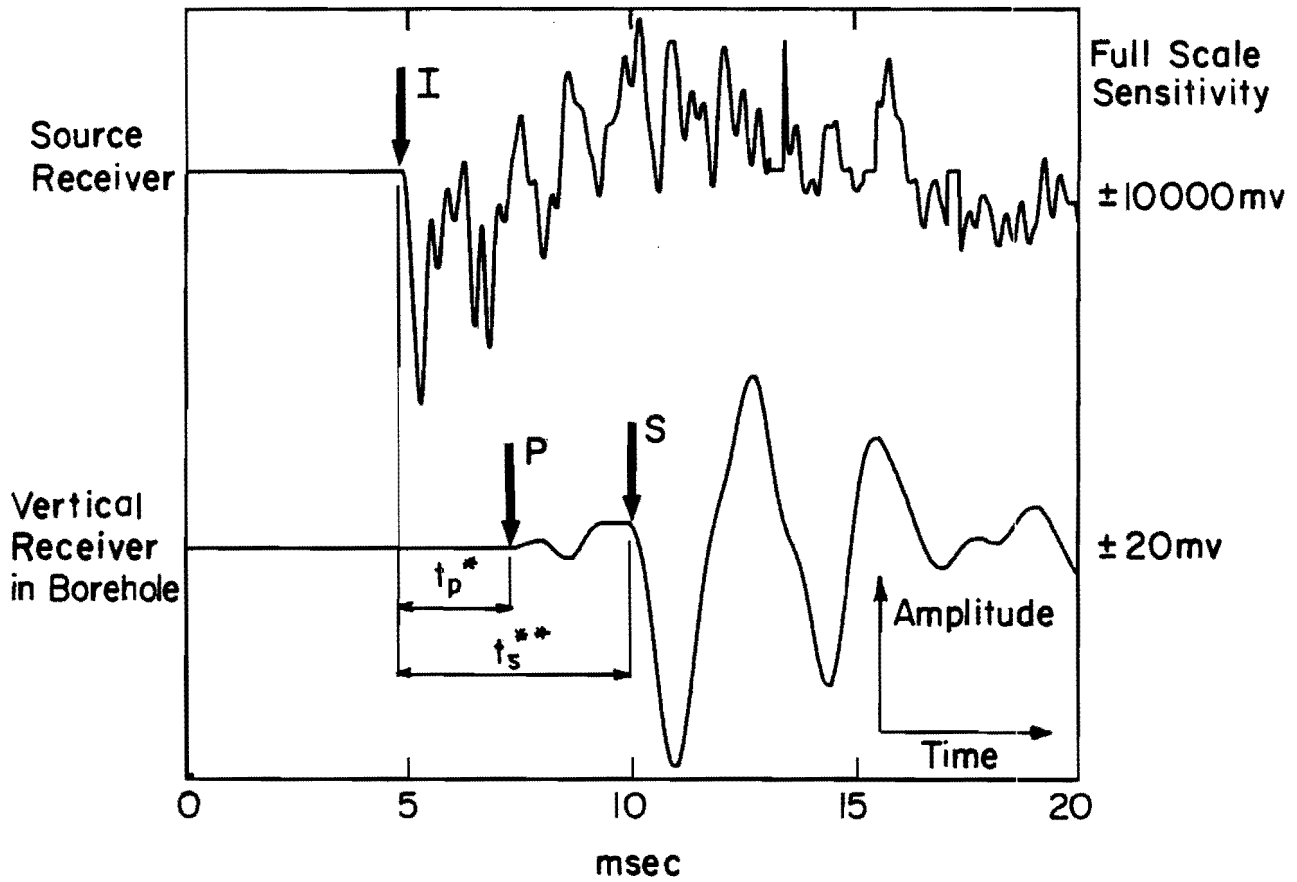
DATA REDUCTION

A typical record detected with vertical geophones is presented in Fig D.7. The upper portion of the figure is the impulse detected by the source geophone. A time delay is used at the beginning of the record so that the triggering point can be easily distinguished. This point is marked as "I" on the record. On the lower part of the figure is the travel time record of the body waves monitored by the vertical geophone at a distance of 3.5 ft from the source. The direct P- and S-wave arrivals are marked by "P" and "S", respectively. Shear and compressional travel times are simply the time differences between point "I" and points "S" or "P", respectively. Although P-wave velocity can be identified on this record, it is preferred that this velocity be determined from a record obtained using a transducer which is oriented in the direction of propagation (i.e., a horizontal geophone). A typical travel time record for a horizontal geophone is shown in Fig D.8. The triggering time and direct arrival of P-wave are marked as "I" and "P" on this record, respectively. The amplitude on the travel time record of the P-



- ① Receiver Borehole
- ② Source Borehole
- ③ Source

Fig D.6. Testing at one depth at the Columbus site.



* P-wave travel time
 ** S-wave travel time

Fig D.7. Typical crosshole travel time record generated with vertical impulse and at a distance of 7 ft.

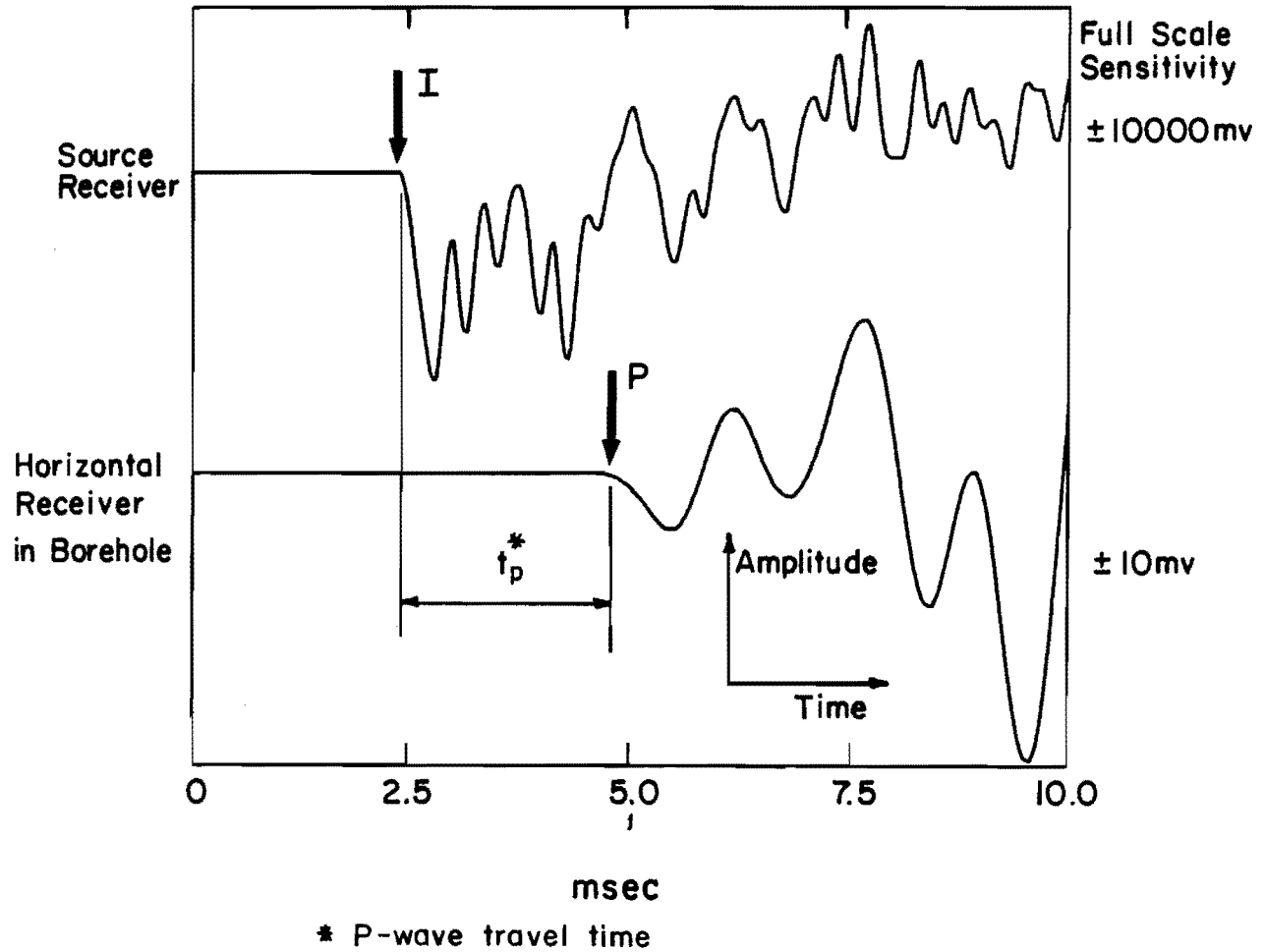


Fig D.8. Typical crosshole travel time record generated with vertical impulse and detected by horizontal geophone at a distance of 7 ft.

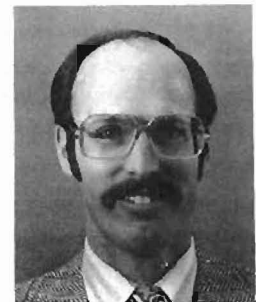
wave is much larger in Fig D.8 than in Fig D.7, because of proper orientation of the receiver.

Propagation velocity is determined simply by dividing the distance between the source and receiver by the travel time over this distance. Moduli are then determined as described in detail in Chapters 2 and 5.

THE AUTHORS

Soheil Nazarian was born in Tehran, Iran on March 28, 1955. In 1973, he graduated from Andisheh (Don Basco) Highschool in Tehran, Iran, and in the same year entered the University of Tehran. He received the degree of Master of Science in Structural Engineering in July 1979. Upon graduation he came to the United States and entered Tufts University in Medford, Massachusetts. In October 1982, he received the degree of Master of Science in Geotechnical Engineering. Since then he has been a Ph.D. student and appointed as a Research Assistant at The University of Texas at Austin.

Kenneth H. Stokoe, II joined the faculty of the College of Engineering at The University of Texas at Austin in 1973. He is presently a Professor of Civil Engineering and is actively involved with several on-going research projects. He has been working in the areas of in situ seismic measurement, laboratory measurement of dynamic soil properties, and the relationship between field and laboratory dynamic measurements for the past fifteen years. He was instrumental in developing the in situ crosshole seismic method for shear wave velocity and shear modulus measurements to the method that is presently used by most geotechnical engineering firms.



In addition to his teaching and research activities, Dr. Stokoe has served as a consultant to federal, state and private organizations in the areas of soil dynamics and geophysics. He is currently serving as a consultant to the Civil Engineering Division and the Earthquake Hazards Mitigation Program of the National Science Foundation.